Computer Modeling in Engineering & Sciences

Tech Science Press

Doi:10.32604/cmes.2025.067724

REVIEW

Advanced Signal Processing and Modeling Techniques for Automotive Radar: Challenges and Innovations in ADAS Applications

Pallabi Biswas[1,#], **Samarendra Nath Sur**[2,*,#], **Rabindranath Bera**[3], **Agbotiname Lucky Imoize**[4] and **Chun-Ta Li**[5,*]

[1]Department of Electronics and Communication Engineering, Sikkim Manipal Institute of Technology, Majhitar, Sikkim Manipal University, Gangtok, 737136, Sikkim, India

[2]Department of Computer Science and Engineering, Sikkim Manipal Institute of Technology, Majhitar, Sikkim Manipal University, Gangtok, 737136, Sikkim, India

[3]Department of Electronics and Communication Engineering, Indian Institute of Information Technology, Kalyani, 741235, West Bengal, India

[4]Department of Electrical and Electronics Engineering, Faculty of Engineering, University of Lagos, Akoka, Lagos, 100213, Nigeria

[5]Bachelor's Program of Artificial Intelligence and Information Security, Fu Jen Catholic University, 510 Zhongzheng Road, New Taipei City, 242062, Taiwan

*Corresponding Authors: Samarendra Nath Sur. Email: samar.sur@ieee.org; Chun-Ta Li. Email: 157278@mail.fju.edu.tw

[#]These authors contributed equally to this work

Received: 10 May 2025; Accepted: 02 July 2025; Published: 31 July 2025

ABSTRACT: Automotive radar has emerged as a critical component in Advanced Driver Assistance Systems (ADAS) and autonomous driving, enabling robust environmental perception through precise range-Doppler and angular measurements. It plays a pivotal role in enhancing road safety by supporting accurate detection and localization of surrounding objects. However, real-world deployment of automotive radar faces significant challenges, including mutual interference among radar units and dense clutter due to multiple dynamic targets, which demand advanced signal processing solutions beyond conventional methodologies. This paper presents a comprehensive review of traditional signal processing techniques and recent advancements specifically designed to address contemporary operational challenges in automotive radar. Emphasis is placed on direction-of-arrival (DoA) estimation algorithms such as Bartlett beamforming, Minimum Variance Distortionless Response (MVDR), Multiple Signal Classification (MUSIC), and Estimation of Signal Parameters via Rotational Invariance Techniques (ESPRIT). Among these, ESPRIT offers superior resolution for multi-target scenarios with reduced computational complexity compared to MUSIC, making it particularly advantageous for real-time applications. Furthermore, the study evaluates state-of-the-art tracking algorithms, including the Kalman Filter (KF), Extended KF (EKF), Unscented KF, and Bayesian filter. EKF is especially suitable for radar systems due to its capability to linearize nonlinear measurement models. The integration of machine learning approaches for target detection and classification is also discussed, highlighting the trade-off between the simplicity of implementation in K-Nearest Neighbors (KNN) and the enhanced accuracy provided by Support Vector Machines (SVM). A brief overview of benchmark radar datasets, performance metrics, and relevant standards is included to support future research. The paper concludes by outlining ongoing challenges and identifying promising research directions in automotive radar signal processing, particularly in the context of increasingly complex traffic scenarios and autonomous navigation systems.

KEYWORDS: Automotive radar; radar waveforms; target direction; tracking; classification

1 Introduction

Next-generation vehicles are equipped with Advanced Driver Assistance Systems (ADAS) designed to enhance driving safety while ensuring a safe and stress-free journey [1]. According to the report provided by the World Health Organization (WHO), road traffic accidents resulted in approximately 1.19 million fatalities in 2023 [2]. The high rate of casualties, significant financial losses, and the growing demand for intelligent safety systems have driven manufacturers to advance autonomous driving technologies [3].

In fully automated vehicles, human drivers are replaced by intelligent systems responsible for both sensing and decision-making. The ADAS framework integrates multiple sensors, including radar, LiDAR, and cameras, to ensure reliable vehicle performance and improve driver assistance. Among these, radar is particularly effective for detecting the range and velocity of objects, processing data efficiently, and operating under challenging weather conditions. LiDAR offers high-range accuracy and superior angular resolution but is susceptible to adverse weather conditions and interference [4]. Cameras provide color distinction, high angular resolution, and accurate target classification but cannot measure velocity and range, and their performance is compromised in low-light and adverse weather conditions [5]. Given these limitations, automotive radar is the primary sensing modality for automated vehicles [6].

Radars were developed as military tools during and after World War II [7]. Over time, the applications expanded to include air traffic control, weather Radars, ground-penetrating radars, guided missile target locating systems, and more. Automotive Radar applications were first developed in the early 1970s as part of a German research program (NTO 49) aimed at reducing road accidents [8]. In recent times, the Euro New Car Assessment Program (NCAP) for European road safety requires Adaptive Cruise Control (ACC), Automotive Emergency Braking (AEB), Lane Change Assist (LCA), etc. In [9], a semi-physical Radar modeling technique has been adopted to observe the accuracy of the probability density function of Radar data and the Radar Cross Section (RCS) values obtained are similar to the values for global vehicle target validation of NCAP.

Automotive Radars are mostly used in the 24 and 77 GHz ranges of the frequency spectrum. A 4 GHz bandwidth, improved range resolution, proper Doppler sensitivity that leads to velocity resolution, and a reduced antenna aperture, which is useful for fitting on vehicles, are the important advantages of using the 77–81 GHz frequency band. Automotive Radars operating in the 24 GHz frequency band are used for ultra-wideband applications. An arrangement of planar grid antenna array for this Radar improves the antenna gain and impedance bandwidth [10]. Performance criteria of automotive Radar include target resolution, range resolution, dynamic range in terms of velocity, and direction of arrival of the received signal. Fig. 1 represents a 360 degree surround sensing by Radar scenario of an autonomous car [11]. A Long Range Radar (LRR) having a range of 10–250 m is mounted in front of a vehicle and is suitable for ACC [12]. Medium Range Radars (MRR) with a range of 1–100 m are fitted on the front and rear sides and are applicable for Lane Change Assistance and warning of rear collisions. Short-range radars (SRRs) with a range of 0.15–30 m are fitted at the four corners of a car and are applicable for parking assist, obstacle detection, etc. [13]. The various radars, along with their respective functions, are depicted in Fig. 1.

Automotive radar systems are generally composed of three main components: the transmitter, the receiver, and the signal processing subsystem. On the transmitter side, the antenna operates using a frequency-modulated continuous wave (FMCW) chirp waveform [14]. Signal processing at this stage involves generating a series of up-and-down chirps using a frequency-generating circuit, which are then transmitted via the antenna. The antenna radiates power that is regulated by design constraints, thereby influencing the transmitter architecture. Notably, the maximum detectable range is proportional to the square root of the transmitted power. The transmitter typically consists of a waveform generator, an upconverter, and a power amplifier. The waveform generator produces a predefined signal, either continuous

or pulsed, at an intermediate frequency (IF). This signal is then converted to a higher radio frequency (RF) via the up-converter and subsequently amplified using a power amplifier with adjustable gain. The transmitted signal reflects off-targets and returns to the radar system, where it is received and mixed with a copy of the transmitted signal, resulting in a beat frequency. The receiver must maximize the signal-to-noise ratio (SNR) to suppress or eliminate unwanted signals and clutter. To achieve this, the receiver includes a low-noise amplifier (LNA) and a down-converter, which utilizes a local oscillator to convert the RF signal back to IF.

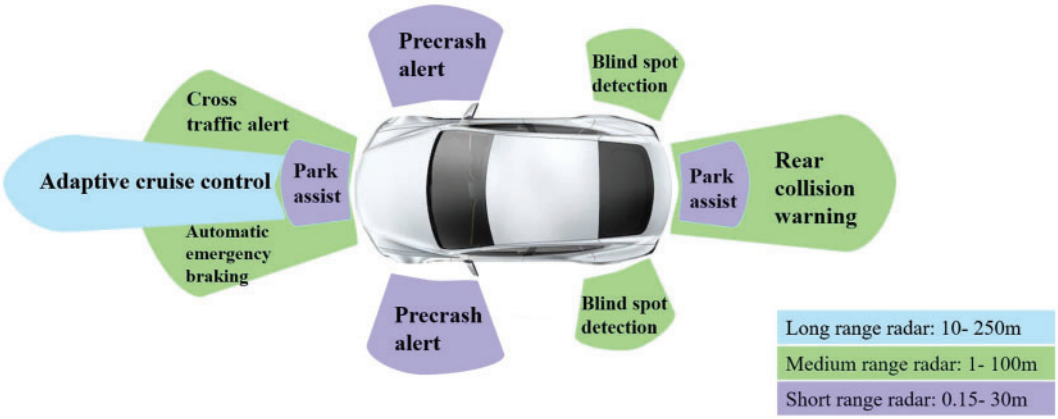

Figure 1: Vehicle in 360° Automotive radar coverage for collision avoidance

The signal processing subsystem plays a crucial role in extracting range and velocity information. It involves applying a Fourier Transform to the beat frequencies to perform range estimation and analyzing the Doppler-induced phase shifts across multiple chirps to measure target velocity. This is typically accomplished through a two-stage Fast Fourier Transform (FFT): a fast-time FFT for range estimation and a slow-time FFT for Doppler estimation, followed by beamforming techniques [15,16]. Direction of arrival (DOA) estimation is performed using array processing techniques, such as digital beamforming. Based on the extracted information, a target list is generated, enabling detection and analysis of target parameters. This is followed by stationary and dynamic target processing, wherein stationary targets undergo classification while moving targets are subject to tracking and classification. A high-level block diagram of the automotive radar signal processing chain is presented in Fig. 2.

Automotive Radar operational hurdles [17]:

1. In urban environments, automotive radar systems are significantly affected by multipath propagation, which arises from reflections of various surrounding objects such as pedestrians, vehicles, road infrastructure, and animals. These objects exhibit varying Radar Cross Section (RCS), velocities, and movement patterns, necessitating high precision in target detection, localization, tracking, and classification. Multipath interference can introduce false target detections, which can adversely impact overall radar performance. Mitigating these effects requires applying advanced signal processing techniques, which, in turn, increases the computational complexity of the system.
2. In automotive radar systems, any object above the road surface that interferes with signal reception is classified as clutter. Clutter originating from nearby obstacles significantly influences the required suppression levels of antenna sidelobes, particularly in the elevation plane. Echoes received through sidelobes can, in some cases, exhibit greater power than returns from weaker targets captured by the main lobe, potentially causing signal interference. Consequently, the design of radar detectors capable

of accurately identifying weak targets in the presence of strong clutter is essential to ensure robust and reliable system performance.

3. Automotive radar systems also encounter significant challenges due to interference, which can be broadly classified into three categories: *self-interference*, *intra-vehicle cross-interference*, and *inter-vehicle cross-interference*. Self-interference arises from reflections of the radar signal off the vehicle's structure, such as the frame or radome, which can hinder the operation of SRR systems. Intra-vehicle cross-interference occurs when multiple radar units installed on the same vehicle have overlapping fields of view, leading to mutual signal disruption. Inter-vehicle cross-interference is induced by radar systems mounted on other vehicles in close proximity, with the severity of interference determined by the relative distance between vehicles and the characteristics of their transmitted waveforms. Addressing these interference sources is critical for maintaining the integrity and reliability of radar-based perception systems in automotive environments.

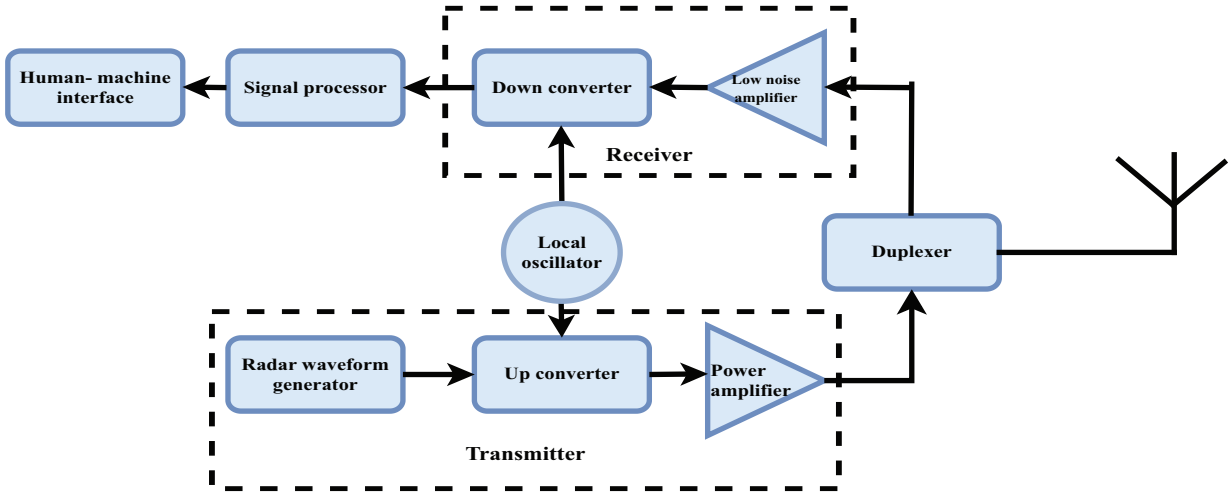

Figure 2: Automotive radar processing system

As stated before, the application areas of automotive radars include ACC, AEB, etc., which further help in the process of vehicle automation. With this ADAS system, the Society of Automotive Engineers (S.A.E.) and the National Highway Traffic Safety Administration have thus standardized six levels of autonomous driving [18]:

1. Level 0: The driver undertakes driving tasks without any automation
2. Level 1: Automation system takes over either steering or acceleration, but the driver monitors, like the Cross Traffic Assist function
3. Level 2: The system takes over functions like adaptive cruise control and brake assist, but the driver still monitors.
4. Level 3: Most tasks are automated, and the system informs the driver when necessary.
5. Level 4: The whole driving task is to be automated and the human driver is to be notified only in undefined cases.
6. Level 5: Fully automated with no driver intervention.

Fig. 3 presents the evolution of automotive Radar for ADAS applications and economic development [19].

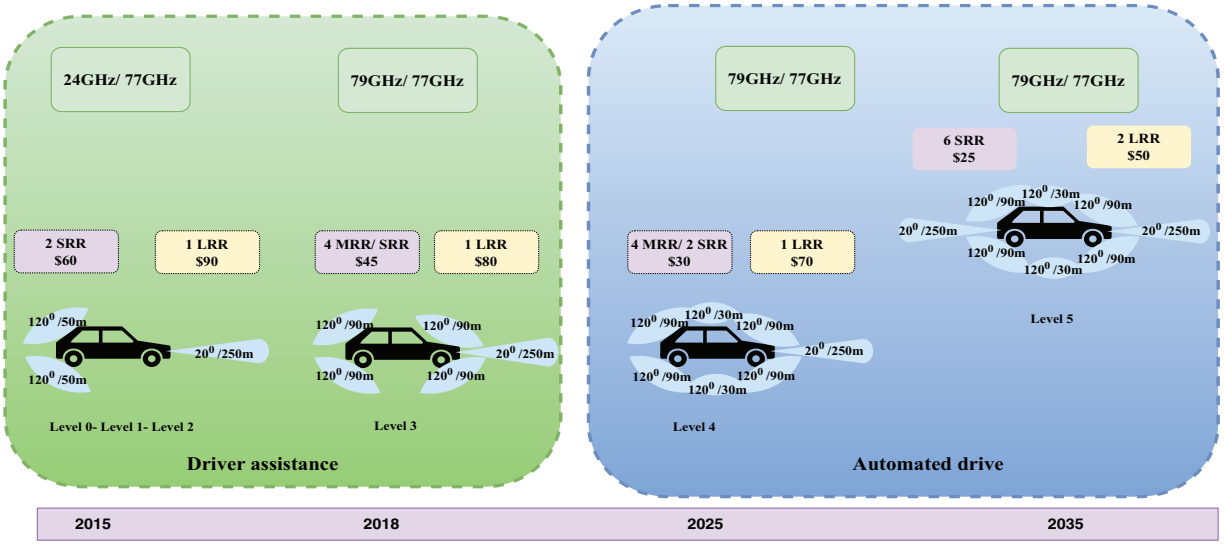

Figure 3: Evolution of automotive radar for ADAS [19]

The contributions of this paper include:

1. A comprehensive overview of automotive radar signal processing techniques, including range and velocity estimation, has been presented. Additionally, a comparative analysis of various waveform types has been conducted, highlighting their respective advantages and limitations in the context of automotive applications. The study also examines different forms of interference encountered in radar systems. Furthermore, a comparative summary of existing review articles on automotive radar offers insight into the current state of research and emerging trends in the field.
2. A detailed analysis of target detection methods and various DOA estimation algorithms has been presented. Comparative evaluations of these algorithms are provided in tabular form, highlighting their respective advantages and limitations. This analysis facilitates a clearer understanding of the trade-offs involved in selecting appropriate DOA estimation techniques for automotive radar applications.
3. Various target tracking algorithms, as proposed in key contributions from existing literature, have been discussed. A comparative table is also included to illustrate the respective advantages and disadvantages of each algorithm, providing insight into their applicability and performance in automotive radar systems.
4. Target recognition and classification using Machine Learning (ML) algorithms has emerged as a significant area of research in automotive radar systems. Various algorithms currently under investigation have been discussed in detail, along with an analysis of their respective strengths and limitations.
5. Key research challenges in the field of automotive radar have also been outlined to support future efforts aimed at addressing these issues and advancing the state of the art.
6. To obtain the training data for the ML algorithms, a large Radar dataset is used that contains a detailed description of the surrounding environment. In this work, the publicly available important datasets are described concisely. Additionally, automotive Radar evaluation metrics and global standards are also provided.

Table 1 presents a comparison between earlier review works on signal processing techniques for automotive radars and this work.

Table 1: An analysis of review works conducted for automotive Radar

Ref.	Year	Paper type	Comparative analysis of waveform	Range and velocity estimation	DOA estimation	Target tracking	Target classification	Algorithm analysis	Radar Dataset analysis
[20]	2023	Review	–	✓	–	✓	–	–	✓
[21]	2019	Magazine	✓	✓	–	–	–	–	–
[22]	2022	Survey	–	✓	✓	✓	✓	–	–
[8]	2021	Review	–	✓	✓	–	–	–	–
[15]	2021	Survey	–	✓	✓	✓	✓	–	–
[17]	2019	Magazine	–	✓	✓	✓	–	–	–
[14]	2018	Survey	–	✓	✓	–	–	–	–
[11]	2017	Magazine	✓	✓	✓	✓	–	–	–
This paper	2025	Survey	✓	✓	✓	✓	✓	✓	✓

The remainder of this paper is organized as follows: Section 2 provides an overview of automotive radar systems, including fundamental mathematical formulations and commonly used radar waveforms. Section 3 presents a detailed analysis of existing research on target detection and Direction-of-Arrival (DOA) estimation techniques. Section 4 discusses various target-tracking methods explored in the literature. Section 5 reviews recent advances in target recognition and classification approaches. Section 6 outlines the key research challenges and potential future directions in the field of automotive radar. Section 7 presents an overview of the various automotive Radar databases available publicly for further research in this field, as well as the standards and parameter evaluation metrics for automotive Radar. Finally, the paper concludes with a summary of key findings.

2 Overview of Automotive Radar

Modern automotive Radar generally applies a frequency-modulated continuous chirp waveform (FMCW), working in frequency ranges of 24 and 76–81 GHz. To detect targets, a series of signals with up chirp and down chirp is generated by a frequency-generating circuit like a phase locked loop (PLL) and transmitted using a transmit antenna [20]. This chirp waveform in the time-frequency domain is presented in Fig. 4, where the transmitted wave, received wave, and beat frequency are identified.

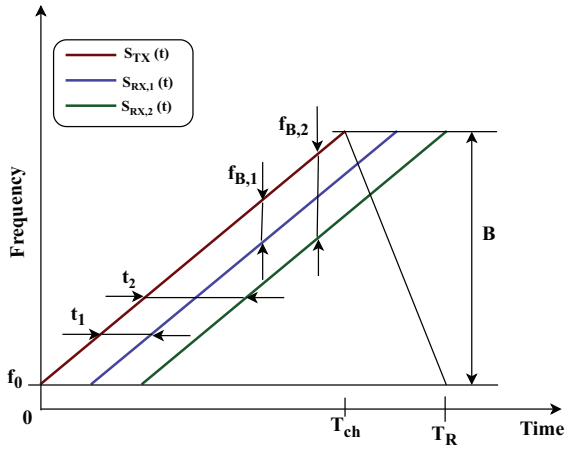

Figure 4: Time vs. frequency domain representation of FMCW radar

The transmitted signal T_x can be expressed as [21],

$$S_{Tx} = A_{Tx}.\cos\left(2\pi f_0 t + \pi k t^2\right) \tag{1}$$

for, $t \in [0 T_{ch}]$, in which T_{ch} is the length of time of one chirp, A_{Tx} is the amplitude of transmitter signal and f_0 is the initial frequency of transmitter signal, $k = B/T_{ch}$ is the chirp's frequency slope with chirp bandwidth presented as B.

A corresponding echo is reflected from the surroundings for each chirp incident on the targets. For simplicity, a target can be considered as a point target. The received signal is a time-delayed and attenuated form of the transmitted signal. The received signal is presented as,

$$S_{R_x} = \sum_{i=1}^{N} A_{T_x}.\alpha_i.\cos\left(2\pi f_0 (t-\tau_i) + \pi k (t-\tau_i)^2\right) \tag{2}$$

where α_i is taken as a damping factor present due to path loss and losses due to reflection corresponding to the received signal from the ith target, and τ_i is the time delay for a round-trip.

2.1 Range Measurement

At the receiving end, the received signal is multiplied by the transmitted signal and then filtered using a low-pass filter to get a signal having IF. The basic mathematical model to estimate the velocity and range of a desired mobile target can be derived from processing this IF frequency signal, which is shown as follows:

$$S_{IF}(t) = [S_{Tx}(t).S_{Rx}(t)] * h_L(t) = \sum_{i=1}^{N} A_{IF,i}.\cos(2\pi f_{B,i} t + \theta_i) \tag{3}$$

in which, $h_L(t)$ is considered as the impulse response of filter and * is a convolution function, $A_{IF,i} = \left(\left(A_{Tx}^2\right) \times \alpha_i\right)/2$ is the received signal's amplitude from ith target, $\theta_i = 2\pi f_0 \tau_i - \pi k \phi_i^2$ is the constant phase of the echo signal reflected from ith target, and $f_{B,i}$ is considered as the beat frequency, that is the dissimilarity of frequency in-between the oscillator and received signal of each point target. This $f_{B,i}$ is directly proportionate to the distance d_i in-between the i-th target and the Radar.

$$f_{B,i} = k\tau_i = \frac{B}{T_{ch}}.\frac{2d_i}{c} \tag{4}$$

Using this $f_{B,i}$ range is measured by the application of the FFT. Thus, Range,

$$R = \frac{c\tau_i}{2} \tag{5}$$

Whether the received signal is coming from a recent chirp or a previous one leads to ambiguity. The maximal unambiguous range can be shown as,

$$R_{max} = \frac{c\ T_{ch}}{2} \tag{6}$$

where T_{ch} is chirp duration. Range resolution is defined as the capability of Radar to differentiate between two targets placed very near to each other. It is expressed as [22],

$$R_{reso} = \frac{c}{2B} \tag{7}$$

This proves that range resolution improves when bandwidth is increased.

2.2 Velocity Measurement

Velocity measurement of a particular target using Radar depends on the Doppler effect. Here, two targets at equal distances but in motion in reverse directions with corresponding velocities v_1 and v_2 are considered. These targets are assumed to be in the same range domain to differentiate based on velocity only. The time-varying delay corresponding to the i^{th} target can be expressed as,

$$\tau_i(t) = \tau_{0,i} + \frac{2v_i}{c}t \tag{8}$$

where $\tau_{0,i}$ is the initial time delay of the round trip of the ith target. Using this delay time, the IF signal might be rewritten as,

$$S_{IF}(t) = \sum_{i=1}^{N} A_{IF,i}.\cos\left(2\pi\left(f_{B,i} + f_{D,i}\right)t + \theta_i\right) \tag{9}$$

where $f_{D,i} = f_0\left(2v_i/c\right)$ is the Doppler frequency. A Range-Doppler map is created for the estimation of velocity in the FMCW Radar model. This Range-Doppler map is calculated by assembling the complex-valued IF signal spectra into matrix form and applying an FFT over the slow-time axis. The velocity can be presented as,

$$v = \frac{\lambda\Delta\theta}{4\pi T_{ch}} \tag{10}$$

For the two targets considered above, the velocities are given as,

$$v_1 = \frac{\lambda\phi_1}{4\pi T_{ch}} \quad and \quad v_2 = \frac{\lambda\phi_2}{4\pi T_{ch}} \tag{11}$$

where ϕ_1 and ϕ_2 are respective phase differences between chirps and λ is the wavelength. Velocity resolution is the capability of Radar to distinguish between two targets' velocities. It is expressed as

$$v_{reso} = \frac{\lambda}{2T_f} \tag{12}$$

where T_f is the duration of the chirp frame.

2.3 Angle Measurement

The position of a particular target is shown in a spherical coordinate system presented as (R,θ,φ) with R as Range, θ as azimuth, and φ as elevation angles. To determine the angle of targets, algorithms such as Multiple Signal Classification (MUSIC) and Estimation of Signal Parameters via Rotational Invariance Technique (ESPRIT) are applied. The Radar usually collects received signal data across multiple discrete dimensions. These dimensions can be modeled using combinations of time, frequency, and space. Since mm-wave bands have smaller wavelengths, this requires smaller aperture sizes, allowing several antenna units to be tightly packed into an antenna array. This results in an active radiation beam that is sharper and stronger, and helps to increase the resolution of angular measurements.

2.4 Waveforms

Automotive radar performance is evaluated based on several metrics, including velocity resolution, range resolution, angular resolution, and target detection probability. The choice of waveform has a

significant impact on these performance parameters. Radar waveforms are generally categorized into continuous wave (CW), pulsed, and modulated types. Modulated waveforms comprise FMCW, Orthogonal Frequency Division Multiplexing (OFDM), and Phase Modulated Continuous Wave (PMCW) [11]. A detailed discussion of these waveform types is provided in the following.

2.4.1 Continuous Wave

In a CW waveform, the transmitted and received signals are processed using a conjugate product, generating a signal corresponding to the specific target's Doppler frequency. However, due to the continuous behavior of this waveform, measuring the delay due to the round-trip is challenging, making range resolution difficult to achieve. Typically, CW radar systems require separate antennas for transmission and reception.

2.4.2 Pulsed Continuous Wave

The duration of a pulse and pulse repetition frequency (PRF) are used for designing this waveform with the required range and velocity estimation. For a pulsed waveform, one antenna system can be used for both transmission and reception processes. Fig. 5 presents a comparative representation of a continuous wave and a pulsed continuous wave.

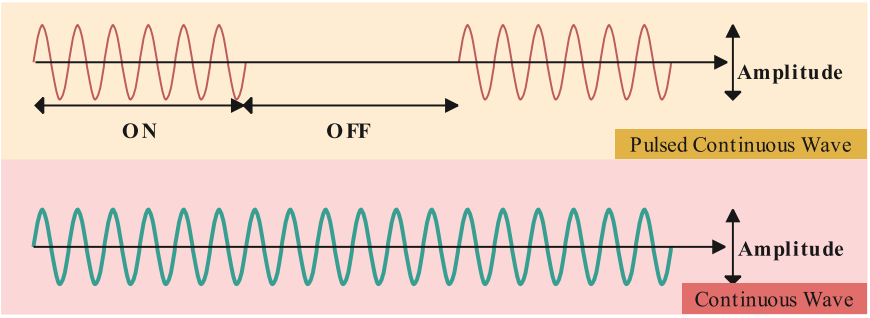

Figure 5: Representation of continuous wave and pulsed continuous wave

2.4.3 Frequency Modulated Continuous Wave

For the FMCW [23] automotive Radar, the carrier signal is modulated by the transmitter by a linear increase of the frequency over time for a predefined interval called a chirp. The main characteristic of FMCW is that the velocity and range of the target can be simultaneously estimated using the 2-dimensional (2D) FFT process. A wide sweep bandwidth improves range resolution as these factors are inversely proportional. The Doppler resolution is determined by the pulse width and the total number of pulses required for this measurement. In the Linear FMCW waveform, the beat frequency for a single mobile target can be derived after the received echo signal is combined with the signal transmitted. Thus, it is composed of a Doppler frequency shift f_d and a frequency component due to range f_b.

$$f_d = \frac{2}{\lambda} v_r \tag{13}$$

$$f_b = 2\frac{R}{c}\frac{B_{sweep}}{T_s} \tag{14}$$

Here, λ is the wavelength of the carrier, v_r is the radial velocity of the target, B_{sweep} is sweep bandwidth, T_s is "sweep time", R is target's range, and velocity of light is taken as c. Fig. 6 presents a linear FMCW waveform for the estimation of the velocity and range of a target.

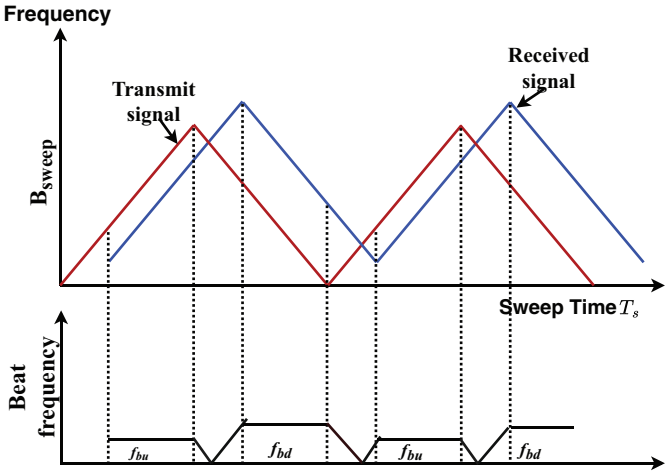

Figure 6: Beat frequency generation using chirp signal to estimate range and velocity

Two beat frequencies, one each for the upward slope f_{bu} and the downward slope f_{bd} of a chirp signal, can be obtained.

$$f_{bu} = f_b - f_d = 2\frac{R}{c}\frac{B_{sweep}}{T_s} - \frac{2}{\lambda}v_r \tag{15}$$

$$f_{bd} = f_b + f_d = 2\frac{R}{c}\frac{B_{sweep}}{T_s} + \frac{2}{\lambda}v_r \tag{16}$$

By applying the FFT on each reflected chirp, the target's range is measured as:

$$R = \frac{cT_s}{4B_{sweep}}\left(f_{bd} + f_{bu}\right) \tag{17}$$

After Range-FFT, another "Fourier transform", "Doppler-FFT" is applied to obtain the velocities of multiple targets

$$v_r = \frac{\lambda}{4}\left(f_{bd} - f_{bu}\right) \tag{18}$$

Stepped FMCW—For this waveform, a sequence of sinusoidal signals is transmitted at distinct frequencies, and the phase shift and steady-state amplitude caused by the Radar channel at each distinct frequency are measured. The inverse discrete Fourier transformation (IDFT) measures the target range. Sparse stepped frequency waveform [24] provides lower levels of range sidelobe for the detection of weak targets. Using a sparse array interpolation method, the sidelobes are reduced, resulting in a mitigation of the likelihood of a "false alarm" during the evaluation of the target angle. *Interrupted FMCW*—In Interrupted FMCW, reception of target echo is allowed only when the timing signal is off. For short-range targets, the total reception time is reduced, making it difficult to detect those targets. But the effect is reversed for long-range targets. So, an arrangement needs to be made between SRR and LRR. An online learning approach based on the

Thompson sampling technique can be applied to identify which FMCW waveform will be beneficial for target classification [25].

2.4.4 Fast Chirp Ramp Sequence Waveform

The advantage of a fast chirp waveform [26] over a usual FMCW waveform is that a 2D-FFT processing enables range and velocity estimation of a target accurately. To collect range information, this 2D-FFT is applied first for each chirp and then across chirps to obtain velocity information. Additionally, the beat frequency signals from targets are greater than the noise corner frequency, providing an improved SNR for detecting weak targets. An example of a fast chirp ramp sequence in the time-frequency domain is indicated in Fig. 7.

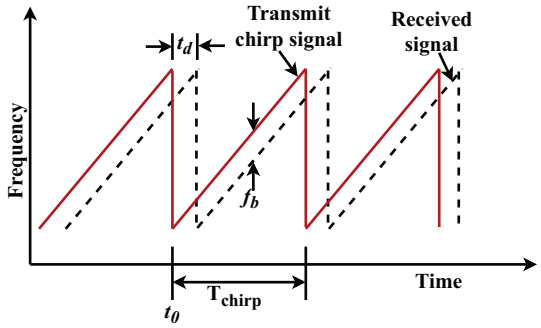

Figure 7: Fast chirp ramp sequence

2.4.5 OFDM Waveform

OFDM [27] is a digitally modulated waveform comprising a set of orthogonal complex subcarriers. In vehicular radar applications, modulation symbols are mapped onto the complex amplitudes of these subcarriers. The orthogonality among subcarriers is ensured by designing each subcarrier to complete an integer number of cycles within the duration of an OFDM symbol, also referred to as the evaluation interval. To mitigate inter-carrier interference (ICI), the subcarrier spacing must exceed the maximum expected Doppler shift.

At the receiver, the radar modulation symbols can be efficiently demodulated using the FFT, making OFDM a suitable choice for digital vehicular radar systems. The range profile is extracted through frequency-domain channel estimation. Range and velocity estimations are performed along two distinct dimensions. Specifically, target velocity estimation can be viewed as a decomposition of the conventional two-dimensional matched filtering process into two one-dimensional matched filters, each is applied independently in its respective measurement domain.

2.4.6 Phase Modulated Continuous Wave

The PMCW waveform [28] consists of a sequence of periodically transmitted symbols that phase modulate a carrier frequency. The estimation of the target range is performed through the correlation between the received and transmitted signals. PMCW radar systems require sampling across the full bandwidth of the transmitted signal, necessitating high-speed sampling and high-resolution analog-to-digital converters (ADCs). Binary PMCW waveforms are commonly employed for automotive applications due to their simplicity and robustness. Binary PMCW is usually used for automotive applications. A PMCW

waveform consists of a few symbols of binary nature I_r (0,1) containing 0-π degree mapping of a carrier frequency. The signal transmitted with R quantity of chirps and a time extent of chirp of T_{ch} is represented as,

$$S_{Tx} = \sum_{r=0}^{R-1} g\left(t - RT_{ch}\right) . \cos\left(2\pi f_0 t + I_r \pi\right) \tag{19}$$

where f_0 is the carrier frequency, and $g(t)$ is a gate function in the time interval of (0, T_{ch}), having unit amplitude. The signal that is received can be represented as,

$$S_{Rx} = A_{Tx} S_T\left(t - \tau_d\right) . \exp\left(j2\pi f_d t\right) \tag{20}$$

where τ_d is the propagation delay. The correlation between the signal received and the signal that is transmitted provides the range information. An FFT is conducted on every range bin in the different sequences to extract Doppler information, which is then used for target velocity measurement. For a stepped-frequency PMCW, the bandwidth of each pulse is reduced when the range resolution is more than assumed limit for that bandwidth [29].

2.4.7 Combined Frequency Shift Keying (FSK) Modulated Waveform and FMCW Waveform

This waveform helps to remove ghost targets and accurately detect multiple targets with high-range resolution for short ranges. Here two-stepped Linear Frequency Modulated Continuous Waveforms (LFMCW), (designated as X and Y) are used, having the same sweep bandwidth and center frequencies, but split by a specific frequency, f_{shift}. Total sweep time is $2NT$ where N is the number of steps and the frequency of each waveform increases by a factor f_{step} after every step. The unambiguous range is dependent on this f_{step} as per the relation, $R = (c/f_{step})$. Multiple targets with varying ranges or velocities are detected based on the N-FFT of both the waveforms and the phase difference between them. In an automotive radar, cost, size, weight, and power (CSWAP) reduction is required, and for this purpose, multiple-input and multiple-output (MIMO) radars are beneficial. MIMO Radar can create virtual arrays of antennas with a bigger aperture by using a smaller number of transmit antennas and receive antennas [30]. For the MIMO, the transmitted signals must be differentiated orthogonally to create the virtual array. This can be attained by Time Division Multiplexing (TDM), Frequency Division Multiplexing (FDM) or Doppler Division Multiplexing (DDM) [31].

Orthogonal waveform using TDM: In TDM MIMO automotive Radar, one transmitting antenna transmits a signal at each time slot. A specific antenna transmits N chirps at each time slot with a switching delay of $\delta t = T_{PRI}$ between antennas (PRI is pulse repetition interval). At every receiver antenna, FFTs with length N_r are applied on every chirp. Doppler FFT of length $2N_d$ chirps are arranged in double matrices as per even and odd chirp series. These subarrays integrate to form a bigger virtual array. In the case of a mobile target, switching delays of the transmit antennas cause a phase shift of the target in a virtual array, which must be corrected before angle estimation. This phase shift is calculated after every target velocity is obtained, depending on the 2D FFT of one receiver antenna or the 2D FFT integration of the respective subarray.

Orthogonal waveform using FDM: In this method, different carrier frequencies modulate the transmitter signals, and then these are separated from each other in a way that the nth FMCW chirp is shifted by frequency $f_{off,n}$. To make the transmitted signals separable at the receiver, differences between every $f_{off,n}$ must be higher than twice the cutoff frequency of the bandpass filter, f_b^{max}. At each receiver, the reflected signal is first joined with the carrier frequency. The transmit signal is separated by frequency shifting, followed by low-pass filtering with cutoff frequency f_b^{max}. This frequency shift and filtering is done M_t times, M_t being the number of transmit antennas, resulting in high-range resolution.

Orthogonal waveform using DDM: In this technique, a total N chirps are transmitted in a sequence with T_{PRI}. All antennas transmit simultaneously, but each transmitted waveform is multiplied by a phase code specific for every antenna and modified within pulses. At the receiver, range FFT is first applied, and then Doppler demodulation in slow time is done on all range bins of the exact chirp to separate the transmit signals. One method for this is to use phase codes where the interference Doppler FFT is transferred to a higher frequency than the highest detectable Doppler frequency f_d^{max}. Interference can hence be removed by low-pass filtering. Another method is to use phase codes, so that the interference Doppler FFT is distributed as pseudo-random noise over the Doppler spectrum. Finally, Doppler FFT can be applied to the demodulated outputs. Another type of waveform, the Random Sparse Step-Frequency Waveform (RSSFW), is presented in [24], where orthogonality is achieved through DDM and provides low-range sidelobe levels for the detection of weaker targets. A joint sparse spectrum and 2D sparse array model helps to obtain higher resolution in Doppler, range, elevation, and azimuth measurements. A comparative analysis [11,32] is presented in Table 2 for understanding vehicular radar waveforms and their features.

Table 2: Comparison of different vehicular radar waveforms

Feature	CW	FMCW	Chirp	OFDM	PMCW
Principle	Measures Doppler shift	Frequency modulation for range and velocity	Uses chirp signals for range and velocity	Uses orthogonal frequency subcarriers	Uses phase modulation for interference resistance
Range measurement	Difficult to determine	Achievable via frequency shift	Achievable via chirp signals	Good due to multi-tone processing	Achievable via phase modulation
Velocity measurement	Direct from Doppler shift	Estimated from beat frequency	Extracted from chirp rate and Doppler shift	High accuracy	Achievable using phase shifts
Interference resistance	Low	Moderate	Moderate	High (due to orthogonality)	High (due to phase coding)
Computational complexity	Low	Moderate	Moderate	High	High
Antenna requirement	Separate Tx/Rx antennas	Single antenna with TDM	Single antenna	Multiple antennas required	Multiple antennas required
Applications	Speed measurement	ADAS, collision avoidance	Automotive and aerospace	High-resolution automotive radar	Short-range automotive radar

Table 3 presents an analysis of the different types of waveforms, generally used for automotive Radar, based on range and Doppler resolution values.

Table 3: A comparative analysis of the resolution corresponds to various waveforms used for automotive Radar

Type of waveforms	Resolution	Properties
Continuous wave	$\Delta f_d = 1/T$	No accurate range resolution
Pulsed CW	$\Delta R = \frac{cT_p}{2}, \quad f_d = 1/T_p$	Range-Doppler measurement trade-off

(Continued)

Table 3 (continued)

Type of waveforms	Resolution	Properties
FMCW	$\Delta R = \frac{c}{2B}, \quad f_d = 1/PT_0$	Range and Doppler information
Fast chirp ramp	$\Delta R = \frac{c}{2B}, \quad v_{reso} = \lambda/2T_f$	2D-FFT provides accurate Range and Doppler measurements
OFDM	$\Delta R = \frac{c}{N\Delta f}, \quad \Delta f_d = 1/PT_N$	Digital Radar, Range and Doppler processing done in two independent dimensions
PMCW	$\Delta R = \frac{c}{2f_{clk}}, \quad \Delta f = F_s/N_{PRBS}$	Digital Coded Radar
Combined FSK and FMCW	$\Delta R = \frac{c}{2B}, \quad \Delta f_d = 1/PT_0$	Maximum range is decided by Δf

B = Radar bandwidth, T = time duration when data is obtained, N = samples used in CW and carriers used in OFDM, T_p = duration of the rectangular pulse, P = number of FMCW or OFDM blocks having duration of t_0 and of T_N, respectively, T_F = duration of the chirp frame, f_{clk} = PMCW binary modulation frequency which is reflected from target while encoded, f_s = sampling rate and N_{PRBS} = length of PRBS in PMCW.

For automotive Radar, conventionally, the FMCW chirp waveform is used due to the advantage of 2D-FFT processing for accurate range and velocity estimation. An RF sweep bandwidth increases the range resolution, and a fast ramp slope helps to achieve maximum unambiguous relative velocity. The fast ramp slope and wide IF bandwidth facilitate the separation of targets in the beat frequency domain, ensuring that the noise from a strong target produces less interference during the detection of a weak target. Recently, however, PMCW Radar has been preferred for automotive applications due to its capability to separate weak RCS targets from those of strong RCS targets. Binary PMCW Radars also provide no range-Doppler coupling and integration of Radar and communication waveforms. Polyphase-coded spread spectrum Radar system can be used for estimation of RCS over ultra-high-frequency radio channels [1,16,33–35].

2.5 Waveform Interference in Automotive Radar Systems

Interference due to Radars occurs when multiple Radars are in proximity, and the interference level depends on the in-between distance and the waveform pattern [36]. A particular vehicle fitted with an interfering Radar present at a distance R, is considered to create interference for a victim Radar. Here, the interfering radar acts as a target for the radar, which is assumed to be a victim. The interference-to-noise ratio (INR) measures the sensitivity of a victim Radar to interference. It depends on the variables of the interfering Radar and the victim Radar, the interfering Radar's signal modulation pattern, and the demodulation process of the victim Radar. The interfering Radar is considered to have a bandwidth B, and at the victim, Radar, the power spectral density (PSD) of the interference is written as [6],

$$PSD_{int} = \left[\frac{P_t G_T \lambda L_{Tx} L_f N_{Tx}}{B\left(4\pi R^2\right)}\right]\left[\frac{G_R \lambda L_{Rx} L_f N_{Rx}}{4\pi}\right]\left(D_f\right)\left(K_{FMCW}\right)$$
$$= \frac{P_t G_T L_{Tx} L_f N_{Tx} \lambda^2 G_R L_{Rx} L_f N_{Rx}}{B\left(4\pi R\right)^2}\left(D_f\right)\left(K_{FMCW}\right) \quad (21)$$

where G_T and G_R = antenna gains for interfering and victim Radars, respectively, λ = Radar signal wavelength, P_T= power transmitted by interfering Radar, N_{Tx} and N_{Rx} = numbers of antennas used for transmission for interfering Radar and receiving antennas of victim Radar, respectively, L_{Tx} and L_{Rx} = transmit loss for interfering Radar and receive loss of victim Radar, respectively, L_f = loss due to fascia of all Radars, D_f = duty factor for the time the interfering Radar works within dwell time and band of victim Radar, varying from 0 to 1, K_{FMCW} = applies to FMCW modulation for interfering and victim Radars and is presented by,

$$K_{FMCW} = \frac{\mathrm{PSD}_I^{Bb}}{\mathrm{PSD}_I^{Rf}} = \frac{\Delta F_I^{Rf}}{\Delta F_I^{Bb}} \quad (22)$$

where PSD_I^{RF} is the PSD of interference in the receiver of victim Radar at RF before down conversion, and PSD_I^{Bb} is the interference PSD at baseband after down conversion in the Radar assumed as a victim, δF_I^{RF} is the sweep bandwidth in RF range of the interfering FMCW Radar, and δF_I^{Bb} is the bandwidth of interference in the receiver of victim FMCW Radar after down conversion to baseband.

2.5.1 FMCW-FMCW Interference

When the victim FMCW signal overlaps with the interfering FMCW signal, this results in a specific type of interference. After down-conversion at the radar receiver, the interference appears as a linear chirp signal that sweeps across the radar's passband, occupying a wide bandwidth. After bandpass filtering, the interference signal becomes an "impulse-like signal" in the time domain. The slope and relative timing of the frequency modulation of both the victim and interfering radars determine the position and width of this interference signal. The difference in frequency modulation (FM) sweep rates between the interfering radar and the victim radar, along with their timing and frequency alignments, determines the bandwidth of the interference observed after down-conversion in the victim radar. Type A: interfering Radar and Radar assumed to be the victim, sweep with similar time duration T_s, start frequency, and start time,

$$K_{FMCW} = \frac{\Delta F_I^{Rf}}{\Delta F_I^{Bb}} = \left|\frac{S_{wI} T_S}{\left(S_{wv} - S_{wI}\right) T_s}\right| = \left|\frac{S_{wI}}{S_{wv} - S_{wI}}\right| \quad (23)$$

Type B: interfering Radar and victim Radar sweeps with similar time duration T_s, start time, and center frequency

$$K_{FMCW} = 2\left|\frac{S_{wI} T_S}{\left(S_{wv} - S_{wI}\right) T_s}\right| = 2\left|\frac{S_{wI}}{S_{wv} - S_{wI}}\right| \quad (24)$$

where Sw_I and Sw_V = FM sweep modulation rates for interfering Radar and victim Radar, respectively. So, the value of K will be 1 if the FM sweep of Radar assumed to be interfering, having a sweep rate S_I, have the same magnitude but is reversed in sign to the sweep rate of the Radar assumed as victim, S_V.

2.5.2 PMCW-PMCW Interference

This kind of interference is noticed when the "interfering PMCW" signal overlaps the victim PMCW signal. A PMCW interference is assumed with arbitrary, noise-type biphase coding with chirp rate $\Delta f_i = \frac{1}{T_c}$ and looks like a spread-spectrum noise-type signal having bandwidth $\Delta f_i = \frac{1}{T_c}$ and carrier frequency f_c. A victim Radar with PMCW is supposed to transmit a noise-type signal that is biphase-coded and has the chirp rate Δf_i and bandwidth $\Delta f_v = \frac{1}{T_c}$ and carrier frequency same as that of interfering PMCW Radar but using a spreading code which is independent, and uncorrelated. The signal received is down-converted at the victim PMCW Radar, with a persistent oscillator frequency (given as $f_i = f_c$), and then demodulated using a delayed version of the PMCW biphase code. The interference is converted into a noise-type signal in the time and frequency domains through downconversion, demodulation. Finally, bandpass filtering in the receiver of the Radar assumed as the victim. The frequency spectrum of this signal is wideband and typically above the level of background noise.

2.5.3 FMCW-PMCW Interference

In both cases of FMCW victim and PMCW interferer or PMCW victim and FMCW interferer, the interference appears like noise in time and frequency domains. The INR is the same.

2.5.4 Interference Mitigation

The techniques for interference mitigation in automotive Radar can be classified into two categories: techniques at the transmitter (such as frequency hopping and timing jitter) and methods at the receiver (such as time domain excision). Transmission techniques are usually designed to ensure that separate Radars transmit in a way where the signals are nearly perpendicular to each other in domains like time, frequency, or polarization. Mostly, interference mitigation is done at the receiver side. For FMCW-FMCW interference, a matched filtering is usually adopted to obtain integration gain for a constant frequency signal considered as a target and the interference spreads as noise [6]. For PMCW on PMCW interference, Code Division Multiple Access (CDMA) ensures that every Radar has a unique spreading code, and the interference becomes a wideband noise signal. An FMCW interference is similar to a jammer in a spread-spectrum system for a PMCW victim Radar, and adaptive filtering can be used for mitigation. A PMCW interference on an FMCW victim can be reduced by separation in the polarization or frequency domain. Additionally, Neural network (NN) methods can be used for mitigating multi-channel interference [37]. The signal separation neural network can separate the interference from the beat signal, making it interference-free, and reconstruct the signal.

3 Target Detection and DOA Estimation

3.1 Signal Processing for Target Detection

A signal processing framework [17] is required for target detection with automotive Radar. An automotive Radar is considered to transmit a series of identical waveforms (like FMCW chirps, PMCW symbols, or OFDM). These transmitted waveforms are reflected from the targets and clutter and received at the receiver end, where they are down-converted as a combination of various Radar signal echoes along with additional noise from the receiver. The work aims to reduce additive noise and detect and then classify echoes obtained from various objects that are separable in the spectral domains of Doppler, range, and Direction of Arrival (DOA). For i = 1, . . . , N targets, the baseband data model present at rth chirp and mth antenna receiver with one transmitter is given by,

$$x_{m,r}(t) = \sum_{i=1}^{N} A_i S(t - \tau_i) \exp(j2\pi f_{di} r T_c) . \exp(j2\pi f_c \Delta\tau_{i,m}) + V_{m,r}(t) \tag{25}$$

where $S(t)$ is the transmitted signal and A_i, i, f_{di} are the amplitude of the ith target, delay in time, and Doppler shift of the ith target, respectively. The difference in time is the time difference between the origin of the array of the antenna and the nth antenna for the ith target, and is denoted as $\Delta\tau_{i,m}$. The additive noise is represented as $V_{m,r}(t)$. Next, the signal received is multiplied by the conjugated transmitted signal. In case of Linear Frequency Modulated (LFM) signal, $S(t) = \exp\left(j\pi B\phi_i^2\right)$.

$$\widetilde{x}_{m,r}(t) = x_{m,r}(t)\, s^*(t) = \sum_{i=1}^{N} \widetilde{A}_i \exp(-j2\pi B\tau_i) . \exp(j2\pi T f_{di} r) . \exp(j2\pi f_c \Delta\tau_{i,m}) + \widetilde{V}_{m,r}(t) \tag{26}$$

where $\widetilde{A}_i = A_m \exp\left(j\pi B\phi_i^2\right)$. For a uniform planar array antenna structure, $\tau_{i,m}$ is linear for horizontal and vertical array elements. So, the above equation contains a product of sinusoids in slow-time l and fast-time t data and a product of sinusoids in antenna array elements. Thus, to obtain Doppler, range, azimuth, and elevation values, the implementation of 4D FFT is required. Before FFT, the signal is sampled with Ts sampling time to get $x[l, r, m] = \widetilde{x}_{m,r}(lT_s)$. Now, the FFT is performed by,

$$\begin{aligned} X[p, q, \theta, \varphi] = & \sum_{m_v=1}^{M} \sum_{m_h=1}^{M} \sum_{r=1}^{R} \sum_{l=1}^{L} x[l, r, m] \exp\left(-j2\pi p \frac{l}{L}\right) \exp\left(-j2\pi q \frac{r}{R}\right) \\ & . \exp\left(j2\pi \frac{d_a}{\lambda} m_h \sin\theta \cos\varphi\right) . \exp\left(j2\pi \frac{d_a}{\lambda} m_v \sin\varphi\right) \end{aligned} \tag{27}$$

where m_h, m_v are the horizontal and vertical antenna indices with d_a as antenna spacing. To detect a target, it needs to be distinguishable in a minimum of one of these parameters. Next, Constant False Alarm Rate (CFAR) detection is used. The CFAR method used in the Doppler range domain, is used where the guard cell is modified and data sorting is eliminated, leading to faster response with improved detection accuracy [38]. The Cell Averaging CFAR (CA-CFAR) is the most common method, where a target is detected for cells that satisfy the following conditions:

$$|X[p, q, \theta, \varphi]|^2 > T_{CFAR} + \sigma_{nv}^2[p, q, \theta, \varphi], \quad \forall\ p, q, \theta, \varphi \tag{28}$$

where T_{CFAR} is the CA-CFAR detection threshold and $\sigma_{nv}^2[p, q, \theta, \varphi]$ is noise variance, estimated around the cell under test. The Cell Averaging CFAR (CA-CFAR) detector determines the power threshold for every bin of the Range angle map, referred to as the Cell Under Test (CUT) [23]. A comparison is made between the CUT and the average of its neighboring cells. The target vehicle is detected when the CUT output power exceeds the average power threshold. The cells immediately adjacent to the CUT, called guard cells, are ignored to avoid corrupting the average power with power from the CUT itself. The process begins with a single cell and is repeated for all cells. An example of the working principle of the CA-CFAR method is presented in Fig. 8.

In Greatest-of-cell-averaging (GOCA-CFAR), two windows are considered on either side of the CUT, each having the same number of training/neighbouring cells. The mean of these two windows is calculated, and the maximum value of these mean values is taken as the threshold value. On the other hand, in Smallest-of-cell-averaging (SOCA-CFAR), the mean of the two windows is calculated, and the minimum value of these is taken as the threshold. In Order static CFAR (OS-CFAR), the values of the training cells are organised in ascending order, and one value is selected. This OS-CFAR detector is used in [39] for targets in micro-motion, and to cluster these targets, the image dilation algorithm is applied. Inclusion of deep learning

techniques such as Convolutional Neural Network (CNN) [40] provides an increased rate of detection of targets compared to CFAR. A comparative analysis of these CFAR methods is presented in Table 4.

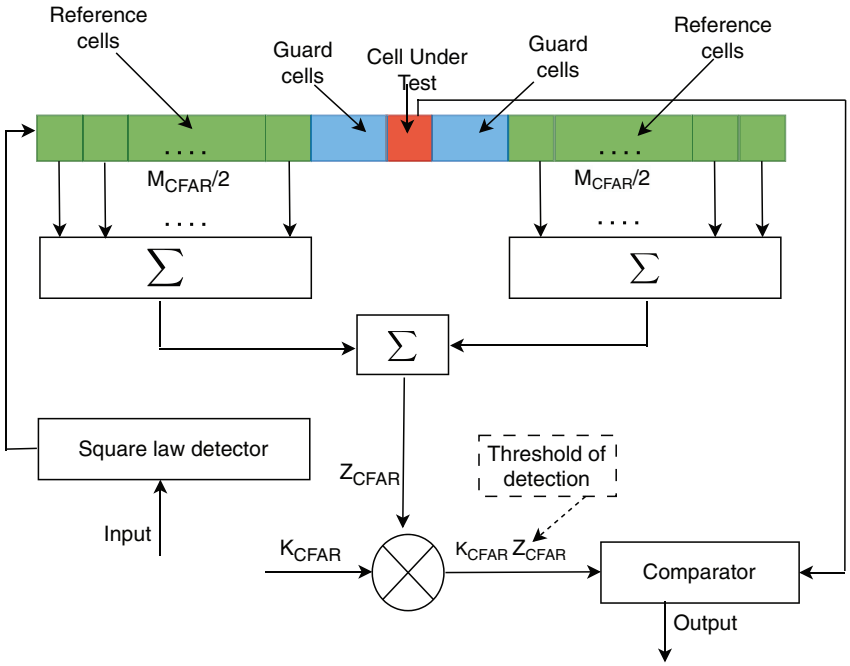

Figure 8: Working principle of the CA-CFAR method

Table 4: A comparative analysis of the CFAR techniques

Type of algorithms	Method of threshold detection	Advantages	Disadvantages
CA-CFAR	Average power of neighboring cells taken as threshold	High SNR in uniform noise	Not beneficial for multiple target detection
GOCA-CFAR	Mean of two windows on either side of CUT calculated and the maximum becomes threshold	Good for false alarm control in clutter	Not beneficial for multiple target detection
SOCA-CFAR	Mean of two windows on either side of CUT calculated and the minimum becomes threshold	Higher false alarm rate	Beneficial for multiple target detection
OS-CFAR	Values of training cells arranged in ascending order and one specific value is taken as threshold	Longer computation duration	Beneficial for multiple target detection

Clustering and tracking methods are adopted for additional detection required for automotive radar. Tracking of the target mainly includes prediction, association, and update procedures, as observed in the case of the Kalman filter. Tracking helps to improve target localization, deduce accurate velocity and trajectory, and create a picture of the target's surroundings. The final task is called classification, where knowledge of

the detected and then tracked target is obtained from echoes received from the target. This is achieved using selected micro-Doppler features, spatial spread, and other parameters.

3.2 Direction of Arrival (DOA) Estimation

Under real-world road conditions, an unknown number of signal echoes from targets in various directions may arrive at the receiver antenna. These target echoes, combined with noise and interference, pose significant challenges for reliable target detection and tracking. To enable accurate beamforming and to place nulls in the direction of interfering signals, precise estimation of the DOA of the desired target signal is essential. Various DOA estimation techniques for target echoes are illustrated in Fig. 9.

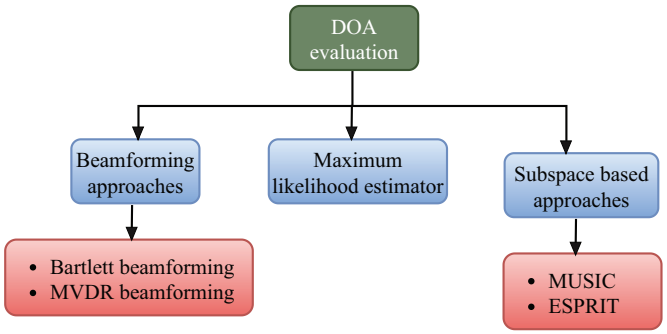

Figure 9: DOA evaluation techniques

A radar signal model is presented in Fig. 10 to estimate the DOA of the received signal.

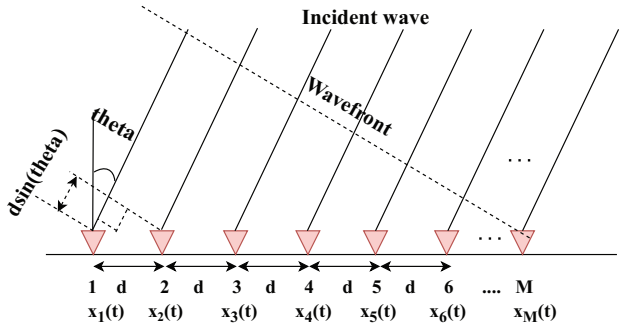

Figure 10: Signal model for DOA estimation

An automotive radar system is considered to contain a series of M antenna elements on which signals from k_t targets are received [23]. The received signal is given as,

$$X(t) = A(\theta) S(t) + N(t) \tag{29}$$

where $X(t) = [x_1(t), ..., x_m(t)]^T$ is the (M × 1) Radar data vector that is received, $A(\theta) = [a(\theta_1), ..., a(\theta_{kt})]$ is the $(M * k_t)$ steering matrix, $S(t) = [s_1(t), ..., s_{kt}(t)]^T$ is the (i × 1) source signal vector and $N(t) = [n_1(t), ..., n_M(t)]^T$ is the (M × 1) sensor noise vector of variance σ^2. The steering matrix is formed of steering vectors, given as,

$$a\left(\theta_i\right) = \left[1, \exp\frac{-j2\pi d\sin\left(\theta_i\right)}{\lambda}, \ldots, \exp\frac{-j2\pi d\left(N-1\right)\sin\left(\theta_i\right)}{\lambda}\right]^T \tag{30}$$

where d is the spacing of elements for a Uniform Linear Array (ULA) antenna, θ_i is the angle of arrival of the signal from the ith source, and T means transpose. For digital beamforming and Minimum Variance Distortionless Response (MVDR), optimization of weights is needed. The weighted combination of the linear nature of sensor outputs is given as,

$$Y\left(t\right) = w^H X \tag{31}$$

With H denoting the Hermitian response. Then the power at the output of the array of sensors is given as,

$$P\left(w\right) = E\left[\left|y\left(t\right)\right|^2\right] = w^H E\left[XX^H\right]w = w^H R_{cm} w \tag{32}$$

where $E[.]$ is the expectation operation and R_{cm} is the input signal covariance matrix. The various DOA estimation methods are described below [41].

3.2.1 Bartlett Beamforming

Beamforming is a technique used to create a desired radiation pattern by coherently combining signals from multiple antennas, each weighted according to its appropriate value. This process enhances signals arriving from a specific direction while suppressing interference and noise from undesired directions. The Bartlett algorithm, also known as conventional beamforming, is used to enhance the signal from a specific direction by compensating for the phase shifts of the incoming wavefront. The optimal weight vector in the Bartlett method ca be written as, $w = a(\theta)$ and the power of the signal at angle θ is obtained as:

$$P_{bart} = \frac{a^H\left(\theta\right)R_{cm}a\left(\theta\right)}{a^H\left(\theta\right)a\left(\theta\right)} \tag{33}$$

The limitations of Bartlett beamforming include: i) Applicable only for a single source of signal, ii) In the presence of multiple sources, it provides low resolution, resulting in ambiguity.

3.2.2 Minimum Variance Distortionless Response (MVDR)

In this algorithm, a persistent gain is maintained for the signal from a desired direction, and a lesser weight is added to the direction of the interfering signal and noise. The weight vector is given as

$$min\left(P\left(w\right)\right) subject\ to\ \left(w^H a\left(\theta\right)\right) = 1 \tag{34}$$

The weight vector for beamforming angle θ is given as,

$$w_{MVDR} = \frac{\mathrm{R}_{cm}^{-1}\,a\left(\theta\right)}{a^H\left(\theta\right)\mathrm{R}_{cm}^{-1}\,a\left(\theta\right)} \tag{35}$$

The power spectrum at angle θ is given as:

$$P_{MVDR} = \frac{1}{a^H\left(\theta\right)\mathrm{R}_{cm}^{-1}\,a\left(\theta\right)} \tag{36}$$

This method provides improved resolution than Bartlett, but not as much as subspace methods. To enhance the angular resolution of beamforming algorithms, a method can be employed to determine the transformation vector that represents the relationship between received signals and create extrapolated elements outside the region of the array's actual antenna elements [42]. With both original and extrapolated signals, the direction of the target echo is estimated with higher resolution.

3.2.3 Multiple Signal Classification (MUSIC)

This method is based on the subspace approach, where the covariance matrix is decomposed into a signal subspace and a noise subspace. The steering vectors are observed to be orthogonal to the noise. In the spatial power spectrum, a peak provides the required direction. Considering the equation of the received signal as shown in (29) and (30), the covariance matrix is presented as,

$$R_{cm} = A(\theta) R_s A(\theta)^H + \sigma^2 I \tag{37}$$

where R_s is the covariance matrix of the signal at the source and I is the identity matrix. The R_{cm} matrix is broken into matrices of eigenvalues and eigenvectors. The size of the subspace of the signal is k_t, and $M - k_t$ eigenvalues of R_{cm} are a part of the noise subspace. For the Eigenvalue Decomposition (EVD), the Hermitian covariance matrix $\mathbf{R}_{cm}$ can be decomposed as:

$$\mathbf{R}_{cm} = \mathbf{U}\mathbf{\Lambda}\mathbf{U}^H \tag{38}$$

where the eigenvalues are sorted as,

$$\lambda_1 \geq \lambda_2 \geq \ldots \geq \lambda_{Kt} > \lambda_{Kt+1} = \ldots = \lambda_M = \sigma^2 \tag{39}$$

The parameters can be defined as,

$$\mathbf{U}_s = [\mathbf{u}_1, \ldots, \mathbf{u}_{Kt}] \quad \text{(signal subspace)} \tag{40}$$

$$\mathbf{U}_n = [\mathbf{u}_{K+1}, \ldots, \mathbf{u}_M] \quad \text{(noise subspace)} \tag{41}$$

The basic principle of the MUSIC algorithm is that for a real source direction θ_{kt}, the steering vector $\mathbf{a}(\theta_{kt})$ is orthogonal to the noise subspace:

$$\mathbf{a}^H(\theta_{kt})\mathbf{U}_n = \mathbf{0}^T \tag{42}$$

Therefore,

$$\mathbf{a}^H(\theta)\mathbf{U}_n\mathbf{U}_n^H\mathbf{a}(\theta) \approx 0 \text{ if } \theta = \theta_{kt} \tag{43}$$

The MUSIC algorithm observes the angles θ_{kt}, such that the signal subspace is observed to be perpendicular to the noise subspace. Thus, the MUSIC algorithm's spatial spectrum is given as,

$$P_{MUSIC} = \frac{1}{a^H(\theta) U_n \mathrm{U}_n^H a(\theta)} \tag{44}$$

The main disadvantages of the MUSIC algorithm are that it requires prior knowledge of the signal sources and its complex computation.

The MUSIC algorithm can be summarised as follows:

1. The sample covariance matrix is computed, using the source covariance matrix
2. The Eigenvalue decomposition of $\mathbf{R}_{cm}$ is done.
3. The noise subspace $\mathbf{U}_n$ is then separated.
4. For each angle θ, $P_{MUSIC}(\theta)$ is evaluated.
5. The DoAs are obtained from the peaks of the pseudo-spectrum.

3.2.4 Estimation of Signal Parameters via Rotational Invariance Techniques (ESPRIT)

This method, ESPRIT, is computationally less complicated than MUSIC as it does not consider all direction vectors. The subspace of incident signals is lengthened by two responses displaced by a recognized vector, using which the DOA can be obtained. The equation of the received signal is presented in (29) and (30). The assumptions for the ESPRIT algorithm can be stated as,

- The array needs to have a structure of translational invariance (e.g., two identical subarrays).
- Prior information is present for the number of sources $K_t < M$.
- The source signals are considered uncorrelated.
- Likewise, the noise is uncorrelated with the signals and spatially white.

Now two overlapping subarrays of size $(M-1)$ are assumed and constructed as:

$$\mathbf{x}_{e1}(t) = \mathbf{J}_{e1}\mathbf{x}(t) \tag{45}$$

$$\mathbf{x}_{e2}(t) = \mathbf{J}_{e2}\mathbf{x}(t) \tag{46}$$

where $\mathbf{J}_{e1}$ and $\mathbf{J}_{e2}$ are selection matrices:

$$\mathbf{J}_{e1} = [\mathbf{I}_{M-1} \quad \mathbf{0}], \quad \mathbf{J}_{e2} = [\mathbf{0} \quad \mathbf{I}_{M-1}]$$

Hence, the subarray outputs can be written as:

$$\mathbf{x}_{e1}(t) = \mathbf{A}_1\mathbf{s}(t) + \mathbf{n}_1(t) \tag{47}$$

$$\mathbf{x}_{e2}(t) = \mathbf{A}_2\mathbf{s}(t) + \mathbf{n}_2(t) \tag{48}$$

Here, $\mathbf{A}_2 = \mathbf{A}_1\mathbf{\Phi}$, where $\mathbf{\Phi}$ is a diagonal matrix containing the phase shifts:

$$\mathbf{\Phi} = \text{diag}(e^{j\psi_1}, \ldots, e^{j\psi_K}) \tag{49}$$

For the estimation of Subspace, the equation form the data matrix:

$$\mathbf{X_e} = [\mathbf{x_e}(1), \ldots, \mathbf{x_e}(N_{es})] \in \mathbb{C}^{M\times N_{es}} \tag{50}$$

The sample covariance matrix is computed as follows:

$$\hat{\mathbf{R}}_{cm} = \frac{1}{N_{es}}\mathbf{X_e}\mathbf{X_e}^H \tag{51}$$

The eigen-decomposition of $\hat{\mathbf{R}}_{cm}$ is computed by using the equation:

$$\hat{\mathbf{R}}_{cm} = \mathbf{U}_s\mathbf{\Lambda}_s\mathbf{U}_s^H + \mathbf{U}_n\mathbf{\Lambda}_n\mathbf{U}_n^H \tag{52}$$

The matrix $\mathbf{U}_s \in \mathbb{C}^{M\times K_t}$ is assumed to span the signal subspace.

For the estimation of Rotational Invariance and Eigenvalue, $\mathbf{U}_s$ is split into two parts:

$$\mathbf{U}_1 = \mathbf{J}_{e1}\mathbf{U}_s \in \mathbb{C}^{(M-1)\times K_t} \tag{53}$$

$$\mathbf{U}_2 = \mathbf{J}_{e2}\mathbf{U}_s \in \mathbb{C}^{(M-1)\times K_t} \tag{54}$$

It is assumed that, $\mathbf{A}_2 = \mathbf{A}_1\mathbf{\Phi}$ and the columns of $\mathbf{U}_s$ span the same space as $\mathbf{A}$, and hence it can be written:

$$\mathbf{U}_2 = \mathbf{U}_1\mathbf{\Psi} \tag{55}$$

for an unknown matrix $\mathbf{\Psi}$.

For the estimation of $\mathbf{\Psi}$, the least squares problem is solved:

$$\mathbf{\Psi} = (\mathbf{U}_1^{\dagger})\mathbf{U}_2 \tag{56}$$

Then the he eigenvalues of $\mathbf{\Psi}$ are computed:

$$\mathbf{\Psi}\mathbf{v}_{kt} = \lambda_{kt}\mathbf{v}_{kt}, \quad kt = 1, \ldots, K_t \tag{57}$$

Every eigenvalue needs to satisfy the following condition:

$$\lambda_{kt} = e^{j\psi_{kt}} = e^{j\frac{2\pi d}{\lambda}\sin(\theta_{kt})} \tag{58}$$

Finally, the angle of arrival can be estimated by using:

$$\theta_{kt} = \arcsin\left(\frac{\lambda}{2\pi d}\arg(\lambda_{kt})\right) \tag{59}$$

The ESPRIT algorithm can be summarised as follows:

1. N_{es} snapshots are collected and computation od the data matrix $\mathbf{X}$ is done.
2. The covariance matrix $\hat{\mathbf{R}}_{cm}$ is evaluated.
3. The signal subspace $\mathbf{U}_s$ is computed from eigen-decomposition.
4. $\mathbf{U}_s$ is then partitioned into $\mathbf{U}_1$ and $\mathbf{U}_2$ with the help of selection matrices.
5. Estimation of $\mathbf{\Psi} = \mathbf{U}_1^{\dagger}\mathbf{U}_2$ is conducted.
6. The eigenvalues λ_k of $\mathbf{\Psi}$ are computed.
7. Finally, estimation of the DoAs is done:

$$\theta_{kt} = \arcsin\left(\frac{\lambda}{2\pi d}\arg(\lambda_{kt})\right)$$

Here, the eigenvalues of ψ are similar to the diagonal elements of ϕ, and DOA is measured using that. The primary disadvantage of the ESPRIT algorithm is its high computational cost. In [41], the authors have introduced a new method where the DOA is obtained by comparison of the difference of phase between two sensors by applying the phase angle of the antenna steering vector having θ as a variable along with the phase of the input signal. This method has the smallest average and standard deviations of errors compared to those obtained from the dissimilarity between the real angle and the evaluated angle using conventional Bartlett and MUSIC algorithms. The authors have used Kurtosis to measure the number of observation values at the center. To improve cross-range resolution in FMCW Radar, discrete Fourier transform (DFT) can be applied for high efficiency, and with the MUSIC algorithm, high angular resolution is obtained for Ultra Wide Band

(UWB) MIMO automotive Radar [43]. A method of pseudo peak suppression can also be applied for angular resolution of targets that are placed closely in angular dimension [44].

A MUSIC algorithm with enhanced beamspace can lessen the computational complexity and storage space, which is beneficial for automotive Radar [45]. The parameter space can be reduced by utilizing prior information to improve beamformer design. To mitigate the consequences of a lower SNR value and incorrect sample covariance in a single snapshot, a modified estimator can be employed, which considers the relationship between a signal with an interference model of sample covariance and the subspace model. Furthermore, to enhance direction estimation for two closely spaced targets, the averaging of sub-matrices of sample covariance evaluation and the utilization of the Toeplitz structure are employed. This new algorithm offers a higher resolution probability than conventional MUSIC at the same signal-to-noise ratio (SNR). For the processing of range and angle, a single-snapshot MUSIC is used in [46], which reduces the computational complexity. Another process involves obtaining DOA with single-snapshot MUSIC and evaluation of the performance with analog-to-digital allocations [47]. A new way for better resolution of angles is the application of a two-stage MUSIC algorithm [48]. Here, a crude estimation is initially performed using MUSIC. However, this estimation won't be accurate if the targets are closely placed and have low SNR. Based on these values, each antenna element is directed to specific directions using a calibration technique that focuses on signals coming from particular directions, as presented in the first stage. The Root Mean Squared Error (RMSE) values of this new method with Root-MUSIC are less than those of standard Root-MUSIC in the low SNR region. In [49], a compressive sensing alternating descent conditional gradient (CS-ADCG) algorithm has been used. Using a gridless process and minimization of the atomic norm, the observation scene has been discretized to prepare an atomic set. The signal sources' angles are obtained by measuring the inner product of this atomic set with fragments from every iteration and are used as primary values for searching. Finally, a function for mapping is made of the sources of the signal, and gradient descent is applied for iterative optimization. This step is conducted in a continuous domain to reduce the off-grid effect. To determine DOA in the presence of interference, the variational mode decomposition method is used. Then, with the signal-to-interference ratio obtained from this algorithm, a weighted MUSIC algorithm is applied for obtaining DOA [50].

The time complexity of MUSIC or MVDR is obtained as $O(M^3)$ where the number of elements of the antenna array is M, and the high latency due to this computational load makes these algorithms impractical for use in automotive Radar systems. In [51], the authors have proposed an efficient MUSIC (E-MUSIC) algorithm that achieves target detection with better resolution at the linear complexity $O(z^2M)$, where z is a user-specific parameter that balances between complex modeling and angular accuracy. The authors approximate large $R \in C^{M\times M}$ using three smaller sketches in the form of $R \approx QB^HQ$, where C^{M*M} is a $M \times M$ complex matrix and $Q \in C^{M\times z}$ comprises of the orthonormal basis for the sketch matrix's range profile, $C \in C^{M\times z}$ that is obtained from R by utilizing a arbitrary but uniform sampling method. $B \in C^{z\times z}$ is a weight matrix that reduces the approximation error. This algorithm utilizes a (16 × 8) sketch matrix, compared to the (16 × 16) covariance matrix of MUSIC, and achieves an accuracy nearly identical to that of MUSIC in high SNR regions for FMCW automotive Radar. A relative comparison between Bartlett, MVDR, MUSIC, and ESPRIT is presented in Table 5.

Table 5: Comparison of Bartlett, MVDR, MUSIC, and ESPRIT

Feature	Bartlett beamforming	MVDR	MUSIC	ESPRIT
Concept	Conventional beamforming method. It scans the spatial domain by calculating the spatial power spectrum with the array steering vector at various angles.	Adaptive beamforming that minimizes interference and noise while retaining a distortion-free response to the desired signal direction.	It uses the eigenstructure of the covariance matrix to separate the signal and noise subspaces.	It avoids the computationally expensive spectral search by taking advantage of the rotational invariance of signal subspaces.
Mathematical basis*	The power spectrum, $P_B(\theta) = \mathbf{a}^H(\theta)\mathbf{R}\mathbf{a}(\theta)$ [52]	The power spectrum, $P_{\text{MVDR}}(\theta) = \frac{1}{\mathbf{a}^H(\theta)\mathbf{R}^{-1}\mathbf{a}(\theta)}$ [53]	The power spectrum, $P_{\text{MUSIC}}(\theta) = \frac{1}{\mathbf{a}^H(\theta)\mathbf{E}_N\mathbf{E}_N^H\mathbf{a}(\theta)}$ [54]	$\mathbf{R} = \mathbf{E}_S\Lambda_S\mathbf{E}_S^H + \mathbf{E}_N\Lambda_N\mathbf{E}_N^H$; $\Psi = \mathbf{E}_S^{(1)\dagger}\mathbf{E}_S^{(2)}$ [55]
Computational complexity**	$O(M)$ [52]	$O(M^3)$ [53]	$O(M^3)$ [54]	$O(M^2)$ [55]
Resolution	Poor; this is due to wide main lobes and high sidelobes [52].	Moderate as it is still limited when sources are closely spaced or correlated [53,56].	High; can resolve closely spaced sources by exploiting noise and signal subspaces. [54,56]	Similar to MUSIC, but performs better for correlated sources [55,56].
Sensitivity to noise	High [52]	Moderate [53]	Low [54]	Low [55]
DOA estimation accuracy	Low; high sidelobes [52,56].	Moderate [53,56].	High; super-resolution [54,56].	High; super-resolution without spectral search [55,56].
Robustness to correlated sources.	Poor [52].	Moderate [53].	Poor unless modified [54].	Excellent [55].
Impact of velocity	High, Velocity fluctuations impact phase coherence, resulting in blurring of the beam pattern and reduced resolution [52].	Moderate, the adaptive nature helps to mitigate some of the effects of velocity, but it is sensitive to covariance matrix errors, particularly with Doppler spread [53].	High, high velocity causes snapshot decorrelation, which reduces performance unless Doppler adjustment is provided [54,57].	Lower, due to direct matrix manipulation, it is less sensitive to velocity than MUSIC, although it is still influenced by fast time-varying channels [55].
Main applications	Simple beamforming [52].	Radar, wireless comm [53].	High-resolution DOA [54].	Array processing, geophysics [55].
Target scenarios	For single target [52].	For closely placed targets [53].	For multiple targets with high-resolution DOA estimation and high accuracy [54].	For multiple targets with high resolution DOA evaluation and high accuracy [55].

Note: *where $\mathbf{a}(\theta)$ is the steering vector; $\mathbf{R}$ is the covariance matrix of the received signals; $\mathbf{E}_N$ is the matrix of noise eigenvectors; $\mathbf{E}_S$ is the matrix of signal eigenvectors; Λ_S and Λ_N diagonal matrices of corresponding eigenvalues. **where M is the number of antennas.

A different method of lowering the computational complexity is by application of digital beam-forming (DBF), which is suitable for dynamic environments as seen in road scenarios of automotive Radar [58]. A 77 GHz automotive Radar uses an improved angular resolution DOA algorithm, which is formed by a bigger virtual array using the relative motion observed between the automotive Radar and targets. The proposed DBF-based method can obtain a crude evaluation of the target angle. The radial velocity produced by the relative motion observed between the radar and targets is taken as if only produced by radar, with the targets motionless. Thus, alongside the vehicle's moving direction, a velocity that differs from its actual velocity can be measured. Lastly, the positions of the array for N_{DBF} number of coherent processing intervals (CPIs) are calculated with high accuracy. All these positions of the antenna array will be joined to form a larger non-uniform array of size MN_{DBF}, with M as the number of antenna units in the array. The computational

complexity results in approximately $O(M\ N_{DBF})$ when applying the DBF method to this virtual array. Another method for obtaining high-resolution DOA for a side-looking Radar is obtained by operating on a limited number of snapshots based on vehicle motion and formulating the steering vector to balance phase error and estimate the time tag [59].

Sparse matrix-based representation of Radar signals can be used for DOA estimation in MIMO Radar [60]. For sparse uniform linear array (ULA) structure, FMCW radar is preferred as it can provide highly accurate range information even in high SNR situations [61]. A sparse matrix depiction is developed for a bistatic model of Radar for 2D-location, i.e., range, DOA, and Doppler estimation [62]. Here, the road is characterized by a Cartesian map using which the targets' coordinates and total multi-path Doppler for target velocity are estimated. In a sparse version of the raw Radar data, after controlling the bistatic formation's geometry, the source vectors have a familiar support set, which helps in the application of group-sparsity (GS) based optimization. This algorithm for estimating 2D location and Doppler performs better compared to MUSIC. A further addition to this algorithm is the application of a 3-dimensional (3D) multi-static FMCW signal model, followed by an evaluation of the multi-target location and Doppler method using the GS methodology [63]. Furthermore, an association of multi-target parameters via cross-correlation and an ESPRIT algorithm, as well as based on Least Squares, is demonstrated. The GS joint shows better results than MUSIC at every level of SNR in the evaluation of Doppler and location. Additionally, the GS method can be used to determine the Doppler frequency first, and then the Doppler parameters are used for obtaining range parameters, and finally, the DOA is evaluated with these target parameters [64]. A signal processing method for DOA measurement based on Compressive Sensing (CS) theory is presented, which provides good resolution and accuracy while allowing an improved degree of design [65]. This algorithm enables the utilization of configurations with sparse antennas, featuring a reduced number of transmitter and receiver channels, while maintaining a larger effective antenna aperture. The authors have provided four sparse reconstruction algorithms along with the MUSIC algorithm. Orthogonal Matching Pursuit (OMP) is better suited for automotive Radar applications, as it offers improved detection efficiency and is faster than MUSIC. A method for ghost target detection is shown in [66] where the CS method is used for angle estimation of direct paths and multipaths.

Deterministic maximum likelihood (DML) is a parametric-based DOA estimation approach that estimates DOA by a projection of vectors of the received signal to the steering matrix's null space. In [67], different transmit signals having orthogonal properties are generated with space-time block codes, and depending on the number of transmit antennas, the transmit signals have their phases shifted at orderly intervals. Each of the signals transmitted is matched to its respective transmitting antenna by applying the DML algorithm to find the proper array for DOA estimation. Upon identifying the signal transmitted from the initial transmitter antenna, the highest velocity to be detected is not compromised, and the accuracy of DOA analysis is improved. When the transmitted signals are not matched, the correlation value of the received echo signal and the steering matrix is degraded, and DOA estimation is worsened, even if the number of targets is appropriately detected. Based on ML assessment [68,69] MARS-a super-resolution real-time DOA used for automotive Radar. Here, the evaluation results from earlier timestamps are used to create an adequate and reduced search space. To decrease computation time, problems at every step are decomposed into separate sub-problems, and the GPU is utilized for parallel computing. Through simulation-type experiments, it has been demonstrated that only MARS can handle up to one hundred bins consisting of reflection points with a resolution of 1° within 1 ms. A DOA estimation based on Fast Variational Bayesian method helps to lessen the high sidelobes in sparse arrays and improve resolution for closely placed reflectors [70]. The implementation of sparse Bayesian algorithms for DOA evaluation, which provides improved accuracy and lower hardware costs, is demonstrated in [71].

Machine learning algorithms for DOA measurement can be classified based on Regression, model order methods, and spectrum [72]. To improve DOA estimation and reduce computational complexity, in [73], the authors utilize a look-up table (LUT) based on data storage, which can mitigate measurement errors. Then, the authors propose Support Vector Machine (SVM), an ML classifier, to decrease the high storage complexity. The ideal azimuth selection issue is considered a multi-classification problem, in which a considerable quantity of training samples is obtained from the ultra-SRR and used to improve the classifier. Depending on these data for training, the SVM algorithm is applied to receive more precise azimuth information in SRR. Table 6 contains a detailed analysis of research works available regarding DOA estimation of targets using automotive Radar.

Table 6: An analysis of research works for DOA estimation

Ref.	Year	Algorithms adopted	Performance metrics and achievements	Drawbacks
[49]	2025	CS alternating descent conditional gradient method for DOA estimation in non-uniform linear arrays.	**(a)** Root mean square error plot of the CS-ADCG method converges with increased SNR, showing that the off-grid effect is not hampering the result. **(b)** With an increasing number of signal sources, this algorithm is better than MUSIC. **(c)** Using real Radar data, when the angle in-between two corner signal reflectors is reduced to 10 and 20 from 30, CS-ADCG reconstructs two sources effectively.	Computation time is slightly more than MUSIC when the number of arrays is 20 in a uniform linear array, a random linear array, and a Coprime linear array.
[63]	2024	**(a)** Group-sparsity method used for multistatic Cartesian 2D range resolution and Doppler estimation. **(b)** Association of multi-target parameters is done using a least-squares-based minimization method.	**(a)** With increasing SNR, GS outperforms the MUSIC-average algorithm in range and Doppler estimation. **(b)** Comparison of the least-square-based pair matching method with the cross-correlation-based ESPRIT pair matching method shows that the former outperforms the latter, considering the probability of successful parameter (DOA and bistatic velocity) association.	Computational complexity due to GS-based optimization and Least Square (LS)-based parameter pairing methods.
[62]	2023	A sparse matrix architecture developed for a bistatic type automotive Radar model for range, DOA, and Doppler estimation.	**(a)** Root mean square error of Doppler decreases with increasing SNR. **(b)** With increasing Radar data size on performance evaluation, the sparsity-based method provides better results than MUSIC in location and Doppler estimation.	Computational cost increases.
[51]	2023	The E-MUSIC that achieves a resolution in target detection with complexity $O(z^2M)$, where z is a user-specific parameter that balances between complex modeling and angular accuracy, and the number of array elements is M.	**(a)** E-MUSIC is computationally fastest among other algorithms like MUSIC and MVDR, considered against array elements. **(b)** Accuracy is almost similar to MUSIC when PSD is plotted against rising SNR values.	Only the line-of-sight channel is studied.

(Continued)

Table 6 (continued)

Ref.	Year	Algorithms adopted	Performance metrics and achievements	Drawbacks
[68]	2022	Based on Maximum Likelihood Estimation, MARS-a super-resolution real-time DOA presented to control approximately 100 bins consisting of reflection points with super-resolution of 1° within the time of 1 msec, beneficial for automotive purposes.	**(a)** With the same number of DOA in 1 bin, the RMSE value against increasing SNR is obtained as 1 deg by only the MARS algorithm. **(b)** Computation time of MARS is lower than MUSIC and ESPRIT.	Performance evaluation with simulation experiment only.
[67]	2020	**(a)** Different transmit signals having orthogonal properties are generated using space-time block codes, and based on the number of transmit antennas, their phases are shifted at regular intervals. **(b)** Each transmitted signal is matched to its transmit antenna by the DML algorithm to find the appropriate array for DOA measurement.	Normalised MUSIC pseudo-spectrum presented against DOA shows accurate DOA estimation of two targets only when true matching of arrays is done.	In true matching of ar-rays, at low SNR, a slight angle estimation error occurs.
[58]	2020	**(a)** Array positions for N_{DBF} number of coherent processing intervals (CPIs) are calculated with high accuracy, and the array positions are joined to form a large non-uniform array of size (MN_{DBF}). **(b)** On application of the DBF method to a virtual array, computational complexity results in about $O(MN_{DBF})$.	The proposed method can better separate two targets in the angular dimension than MUSIC, sparse recovery-based methods.	Angular resolution is not accurate at 0 SNR, and is possible only with higher values.
[45]	2020	**(a)** Enhanced beam-space MUSIC algorithm to reduce parameter space by utilizing prior information to improve beam-former design. **(b)** Modified MUSIC estimator used to lessen the impact of low SNR and wrong sample covariance in one snapshot. **(c)** Considers relation between a signal-plus-interference model of sample covariance and a subspace model.	**(a)** With target number = 1, the performance of this algorithm is better for the mean deviation and standard deviation of the angle estimated compared to beamforming MUSIC and classical MUSIC. **(b)** With the same angular separations, this algorithm has a better probability of resolution under the same SNR.	Beamformer design is unsuitable for a restricted Field of View (FOV). DOA evaluation is done on a specific Doppler and range cell that contains one or more targets.
[42]	2019	**(a)** DOA estimation method to extract the connection among the received echo signals and create extrapolated elements outside the region of the actual array of antenna elements. **(b)** With both original and extrapolated signals, DOA is estimated with higher resolution, almost 99% with expanded signals.	**(a)** Bartlett algorithm with the suggested method provides the best resolution probability and least RMSE, compared to conventional Linear Least Squares. **(b)** Lower computational complexity.	Computational complexity marginally increased.

(Continued)

Table 6 (continued)

Ref.	Year	Algorithms adopted	Performance metrics and achievements	Drawbacks
[73]	2019	**(a)** Uses a LUT as a data storage-based method for outputting azimuth angle. **(b)** SVM classifier used to decrease high storage complexity. Depending on the training data, the SVM algorithm is applied to obtain more accurate azimuth information in SRR.	**(a)** Average azimuth error increases with decreasing range value. **(b)** LUT and proposed SVM are more robust to this.	
[43]	2018	DFT applied for high efficiency, and with the MUSIC algorithm, high angular resolution is obtained in UWB MIMO Automotive Radar.	**(a)** In the range vs. angle plot, the spectra for a car are narrower for super-resolution than those of the beamforming method. **(b)** The DFT-MUSIC algorithm provides better resolution than the DFT-BF algorithm.	DFT-MUSIC is computationally slower than DFT-BF.
[65]	2018	**(a)** Method based on CS theory provides good resolution and accuracy while allowing a better front-end design. **(b)** Uses a sparse configuration of antennas with fewer transmitter and receiver channels and a big effective antenna aperture.	**(a)** Accuracy of the different estimators with RMSE between valid target detections and their positions is considered. **(b)** False alarm ratio, probability of detection, and detection efficiency are measured. **(c)** OMP reconstruction algorithm provides better detection efficiency and is faster than MUSIC. **(d)** Sparse reconstruction algorithms capable of resolving two closely-spaced targets due to the increased aperture of the sparse array.	Sparse reconstruction requires more computational time than FFT and is more dependent on hyperparameter tuning.
[41]	2017	**(a)** DOA estimation by comparison of a phase difference between two Radars using the phase angle of the steering vector. **(b)** Kurtosis measures how many observation values are present at the center.	**(a)** Average values and "standard deviations of errors" obtained from the difference between actual angles and estimated angles, which shows the proposed method has a smaller average error. **(b)** The Kurtosis value of this algorithm is 31.9140, suggesting main lobes with large peak values and side lobes have smaller values, providing better resolution.	As SNR changes, the method has an error of DOA estimation like for MUSIC and Bartlett, but with more computational complexity.
[48]	2017	**(a)** Crude estimation is done using MUSIC. **(b)** Based on these values, each antenna element is turned to specific directions using a calibration technique focusing on signals from target directions obtained in the first stage.	MUSIC with this technique results in lower RMSE values at low SNR regions compared to conventional MUSIC.	In a high SNR region, the approximation error is observed when estimated phase delays are multiplied by the received signals.

Table 7 contains an analysis of various DOA estimation algorithms.

Table 7: An analysis of various DOA estimation algorithms

Ref.	Year	Algorithms adopted	Advantages	Drawbacks	Scenarios
[49]	2025	Compressive sensing alternating descent conditional gradient method for DOA estimation in non-uniform linear arrays.	**(a)** Off-grid effect is not hampering the result. **(b)** Using real Radar data, the algorithm can reconstruct two sources effectively when the angle between two corner reflectors is reduced.	Computation time is slightly more than MUSIC when the number of arrays is much less.	Urban roads.
[63]	2024	**(a)** Group-sparsity method. **(b)** Association of multi-target parameters is done using least-square-based minimization method.	The least-squares-based pair matching method is good for the probability of successful parameter (DOA and bistatic velocity) association,	Computational complexity.	Urban roads.
[62]	2023	GS based algorithm.	With increasing Radar data size on performance evaluation, the sparsity-based method provides a better result than MUSIC.	Computational cost increases.	Urban roads.
[51]	2023	E-MUSIC algorithm.	E-MUSIC is computationally fastest among algorithms like MUSIC, and MVDR, considered against the array elements.	Only the line of sight channel is studied.	Highway.
[68]	2022	MARS-based on Maximum likelihood.	With the same number of DOA in 1 bin, the RMSE value against increasing SNR is obtained as 1 deg by only the MARS algorithm.	Performance evaluation with simulation experiment only.	Dynamic driving situations on urban roads.
[67]	2020	Deterministic Maximum Likelihood.	Accurate DOA estimation of two targets only when true matching of arrays is done.	In true matching of ar-rays, at low SNR, a slight angle estimation error occurs.	Highway.
[58]	2020	Digital Beamforming method to virtual array.	Two targets are separated better in the angular dimension.	Angular resolution is inaccurate at 0 SNR, and is possible only with higher values.	Dynamic environment such as on a highway.
[45]	2020	Enhanced beam-space MUSIC algorithm.	With target number = 1, the performance of this algorithm is better compared to beamforming MUSIC and classical MUSIC.	Beamformer design is unsuitable for a restricted Field of View (FOV).	Dense traffic condition.
[42]	2019	DOA estimation with both original and extrapolated signals.	Bartlett algorithm with the suggested method provides a higher resolution probability and lower RMSE when plotted against SNR.	Computational complexity marginally increased.	Urban roads.
[73]	2019	**(a)** LUT as a data storage-based method. **(b)** Support Vector Machine.	LUT and proposed SVM are more robust to azimuth error when plotted against the number of data samples.		Urban roads.

(Continued)

Table 7 (continued)

Ref.	Year	Algorithms adopted	Advantages	Drawbacks	Scenarios
[43]	2018	DFT applied with MUSIC algorithm.	DFT-MUSIC algorithm provides better angular resolution.	DFT-MUSIC is computationally slower than DFT-BF.	Parking area of university campus with static targets and slowly moving targets.
[65]	2018	Method based on Compressive Sensing.	Sparse reconstruction algorithms can resolve two closely-spaced targets due to the increased aperture of the sparse array.	Sparse reconstruction requires more computational time compared to FFT and is more dependent on hyperparameter tuning.	Outdoor parking area.
[41]	2017	Comparison of the phase difference between two Radars using phase angle of steering vector.	the kurtosis value of this algorithm is 31.9140, providing better resolution.	As SNR changes, the method has more computational complexity.	Urban roads and parking area.
[48]	2017	**(a)** Crude estimation is done using MUSIC **(b)** The Antenna element is turned in specific directions using a calibration technique	Lower RMSE values at low SNR region, compared to conventional MUSIC	In high SNR region, approximation error is observed when estimated phase delays are multiplied by received signals.	Highway.

4 Target Tracking

After target detection by Radar, filtering and tracking techniques for obtaining target motion dynamics are required to stay informed about the target's position and avoid collision [74,75] as in the ACC application. Different target modeling models are present, like dynamic target modeling and static target modeling, which are further categorized into occupancy grip mapping, amplitude grid mapping, and free space mapping [76]. Fig. 11 draws a flowchart of the target tracking signal processing method.

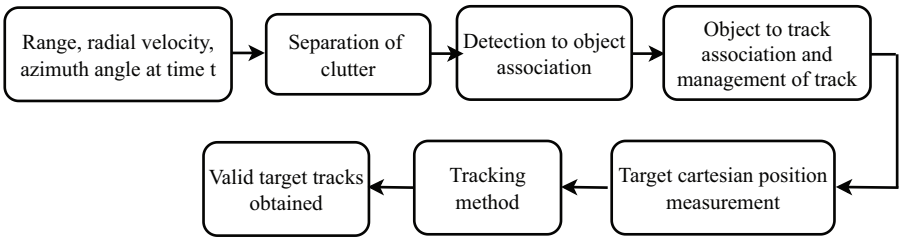

Figure 11: Signal processing for target tracking

The target parameters measured are range, velocity, and azimuth angle obtained at time instant t. The target is separated from clutter by discriminating between moving and stationary targets, where stationary targets are not considered. Object association is achieved by grouping multiple detections from the same target into a single object. When an object does not match any existing track, a new track is initiated, resulting in valid and false tracks. Only valid tracks of real targets are input to the tracking filter. The target position represented in Cartesian coordinates obtained from range and angle measurements is fed to tracking filters. The output from the tracking filter is a valid track for a particular target.

The main characteristics of multi-target tracking are [77,78]:

1. Motion model for the target.
2. Prediction and update of the target state.
3. Data association of measurements of tracks.
4. Target Track Management applied for track initiation, confirmation of track, and termination of track.

4.1 Motion Model for Target

To detect a target vehicle, motion models are utilized, where the parameters of the target are assembled from sensor data. These models are designed according to the movement of vehicles and classified as constant velocity (CV), constant acceleration (CA), constant turn rate (CTR), and constant turn rate and acceleration (CTRA).

4.2 Prediction and Update of Target State

Track initiation establishes a sufficiently accurate track in terms of position, velocity, and direction within the shortest time possible. The Kalman filter (KF) is typically used to estimate the location of actual targets at the current instant in time, utilizing prediction and update processes. The Bayesian method is also being introduced for this purpose.

4.2.1 Kalman Filter

The KF is a recursive filter used to estimate the state of a discrete-time linear type dynamic system from noise-filled measurements. It consists of a Prediction step and an Update step. *Prediction step:* A new value called the predicted value is assumed based on the initial value, and then the error present in the prediction is obtained according to various noises in the Radar system. Predicted value,

$$\mathrm{x}'_t = F.x_{t-1} + W_{t-1} \tag{60}$$

where F is the state transition matrix, x is the mean state vector having position and velocity values of the target, W is the Gaussian state noise vector, and t is the time stamp. The covariance matrix can be denoted as,

$$\mathrm{P}'_t = F.P_{t-1}.F^T + Q \tag{61}$$

where Q is noise and T stands for transpose. *Update step:* The actual measurement coming from the Radar is obtained and named as the measured value. The difference between the measured and predicted values is evaluated, and then it is decided which value to keep based on the Kalman gain. Based on the Kalman gain, these new values and new errors are calculated, which will be the predictions done by the KF in the first iteration. The Kalman gain is the parameter that determines the weight assigned to predicted and measured values. It determines whether the actual value is closer to the expected value or the measured value. The output of this Update step is fed back to the predicted state, and this cycle continues until the error between predicted and real values conve rges to zero.

$$KG_t = \frac{error\ in\ prediction}{error\ in\ prediction + error\ in\ measurement} = \frac{\mathrm{P}'_t H^T}{H\,\mathrm{P}'_t H^T + R_n} \tag{62}$$

where H is state transition matrix containing no unwanted information, R_n is measurement noise. The value of Kalman gain ranges from 0 to 1. When the value is closer to 0, the predicted value approaches the real

value, and when the value is closer to 1, the measured value approaches the real value.

$$x_t = \mathrm{x}'_t + KG_t.\left(Z_t - H\mathrm{x}'_t\right) \tag{63}$$

where Z_t is the actual measured value from Radar and the term $\left(Z_t - H\mathrm{x}'_t\right)$ denotes the difference between measured value and predicted value.

$$P_t = \left(I - KG_t.H\right).\mathrm{P}'_t \tag{64}$$

These new x_t and P_t values will be sent for the next prediction step, and the cycle continues. Fig. 12 shows a pictorial presentation of the Kalman filter algorithm.

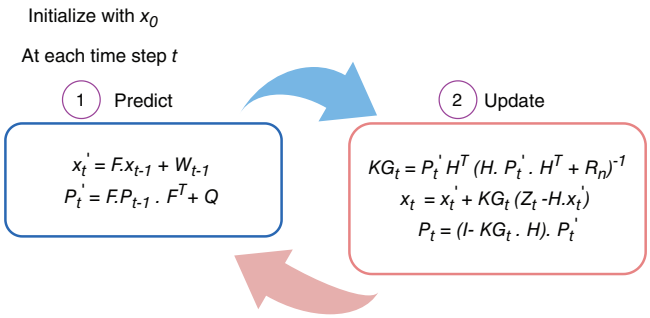

Figure 12: Kalman filter algorithm

4.2.2 Extended Kalman Filter (EKF)

The limitation of the "Kalman filter" is that it works with a Gaussian distribution and linear functions. Radar data involves non-linear functions, which must be approximated to make them linear. This approximation is typically performed using the Taylor series, and the EKF can be applied afterward. *Prediction step:* The prediction step is similar to the Kalman filter.

$$Predicted\ value,\ \mathrm{x}'_t = F.x_{t-1} + W_{t-1} \tag{65}$$

where F is a matrix of state transition, x is the mean state vector having position and velocity values of the target, W is the Gaussian state noise vector, and t is the time stamp. The covariance matrix can be denoted as,

$$\mathrm{P}'_t = F.P_{t-1}.F^T + Q \tag{66}$$

where Q is noise and T stands for transpose. *Update step:* the difference in-between the measured value and the actual value is given as,

$$y = Z_t - h\mathrm{x}'_t \tag{67}$$

where Z_t is the actual measured value from Radar in polar coordinates and h is a function that specifies how position and velocity are mapped to polar coordinates.

$$Total\ error, S = H_j\mathrm{P}'_t\mathrm{H}_j^T + R \tag{68}$$

$$Kalman\ Gain, KG_t = \frac{\mathrm{P}'_t \mathrm{H}_j^T}{S} \tag{69}$$

where H_j is the Jacobian matrix, which is the first-order derivative of the Taylor series. Now,

$$x_t = \mathrm{x}'_t + KG_t.y \tag{70}$$

$$P_t = \left(I - KG_t.H_j\right).\mathrm{P}'_t \tag{71}$$

Fig. 13 shows a pictorial presentation of the Extended Kalman filter method.

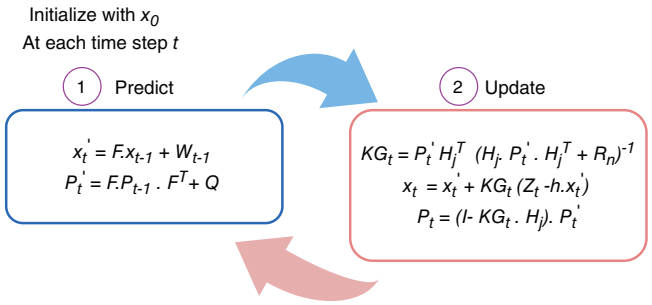

Figure 13: Extended Kalman filter algorithm

4.2.3 Unscented Kalman Filter (UKF)

The UKF is similar to the EKF and tries to address its problems. Here, the transformation is a nonlinear unscented transformation and is considered a replacement for the linearization process in EKF. In this method, a precise nonlinear function is employed to approximate the probability distribution of the state.

4.2.4 Bayesian Filter

To work with non-Gaussian Radar systems, Bayesian filtering and the particle filter (PF) are sometimes employed. With the help of random samples, this method estimates the state Probability Density Function (PDF). The model for the system can be shown as,

$$x\left(t\right) = F\left(x\left(t-1\right), V_n\left(t-1\right)\right) \tag{72}$$

where F is a transition matrix and V_n is zero-mean white noise of known PDF. The equation for measurement is shown as,

$$Z\left(t\right) = H\left(x\left(t\right), W\left(t\right)\right) \tag{73}$$

where H is taken as the transition function and W is taken as zero-mean white noise. The PF algorithm can approximate the posterior PDF P(x(t)|Z(1:t)) by particles, which are a set of weighted random samples. The first prior distribution of the state P(x(0)) and PDF P(x(t−1)| Z(1: t−1)) at time (t−1) are assumed to be known. The PDF is written as,

$$P\left(x\left(t\right)|Z\left(1:t-1\right)\right) = \int P\left(x\left(t\right)|x\left(1:t-1\right)\right) P\left(x\left(t-1\right)|Z\left(1:t-1\right)\right) dx\left(t-1\right) \tag{74}$$

The prediction is then updated with the help of the current measurement y(t) based on Bayes' theorem,

$$P\left(x\left(t\right)|Z\left(1:t\right)\right)=\frac{P\left(y\left(t\right)|x\left(t\right)\right)P\left(x\left(t\right)|Z\left(1:t-1\right)\right)}{P\left(Z\left(t\right)|Z\left(1:t-1\right)\right)} \tag{75}$$

in which, P(y(Z)|Z(1:t−1)) is a normalizing constant. The optimal state can be derived as

$$E\left(x\left(t\right)|Z\left(1:t\right)\right)=\int x\left(t\right)P\left(x\left(t\right)|Z\left(1:t\right)dx\left(t\right)\right) \tag{76}$$

A limitation of this method is that the unknown integrals are hard to compute, so approximations are needed.

A single target localization method by applying a collocated MIMO-monopulse approach to FFT processing is adopted in a real-life experiment [79]. To improve the velocity uncertainty of a moving target, a cascaded KF as described in [80], can be applied, where KF is first applied on polar coordinates to derive velocity and predict the acceleration. Next, an EKF is used to improve velocity measurements and minimize measurement error when the motion state is in Cartesian coordinates, and measurements are provided in polar coordinates. An improved adaptive EKF is used in [81] to enhance the robustness and accuracy of the tracking process. A cubature Kalman filter (CKF) applies the cubature rules to approximate recursive Bayesian estimation integrals with a Gaussian assumption. The square-root CKF (SRCKF) algorithm distributes the factors, which are the square roots of the predicted and posterior error covariance matrices, to prevent the square rooting of the matrix. The iterative SRCKF algorithm in [82], iteratively optimizes the SRCKF measurement and update processes by the Gauss-Newton method, leading to a lower error component. In [83], a threshold method is first used to filter out ghost targets and empty targets. This is followed by application of the Adaptive Interactive Multiple Model Kalman Filter and the Hungarian algorithm for association and tracking of multiple targets, which reduces the error as compared to conventional UKF algorithms. In [84], a multi-target tracking algorithm based on a 4D Radar point cloud has been proposed for obtaining the intensity, location, velocity, and structure of the targets. The method provides compensation for point cloud clustering, velocity, static state, and dynamic state updates, as well as 3D border generation of the dynamic target using the Kalman filter, contour updates of the static target, and a target trajectory control procedure. Tracking of targets in the presence of velocity ambiguity requires a tracking algorithm with TDM where disambiguation of Doppler is done before angle estimation [85].

A reweighted robust PF (RR-PF) is proven to improve state values in a nonlinear model and is more robust to outliers [86]. The method utilizes inputs from the particle weights of true particles and filters out inputs from unreliable particles through the discriminative treatment of detected Radar data. A track-before-detect (TBD) algorithm uses the targets' kinematic constraints on road and graph theory algorithms to define every plot as a potential target or clutter [87]. The algorithm involves a discriminant metric, which refers to mathematical calculation rules of a plot and its trajectory, followed by the state transition of the plot, and requires transition conditions. The post-processing is done for motion state estimation of confirmed targets, after which significant results in target detection and effective clutter removal are observed. A multi-frame TBD can adjust the threshold value of detection depending on the existence of mobile targets present within the Radar field-of-view and also considers the self-positioning errors of the ego vehicle [88]. Another application of TBD is the motion compensation technique on the dynamic programming-based TBD [89], which works for ground Radars to decrease the error of the conventional algorithm. In [90], the Cramer-Rao lower bound method is applied to detect the location and velocity of a mobile target, and an active sensing application is further used to improve tracking accuracy.

Linear Regression with KF: A machine learning algorithm like Linear regression can be applied with KF for more accurate estimation of target parameters. Linear regression helps identify a statistical relationship between an independent variable and a dependent variable. Here, time (t) can be assumed as independent and 'x' or 'y' position as dependent variables. It is believed that the relation between time and position is of second order polynomial and hypothesis is $h_\theta(t) = \theta_0 + \theta_1 t + \theta_2 t^2$, where, θ is weight determined by LR.

The motion in both 'x' and 'y' directions is trained using the last position values or training examples and these weights. Final estimated position values are calculated by applying KF. The expected outcome is to minimize the total error in prediction.

4.3 Data Association and Measurement of Tracks

Data association is used to combine multiple detections from the same target into a single object. If an object does not match the current track, a new track has to be initialized. Thus, valid and false tracks are produced. The valid tracks are considered for updating the states [91]. In the global nearest neighbor (GNN) algorithm, the association depends on the minimum Euclidean distances between measured and predicted values. However, this algorithm performs poorly in high-clutter regions.

The Joint Probabilistic Data Association Filter (JPDAF) algorithm is more efficient for tracking targets, where the probability of $\beta_{i,j}$ is measured, which shows a measure of i obtained from a target track j. In this case, measurements from targets are assumed to be of a Gaussian distribution, whereas the clutter is uniformly generated. A hypothesis tree is created by the hypothesis filter, considering three associations: a measurement will either belong to an existing track or a new one, or it is due to a false alarm. The probability of each hypothesis is based on the Bayes rule, and the likelihood of each association is calculated. The Hungarian algorithm is an assignment algorithm used to find an appropriate "target track assignment" for a specific cost matrix. The cost matrix is square and contains elements $C_{i,j}$, which denote the cost for the measurement assignment i to target track j. The elements are calculated from the likelihood function, which is determined by radar properties such as measurement noise, the probability of target detection, and the detection of false alarms for the initialization of track and target properties.

A micro-Doppler-based leg tracking framework for pedestrian detection to enable behavioral signs within one measurement cycle has been presented in [92]. A model is designed to estimate the spatial movement of the feet, segment the body in a vertical format, and extract the reflection points resulting from leg movement. An elevation-resolving antenna is used. Then, EKF is used for target tracking. After data association is completed with Joint Probabilistic Data Association (JPDA), the reflection points can be assigned to a particular leg. Then the location, kinematic data, and velocity of each foot can be filtered. In [93], an Interacting Multiple Model (IMM) algorithm with the JPDA algorithm is shown to achieve tracking of multiple maneuvering targets. Since the effect of this algorithm is less pronounced in the nonlinear case, UKF with Doppler measurement is applied to achieve better position and velocity accuracy. In [94], the spatial distribution of the measurement model produced by a target vehicle is presented using a variational Gaussian mixture (VGM) model. For mapping of the extended target tracking problem, the Probability Generating Functional formulation has been used.

An adaptive strong tracking extended KF (ASTEKF) helps to lessen the impact of state transitions and parameter changes on the measurement process and for better resilience to interferences [95]. The adaptive attenuation factor is updated whenever the time fading factor changes, helping to mitigate the divergence problem in a tracking process. This algorithm offers enhanced capacity to track abrupt changes in the target's motion states. A number of clustering algorithms are used for identification, investigation, and tracking of targets [96]. The Density Based Spatial Clustering of Applications with Noise (DBSCAN) clustering algorithm can be applied to range-angle data to obtain the centroids of the cluster points, which then provides

the target position [97]. An imaging method for a target moving at high speed utilizes the Doppler Range Processing (DRP) method to achieve velocity and range resolutions, thereby obtaining coherent integration gains through range-Doppler processing [98]. Initially, Doppler processing is performed using the FFT on slow-time samples. A velocity bin interpolation method, and lastly, processing of the range is done via FFT over Doppler migration lines. The complexity of computation of this algorithm is calculated as $O\left(NL\log\left(NL\right)+NL\right)$, where N is the number of samples in PRI, and L is the periods of chirps in a CPI.

A hybrid smooth variable structure filter (SVSF) is presented in [99] by combining generalized time-varying smoothing boundary layer (GVBL) and Tanh-SVSF to prevent parameter sensitivity and control the unwanted chattering matter. A non-linear generalized variable smoothing boundary layer (NGVBL) parameter is used to create a hybrid switching scheme that leads to an ideal Kalman filter (KF) in cases of low model uncertainty. For solving data association and clustering problems, a Deep Neural Network (DNN), called Radar Tracking Network or *TrackNet*, can be used, which applies point clouds of Radar data from several time stamps to get desired objects on the road and provide the information on tracking [100]. In this architecture, features are extracted independently for each cell and timestamp using a *PointNet++*-based method that incorporates long-distance point sampling and multi-scale grouping. This is followed by processes of convolution and max-pooling applied to smaller point clouds within each cell. For extended object tracking, a measurement modeling and estimation method, known as the data-region association process, partitions an object into several regions. A simple measurement distribution is performed over each area, and a complex method is applied to the target [101]. Also, a new gating method is used for data association.

4.4 Target Track Management

For multiple targets, a management process is required to filter false alarms and efficiently track them under changing detectability scenarios [102]. Tracks can be classified into two categories: provisional and verified tracks. After each measurement round, the values are updated and verified in the first phase. The remaining measurements are tested for association with provisional tracks in the second phase. If these measurements do not correlate with known tracks, they initialize new provisional tracks. After further examination, these tracks become either confirmed or deleted. For this purpose, the M/N test can be applied, where a provisional track is confirmed if a minimum M number of detections is obtained for N scans of data. If K or fewer detections are obtained for N scans, the provisional track is rejected. A composite method can be formed by combining two or more M/N tests by a logical OR operation. This will provide more accurate results with little increase in computational difficulty. For target tracking, a medium access control (MAC) technique has been adapted so that automotive Radars can have a common channel and suggest the best MAC parameter for a particular vehicle and corresponding road traffic [103]. Table 8 contains a detailed analysis of research works available regarding target tracking using automotive Radar.

Table 8: An analysis of research works for target tracking

Ref.	Year	Algorithms adopted	Performance metrics and achievements	Drawbacks
[102]	2025	**(a)** Track management methods: Naïve approach, track history-based, and existence probability-based. **(b)** The Naïve method is used in sensor-to-sensor track fusion architecture where all sensors are assumed to detect and track all targets within their respective field-of-view. **(c)** For the track history-based method, the history of a target track's association is used to confirm the track in multi-target tracking. **(d)** In the existence probability method, a probability value is set to a global track and is compared to a threshold value to determine track confirmation and deletion.	**(a)** Performance metrics include precision, recall and Multiple Object Tracking Accuracy (MOTA) and F-measure F1 score. **(b)** The Recall value of the Radar is higher than that of a camera. **(c)** The Existence probability-based method, depending on the sensor to global Dempster-Shafer rule, creates a balance between recall and precision and high F1 and MOTA scores, providing better performance than other methods.	The Existence probability-based method does not provide a better recall value than the central tracking algorithm.
[95]	2024	**(a)** Adaptive strong tracking extended Kalman filter to prevent filtering divergence problem. **(b)** DBSCAN algorithm to merge target tracks on the real main route. **(c)** Data association is done with JPDA.	**(a)** Root mean square errors in location and velocity are lower using ASTEKF than with EKF and strong tracking extended KF (STEKF). **(b)** Target vehicle's filtered tracks are almost the same as the real track, as it changes roads and velocity filtering values intersect fast with lesser error.	Only the Constant acceleration motion model is considered.
[84]	2023	**(a)** 4D Radar cloud-based measurement model for obtaining intensity, location, velocity, and structure of targets for tracking. **(b)** The binary Bayesian filtering technique is applied to identify the size of dynamic and static targets. **(c)** Kalman filter used for dynamic target tracking.	If the radial velocity is less, rotation angle estimation is done from velocity measurements from many points, and a smaller range is better for obtaining the rotation angle.	Research is required for motion models of moving targets and pose estimation of the ego-vehicle.
[92]	2022	**(a)** Micro-Doppler-based leg tracking framework for pedestrian detection to enable behavioral signs within one measurement cycle. **(b)** EKF is used for target tracking. **(c)** Data association was done with JPDA, reflection points were set to respective legs, and finally, filtering of each foot's velocity, position, and kinematic data.	**(a)** Micro-Doppler spectrum of the lower body of a pedestrian, dependent on time range, shows tracking of a foot movement. **(b)** Required for determining the state of a pedestrian, like drunk or not, for safety purposes.	Data association conflict arises if targets are close to one another.
[99]	2022	**(a)** Hybrid SVSF presented by combining generalized time-varying boundary layer (GVBL) and Tanh-SVSF to prevent parameter sensitivity and control unwanted chattering phenomenon. **(b)** Non-linear GVBL parameter to create a hybrid switching scheme for ideal Kalman filtering in case of low model uncertainty. **(c)** NGVBL-SVSF corrects the optimization problem and gets a quasi-optimal NGVBL parameter.	**(a)** NGVBL-SVSF compared to common SVSF and Tanh-SVF, considering parameters like Root Mean Square Error of target's position and velocity measurements and track continuity. **(b)** NGVBL-SVSF attains the least RMSE in low model and high uncertainty level cases.	Cost of NGVBL-SVSF is more than Kalman filter, common SVSF, due to hybrid switching.
[86]	2022	**(a)** For the generative model, the Bayesian algorithm is used to treat the weights of each entry in measurement data probabilistically. **(b)** Reweighted robust particle filter method uses inputs from particle weights of reliable particles and deteriorates the inputs from unreliable particles by discriminative treatment of detected Radar data, to improve state estimates in a nonlinear model.	**(a)** RMSE and Normalized Mean Squared Error (NMSE) are performance metrics observed against outlier ratios. **(b)** This method has the lowest NMSE and average Mahalanobis distance throughout the range of outlier ratios compared to other particle filters. **(c)** Better trajectory tracking of pedestrian.	In detecting walking pedestrians with real data, few fluctuations were observed.

(Continued)

Table 8 (continued)

Ref.	Year	Algorithms adopted	Performance metrics and achievements	Drawbacks
[87]	2021	**(a)** Track-before-detect algorithm uses kinematic constraints of targets on the road and graph theory algorithms to define every plot for a potential target or clutter. **(b)** Involves a discriminant metric, referring to mathematical calculations of a plot and its trajectory. **(c)** Next, the state transition of the plot that describes a state variable in the case of plots. **(d)** Post-processing for motion state estimation of confirmed targets.	**(a)** Probability of detection (PD), Receiver operating characteristic (ROC), and clutter elimination rate are performance metrics. **(b)** In PD vs. signal-to-disturbance ratio (SDR), TBD shows better performance in the detection of target and high clutter elimination rate. **(c)** With different SDRs, this method provides better target detection and clutter elimination compared to successive track cancellation algorithms.	TBD can not perform properly in case of a large signal loss.
[98]	2021	**(a)** Imaging method for target moving with high speed, Doppler Range processing (DRP) used to achieve velocity and range resolutions and obtain coherent integration gains of range-Doppler processing. **(b)** Doppler processing is performed via FFT on slow time samples, then a velocity bin interpolation method, and lastly, range processing is done with FFT.	**(a)** Considering point spreading functions of moving target in range-Doppler plot, DRP performs better than conventional Range-Doppler Processing (RDP). **(b)** DRP has the same coherent integration gain for different Radar bandwidths and target velocities.	The results are proven theoretically only.
[93]	2021	**(a)** IMM with JPDA is proposed to achieve tracking of multiple targets in the case of maneuvering targets. **(b)** DUKF applied for better position and velocity accuracy.	**(a)** Smaller correlation coefficient results in smaller range RMSE and range average RMSE. **(b)** Value of RMSE of velocity tracking and RMSE of velocity average is largest at zero correlation coefficient value. As the correlation value becomes negative, RMSE values decrease.	The algorithm cannot correctly derive the target motion state of a high-velocity vehicle with maneuvering acceleration. The accuracy of target range tracking is reduced.
[100]	2020	For solving data association and clustering problems, Radar TrackNet applied Radar data point clouds from several time stamps to detect desired objects on the road and provide tracking information. The IMM with JPDA is proposed to achieve multi-target tracking of maneuvering targets.	Radar TrackNet provides improved performance with multiple object tracking accuracy and precision values compared to classification-assisted and basic clustering tracker methods.	Probability of missing an actual track is more than showing false tracks.
[94]	2020	**(a)** Spatial distribution of measurement model produced by a target vehicle presented using a variational Gaussian mixture (VGM) model. **(b)** For mapping of the extended target tracking problem, the Probability Generating Function formulation is used.	Plot of Wasserstein distance vs. traces from Nusense's data set shows the algorithm has improved performance in terms of average Wasserstein distance (WSD) and median WSD.	Computationally complex.
[80]	2018	**(a)** Kalman filter applied on polar coordinates to derive velocity and acceleration. **(b)** Extended Kalman filter used to improve velocity measurements and minimize the measurement error where the motion state is in Cartesian coordinates.	Cascaded KF can estimate the velocity ambiguity number whether the target velocity is at the hopping stage or not. The algorithm is not tested on a real road environment.	
[77]	2018	**(a)** UKF applied to CTRA motion model. **(b)** Tracking accuracy improved by linear regression technique. **(c)** JPDA algorithm applied for data association to update the state estimate of the target. **(d)** For track management, the M/N test is used to determine tentative tracks for approval or deletion.	**(a)** Root Mean Square (RMS) error in target position over time proves the accuracy of the CTRA-UKF model on highly curved tracks, compared to the KF model with constant velocity and constant acceleration models. **(b)** Considering different probabilities of detection, clutter density, and high and low resolution of Radars, RMS error in velocity is constant for the CTRA-UKF model.	For low-resolution radars, selecting or deleting tracks is considered after many cycles to prevent errors in the track management step.

(Continued)

Table 8 (continued)

Ref.	Year	Algorithms adopted	Performance metrics and achievements	Drawbacks
[82]	2018	**(a)** Iterative SRCKF iteratively improves the SRCKF process, leading to a lower error component. **(b)** To obtain cubature points and weights, a three-order cubature rule is used. **(c)** Instant time is updated, and then measurement update is done with the Gauss-Newton nonlinear iteration process.	**(a)** Mean square relative error of radial distance for SRCKF and ISRCKF filters shows that the latter has a lower error than the former. **(b)** Mean square relative error (MSRE) of radial distance improves with increasing iteration number, providing better filtering.	On-road experiments are not present.

Table 9 contains an analysis of various algorithms for target tracking using automotive Radar.

Table 9: An analysis of various target tracking algorithms

Ref.	Year	Algorithms adopted	Advantages	Drawbacks	Scenario
[102]	2025	**(a)** Track management methods: Naïve approach, track history-based, and existence probability-based. **(b)** track fusion architectures: sensor to sensor and global.	**(a)** Recall value of Radar is higher than a camera. **(b)** Existence probability-based method, depending on the sensor to global Dempster-Shafer rule, provides high F1 and MOTA scores, providing better performance than other methods.	Existence probability-based method does not provide better recall value than central tracking algorithm.	Dynamically changing road conditions.
[95]	2024	**(a)** Adaptive strong tracking extended Kalman filter. **(b)** DBSCAN algorithm to merge target tracks on a real main route. **(c)** Data association is done with JPDA.	**(a)** Root mean square errors in position and velocity are lower using ASTEKF. **(b)** Target vehicle's filtered tracks are almost the same as the real track, as it changes lanes and velocity filtering values converge fast with lesser error.	Only the Constant acceleration motion model is considered.	Road traffic scenario.
[84]	2023	**(a)** millimeter-wave Radar 4D point cloud-based measurement model. **(b)** For identifying the size of dynamic and static targets, a binary Bayesian filter was applied. **(c)** KF.	If the radial velocity is less, rotation angle estimation is done with velocity measurements from multiple points, and a shorter range is better for obtaining the rotation angle.	Research is required for motion models of moving targets and pose estimation of the ego-vehicle.	Roads with static and dynamic targets.
[92]	2022	**(a)** Micro-Doppler-based leg tracking framework for pedestrian detection. **(b)** EKF. **(c)** Data association is done with JPDA.	Micro-Doppler spectrum of the lower body of a pedestrian, dependent on time range, shows tracking of a foot movement.	Data association conflict arises if targets are close to one another.	Roads for pedestrians.
[99]	2022	**(a)** Hybrid SVSF presented by combining GVBL and Tanh-SVSF. **(b)** Non-linear GVBL parameter with SVSF.	NGVBL-SVSF attains the lowest RMSE in both low and high-uncertainty-level cases.	The cost of NGVBL-SVSF is higher than that of the Kalman filter, common SVSF, due to the hybrid switching.	Urban roads.
[86]	2022	Reweighted robust particle filter.	the proposed method has the lowest NMSE and lowest average Mahalanobis distance throughout the range of outlier ratios compared to other particle filters.	In detecting walking pedestrians with real data, few fluctuations are observed.	Roads for pedestrians.
[87]	2021	Track-before-detect algorithm uses kinematic constraints of targets on the road and graph theory algorithms.	In PD vs. SDR, TBD shows better performance in target detection and a high clutter elimination rate.	TBD can not perform properly in case of a large amount of signal loss.	Roads with less traffic.

(Continued)

Table 9 (continued)

Ref.	Year	Algorithms adopted	Advantages	Drawbacks	Scenario
[98]	2021	Imaging method for target moving with high speed, Doppler Range processing used.	Considering point spreading functions of moving target in the range-Doppler plot, DRP performs better than conventional RDP.	The results are proven theoretically only.	Roads with fast moving cars
[93]	2021	**(a)** IMM algorithm with JPDA algorithm. **(b)** DUKF applied.	IMM-JPDA-DUKF provides improved accuracy with the maneuvering target.	The algorithm is unable to correctly derive the target motion state of a high-velocity vehicle with maneuvering acceleration.	Curved roads with multiple targets.
[100]	2020	Deep neural network Radar TrackNet.	Improved performance with multiple object tracking accuracy and precision values compared to basic clustering tracker methods. The probability of missing an actual track is greater than showing false tracks.		Urban roads with pedestrians and different types of vehicles.
[94]	2020	Probability Generating Functional formulation used.	Plot of Wasserstein distance vs. traces from Nusense's data set shows the algorithm has improved average WSD and median WSD performance.	Computationally complex.	Urban roads.
[80]	2018	**(a)** Kalman filter applied on polar coordinates. **(b)** EKF is used to improve velocity measurements and minimize the measurement error where the motion state is in Cartesian coordinates.	Cascaded KF can estimate the velocity ambiguity number whether the target velocity is at the hopping stage.	The algorithm has not been tested on a real road environment.	Simulation environment considers long roads.
[77]	2018	**(a)** UKF applied to Constant Turn Rate and Acceleration (CTRA) motion model. **(b)** Linear regression technique. **(c)** JPDA algorithm applied for data association. **(d)** For track management M/N test is used.	RMS error in target position over time proves the accuracy of the CTRA-UKF model on highly curved tracks.	For Radar with low resolution, the decision to select or delete tracks is considered after a large number of cycles to prevent errors in the track management step.	Curved roads with multiple vehicles.
[82]	2018	**(a)** Iterative SRCKF. **(b)** To obtain cubature points and weights, a three-order cubature rule is used. **(c)** Measurement update is done with the Gauss-Newton nonlinear iteration process.	MSRE of radial distance improves with increasing iteration number, providing better filtering.	On-road experiments are not present.	Simulation model of urban roads.

5 Target Recognition and Classification

The road scenario in which automotive Radar operates is very cluttered, so the classification of targets with high accuracy is essential. A flowchart for the target recognition and classification process is depicted in Fig. 14. Using the raw Radar data, a potential target is observed and its features like RCS, range, and Doppler are extracted.

A training data set containing representative Radar data examples is required. Now, the data measured from the target is considered along with the training data. The result is classifying the new data, i.e., the new target, into different classes or categories. The target recognition problem in Radars can be addressed from an ML algorithm perspective. The principle of an ML is to find the direction from a group of unknown data and then utilize this to predict the next step in advance or classify the remaining data. ML algorithms are divided into three types: Supervised learning algorithms, Semi-supervised learning, and Unsupervised learning

algorithms. The supervised methods are applied when training datasets are available to predict the output of the algorithm, and the well-known examples include K-Nearest Neighbor (KNN) algorithm, Support Vector Machine (SVM) algorithm, and Artificial Neural Networks (ANN). Semi-supervised methods are used when labeled data is insufficient and unlabeled data is used for training the algorithm; certain Convolutional Neural Networks (CNNs) fall into this category. Unsupervised algorithms such as K-means clustering and Principal Component Analysis (PCA) are applied when labeled data is not available for training purposes.

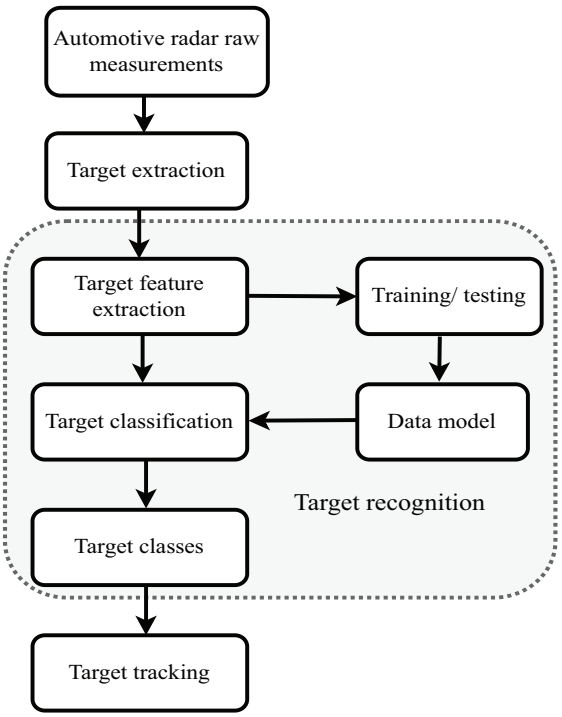

Figure 14: Signal flowchart of automotive radar for target recognition and classification

5.1 K-Nearest Neighbor (KNN) Algorithm

In the scenario of Automotive Radar data, the supervised learning algorithm, KNN algorithm [104], can be used to classify Radar signals into different categories based on their similarity to other signals. To derive this classifier, a training set containing representative examples of the Radar data is required. Data obtained from the Range-Doppler map is considered. The main steps for the KNN algorithm can be written as:

1. Calculation of distance between the fresh data point, known as query, and every data point in the training dataset with the help of a distance metric, e.g., Euclidean distance as used here:

$$Distance = \sqrt{(X_2 - X_1)^2 + (Y_2 - Y_1)^2} \tag{77}$$

   where X_2 and Y_2 are the new Velocity and Range values, respectively, and X_1 and Y_1 are the existing velocity and Range values from the training dataset;
2. This equation is conducted on each existing data point with the new data;
3. Once all distances are obtained, these are sorted in ascending order to find the k-nearest neighbors;
4. The k-nearest neighbors with the smallest distances are selected with k value, usually in odd numbers as 3 or 5;

5. Lastly, the class of the query point is obtained based on the majority class among the k-nearest neighbors.

5.2 Support Vector Machine (SVM) Algorithm

The SVM is a set of supervised learning algorithms used to classify targets, regression, and outlier detection [23]. The SVM algorithm chooses the decision threshold from an indefinite quantity of probable ones, leaving the biggest margin between the nearest data point and the hyperplane, called support vectors. A classifier of linear type is of the form,

$$f(x) = \mathrm{w}_s^T x + b \tag{78}$$

where w_s is weight vector and b is bias. Let the available dataset be $x_1, \ldots, x_n$ and the two class labels are termed as $y_i = (-1, 1)$. The decision threshold is defined as,

$$y_i \left(\mathrm{w}_s^T x + b\right) \geq 1 \quad \forall i \tag{79}$$

The issue of optimization is stated as,

$$Minimize : \frac{1}{2} \|w_s\|^2, \ \ subject\ to : y_i \left(\mathrm{w}_s^T x + b\right) \geq 1 \ \ \forall i \tag{80}$$

This problem is expressed by defining the Lagrangian

$$L = \frac{1}{2} \|w_s\|^2 + \sum_{i=1}^{n} \beta_i \left(1 - y_i \left(\mathrm{w}_s^T x + b\right)\right) \tag{81}$$

where β_i are the Lagrange multipliers. Considering derivatives of L with reference to $\frac{1}{2} \|w_s\|^2$ and b and making the result equal to zero, the final results are obtained,

$$w_s = \sum_{i=1}^{n} \beta_i y_i x_i \sum_{i=1}^{n} \beta_i y_i = 0 \tag{82}$$

After substituting w_s into L, the result is obtained as,

$$L = \sum_{i=1}^{n} \beta_i y_i - \frac{1}{2} \sum_{i=1}^{n} \sum_{i=1}^{n} \beta_i \beta_j y_i y_j \mathrm{x}_i^T x_j \tag{83}$$

The initial problem of optimization can be finally given as,

$$Increased\ to\ maximum : \sum_{i=1}^{n} \beta_i y_i - \frac{1}{2} \sum_{i=1}^{n} \sum_{i=1}^{n} \beta_i \beta_j y_i y_j \mathrm{x}_i^T x_j \ \ liable\ to : \sum_{i=1}^{n} \beta_i y_i = 0, \ \ \beta_i \geq 0 \tag{84}$$

So, if β_i is provided, then w_s will be obtained and finally the margin $m = \frac{2}{\|w_s\|}$ can be calculated.

A classifier based on bidirectional long short-term memory (LSTM) applies the feature of relative velocity, range, and signal amplitude to classify targets at ground level and targets at overhead on real roads, useful for collision avoidance [105]. FFT and cell-averaging CFAR (CA-CFAR) have been used for the implementation of this LSTM, which provides a precision of around 98.18% inside a range of value 13 m and a correctness of around 94.97% within a range of 20 m. A convolutional LSTM and a convolutional gated recurrent unit (GRU) are used to obtain the dynamics of input of the time-series range-velocity (RV) images to perform classification of the target [106]. The proposed network comprises one convolutional recurrent

layer, whose input is 2D time series signals received from an automotive Radar, a convolutional layer, and a fully connected layer. In [107], three types of neural network (NN) architectures are presented, namely, Visual Geometry Group (VGG16) but a scaled-down version, the ResNET-50 for better generalization, and a supervised algorithm Convolutional Neural Network (CNN) with LSTM, to extract features from segments of the micro-Doppler spectrogram. For target classification using the height, length, and width of a target, 3D point cloud data can be launched in orthogonal directions onto the yz, xy, and zx planes, respectively, to create images of three types [108]. A parallel input CNN or a serial input CNN is used to classify images of targets after detection from three features into one of the four types of targets, such as pedestrian, cyclist, sedan, or Sport Utility Vehicle (SUV). A Radar range-Doppler flow and a method for radial acceleration for clustering of Radar data point cloud helps in effective clustering in congested traffic conditions on urban roads [109]. This clustering is an unsupervised learning algorithm. DNN algorithm provides better classification of targets even if a specific target try to be imitate other targets [110]. In [111], a classification method based on phase estimation is proposed for pedestrians and vehicles. After the extraction of phase patterns obtained from received signals reflected from different targets and differences in phase, these are taken as inputs for a DNN.

A hybrid method of SVM and CNN techniques for target classification is proposed in [112]. At first, the range-Doppler image is obtained by 2D DFT, followed by the extraction of features of targets by CA-CFAR and a DBSCAN algorithm. Then, SVM is applied for the first stage classification, and finally, the remaining image samples with no identified category are used as input into the CNN to retrain. Based on conventional RCS, Root Radar Cross Section (RRCS) is defined in [113], for real-time target classification using 77 GHz FMCW Radar. The RRCS is determined by using the amplitudes of the received and transmitted signals from the frequency domain. Hence, the reflection characteristics of targets can be extracted from the amplitude of the transmitted signal. The SVM can be applied to pedestrian and vehicle classification based on the proposed characteristics obtained from RRCS. Another method of using SVM in conjunction with a Deep Learning (DL) model, specifically *You Only Look Once (YOLO)*, for classifying vehicles and humans is presented in [114]. The range-angle Cartesian plot is transformed into an image and used for training and classification with the YOLOv3 model. The SVM utilizes target boundary boxes from the YOLO V3 model to enhance classification, and by combining each result, the classification performance is further improved. The YOLO V3 is also presented in [115] for classifying humans, vehicles, and aerial vehicles, such as drones. This is applied after detecting range and angle using a rotating millimeter-wave (mmWave) FMCW Radar, where the range is calculated from Analog-to-Digital converter (ADC) samples, and the angle axis is calculated from the rotational frames. Another application of YOLO trained using a transformed range-angle domain is presented in [116]. In a Radar image, YOLO studies the bounding box and probability of class as a regression problem, assuming the location and type of the target by only looking at the image once, hence the name. These images are partitioned into grid cells, where each cell consists of bounding boxes and a confidence score, representing the likelihood of the target's presence based on the intersection over union (IoU). The performance of this model is presented in mean average precision (mAP). YOLO V4 is used in [117] also for obtaining IoU values. The YOLO V5 model has been utilized for human classification to achieve improved accuracy [118]. The DL can be applied to data of imaging Radar to classify vehicles, pedestrians, and cyclists and estimate their direction [119].

In [120], the classification of pedestrians' speed rate and movement of hands is done by applying unsupervised Principal Component Analysis (PCA) for the extraction of features. Then supervised classification algorithms like SVMs and KNN are used to classify between fast walk, slow walk, and slow walk while keeping hands in pockets of pedestrians. A high fidelity physics-based simulation method has been used in [121] for obtaining several spectrograms from the micro-Doppler parameters of the vulnerable road users like pedestrians. This is the training data for a 5-layer convolutional neural network, which achieves nearly

100% classification accuracy after five iterations. A method based on the Hough transform can be used to determine the direction of movement and the size of the vehicle [122]. An integrated method of classifier and tracking by KF leads to better tracking association and classification [123]. UKF is applied to a constant radial velocity model in Cartesian coordinates to track the location and velocity of the targets, and classification is performed using the KNN algorithm for stabilized classification of pedestrians and cyclists. The KNN algorithm is best suited for classification of vehicles by a type of bistatic Radar called the forward scattering Radar [124].

Considering the information obtained from a target's statistical RCS, the classification accuracy of around 90% and more has been achieved by the usage of Artificial Neural Network (ANN) [125]. In continuation of this work, more classification models have been introduced in [126], for different types of data from mmwave Radar, like distributed RCS data classification, 2D range-azimuth angle Radar images classification is proposed for Radars that scan in the direction of azimuth and Radar images in 3D for Radars which have elevation and azimuth beam-steering capability. Suppose targets are observed at long range, or Radar doesn't have imaging capability. In this case, methods based on statistical RCS and data from the time domain are employed, and an ANN model is applied for classification. Meanwhile, the CNN model is applied for classification based on range-phase images of radar data for short-range targets and radars with beam-steering. This paper shows that the model based on 3D Radar images shows the best classification results. CNN applied on dual automotive Radar system provides improved target classification [127]. A lightweight deep learning method based on the level of reflection of Radar data is used in [128] for target classification. Table 10 contains a detailed analysis of research works available regarding target recognition and classification using automotive Radar.

Table 10: An analysis of research works for target classification

Ref.	Year	Algorithms adopted	Performance metrics and achievements	Drawbacks
[119]	2025	**(a)** Spatial clustering method based on density to imaging Radar data projected in X-Y domain to cluster target data and filter out remaining data as noise. **(b)** Dividing out of data points on the X-Y domain is changed to an image and used as input to a DL network to classify the target and detect its direction of movement.	**(a)** Accuracy of classification is highest with 96.10% compared to ResNet50, GoogleNet. **(b)** This method showed the lowest average RMSE to assess the correctness of estimating the target's moving direction, at 9.68%, compared to other methods with the shortest runtime of 0.1 s.	In the case of pedestrians, the RMSE of the estimated angle is higher than that for cyclists and vehicles, making it difficult to predict the pedestrian's moving direction.
[105]	2024	**(a)** The Neural network is a Bidirectional long short-term memory-based classifier that uses the relative velocity, range, and signal amplitude to classify targets at overhead and road level targets on a real road. **(b)** FFT and cell averaging CFAR are used to implement the algorithm.	Classification of the reflector's installation height is observed to be accurate when the distance in-between the reflector and the Radar ranges from 13 to 3 m.	Percentage of *overhead*data wrongly predicted as *ground* is more than that of *ground* data wrongly predicted as *overhead*, and this increases with classification distance.
[108]	2022	**(a)** For classification using the height, length, and width of a target, a cloud of data comprising 3D points is projected in orthogonal directions onto the yz, xy, and zx planes, respectively, to create images of three types. **(b)** Parallel input CNN classifies targets using three parallel images after training.	**(a)** Classification accuracy for SUVs is highest, next for sedans and for pedestrians, and lastly for cyclists. **(b)** With increasing hidden layers from 1 to 5, classification accuracy remained almost the same, but training time increased.	Cyclists have spatial size the same as pedestrians and thus tend to be wrongly classified as pedestrians.

(Continued)

Table 10 (continued)

Ref.	Year	Algorithms adopted	Performance metrics and achievements	Drawbacks
[123]	2021	**(a)** UKF is applied to a constant radial velocity model in Cartesian coordinates. **(b)** Classification is done using the KNN algorithm for the stabilized classification of pedestrians and cyclists. **(c)** Integration of output from the classifier into the tracker helps to process uncertainty related to the target state.	Micro-Doppler images show less misclassification between closely related targets, such as teenagers and men, or between cyclists, compared to results obtained using a stand-alone classifier.	Only simulation model developed in MATLAB.
[115]	2021	**(a)** Range bin obtained from ADC samples in frequency bins and range calculated by applying a 1-dimensional FFT of the sampled IF signal. **(b)** Field of View is divided into angle bins. **(c)** YOLO V3 applied on data from angle vs. range heatmap plot.	**(a)** Precision: ratio of appropriately predicted positive results to predicted positive results. **(b)** Recall: ratio of rightly predicted positive results to results in the real positive class. **(c)** Specificity: ratio of actual negatives to all negatives. **(d)** F1 score: combining recall and precision. **(e)** Classification accuracy value of 97.4% obtained, based on above parameters.	For closely placed targets, bounding boxes overlap in range-angle maps. To resolve targets, these boxes must be made distinguishable, increasing complexity.
[126]	2021	**(a)** The proposed algorithm is based on statistical RCS values and data from the time domain, utilizing an ANN model for classification. **(b)** For short-range targets and Radars with beam-steering, the CNN model is applied for classification based on range-phase images of Radar data. **(c)** CNN is used for Radar that provides azimuth-elevation angle images and 3D images.	Image-based classification provides more accurate results compared to Doppler-based methods. The performance of the former remains the same for stationary targets, unlike the latter method.	Radar with imaging ability is more complicated than usual MIMO Radar.
[114]	2020	**(a)** Range-angle (RA) cartesian plot of Radar data transformed into an image form and utilized for training of target and classification of target with YOLO V3. **(b)** Detection points obtained from range-angle (RA) data through order static CFAR and range, RCS, angle, mean, variance, and kurtosis extracted from this matrix. **(c)** SVM gets target boundary boxes from the YOLOV3 model to improve classification.	Considering classification accuracy, the proposed method outperforms YOLO and SVM with target boundary boxes.	The accuracy of classification in humans is slightly lower than that of vehicles due to consistent changes in the arms and torsos of humans.
[116]	2020	**(a)** YOLO studies the bounding box and image class probability as a regression problem and assumes the location and type of target by only looking at the image once. **(b)** Images used for input are partitioned into grid cells, representing the chances of the presence of a target that depends on the IoU.	**(a)** Performance presented in mAP, called a general DL performance index, and in this paper, mAP with the threshold value of 0.5 IoU is obtained as 93.44%. **(b)** The Proposed method shows better recognition for long vehicles compared to SVM.	Classification performance of pedestrians is lower than that of trailers and cars.

(Continued)

Table 10 (continued)

Ref.	Year	Algorithms adopted	Performance metrics and achievements	Drawbacks
[120]	2020	**(a)** PCA is for the extraction of possible features, and t-SNE is used to decrease data dimensionality. **(b)** SVM and KNN are used to classify between fast walking, slow walking, and slow walking with hands in pockets of pedestrians.	**(a)** Range-Doppler plot and Doppler vs. time plot show that the slow walk and fast walk of the pedestrian are easier to distinguish. **(b)** Considering FMCW Radar, SVM provides better classification precision than KNN.	Slow walking with hands in pockets is the same as walking with free hands, which is not easily recognized.
[125]	2019	With information from a target's statistical RCS, the classification of a target is done using an Artificial Neural Network.	**(a)** A Huge amount of RCS images from various targets with varying aspect angles but at the exact range are considered. **(b)** At the range of 10 m, the accuracy of recognition is observed to be 99%.	The Accuracy of classification decreases with an increase in distance to the target.
[112]	2019	**(a)** A Hybrid method of SVM and CNN techniques for target classification is proposed. **(b)** Range-Doppler image obtained by 2D DFT, followed by extraction of features of targets by CA-CFAR and DB-SCAN. **(c)** SVM applied for first stage classification for classifying vehicle samples. **(d)** Remaining image samples with no identified category are used as input into the CNN to retrain.	**(a)** Precision: a measure of correctly predicted positive results to total predicted positive results. **(b)** Recall: a measure of rightly predicted positive results compared to results in the real positive class. **(c)** To improve recall for cyclists in the SVM method and precision of the same in CNN, this hybrid method is used.	Complex computational model.
[111]	2019	**(a)** Classification method based on phase estimation proposed for pedestrians and vehicles. **(b)** Phase patterns obtained from received signals and the phase differences are taken as inputs for a DNN.	**(a)** Accuracy of classification increases with an increasing number of nodes present in the hidden layer of the NN and is maximum at 25. **(b)** Accuracy decreases with an increase in hidden layers and so is set to 1. **(c)** With these parameters and input of phase difference, higher accuracy is observed.	Large amount of Radar data is required for better classification accuracy.
[106]	2018	Convolutional LSTM and convolutional GRU are used to obtain the dynamics of the input time-series RV images and classify a target.	**(a)** Activation function relu or tanh is used. **(b)** The ReLU-based model performs better than the baseline one	Complex computation.
[107]	2018	Three types of neural network architectures presented, VGG16, but a scaled-down version, the ResNET-50, and CNN with LSTM, to extract features from segments of micro-Doppler spectrogram	**(a)** CNN-LSTM provides better classification (93–83)% for car and pedestrian. **(b)** VGG provides accuracy of about 80% for car, pedestrian and bicycle.	Problem of overfitting for cases when less data is available. It is unable to detect differences in spectrograms of multiple target types.
[113]	2017	**(a)** The RRCS is defined by the amplitudes of the transmitted and received signal in frequency and used for the target classification. **(b)** Magnitude value of RRCS, moving outline along RRCS, and slopes around RRCS is obtained from distance-regulated FFT. **(c)** SVM is applied based on the above features.	**(a)** SVM applied on each feature separately shows that higher classification accuracy is obtained using the magnitude value of RRCS. **(b)** Better accuracy is obtained when all three features are used together for classification rather than using one or two features	

Table 11 contains an analysis of various algorithms used for target classification by automotive Radar.

Table 11: An analysis of various target classification algorithms

Ref.	Year	Algorithms adopted	Advantages	Drawbacks	Scenarios
[119]	2025	**(a)** Density based spatial clustering method. **(b)** Deep learning network for target classification and detection of its moving direction.	**(a)** Accuracy of classification is highest with 96.10% compared to ResNet50, GoogleNet. **(b)** This method showed the lowest average RMSE to assess the accuracy of estimating the target's moving direction, at 9.68%, compared to other methods with the shortest runtime of 0.1 s.	In the case of pedestrians, the RMSE of the estimated angle is higher than that for cyclists and vehicles, making it difficult to predict the pedestrian's moving direction.	Urban roads.
[105]	2024	Neural network, a classifier based on Bidirectional LSTM.	Classification of the reflector's installation height is observed to be accurate when the distance in-between the reflector and the Radar ranges from 13 to 3 m.	Percentage of overhead data wrongly predicted as ground is more than that of ground data wrongly predicted as overhead, and this increases with classification distance.	Road with static targets like buildings.
[108]	2022	**(a)** Cloud data is put across in orthogonal directions onto the yz, xy, and zx planes, respectively, to create images of three types. **(b)** Parallel input CNN and serial input CNN.	Classification accuracy for SUVs is highest for sedans, pedestrians, and cyclists. Cyclists have a spatial size similar to that of pedestrians and thus tend to be wrongly classified as pedestrians.		Urban roads with pedestrians and various kinds of vehicles.
[123]	2021	**(a)** UKF is applied to a constant radial velocity model in Cartesian coordinates. **(b)** Classification is done using the KNN algorithm. **(c)** Integration of output from classifier into the tracker.	Micro-Doppler images show less misclassification between closely related targets, such as teenagers and men, or between cyclists, compared to results obtained using a stand-alone classifier.	Only simulation model developed in MATLAB.	Simulation of roads for cyclists and pedestrians.
[115]	2021	YOLO V3 applied to data from angle vs. range heatmap plot.	A classification accuracy value of 97.4% was obtained based on precision, recall, specificity, and F1 score.	For closely placed targets, bounding boxes overlap in range-angle maps. To resolve targets, these boxes are to be made distinguishable, increasing complexity.	Urban roads.
[126]	2021	**(a)** Targets at the long-range or if the Radar sensor doesn't have the ability for imaging, methods used are based on statistical RCS value and data from the time domain with an ANN model. **(b)** For short-range targets and Radars with beam-steering, the CNN model is applied. **(c)** CNN is used for Radar that provides azimuth-elevation angle images and 3D images.	Image-based classification provides more accurate results compared to Doppler-based methods.	Radar with imaging ability is more complicated than usual MIMO Radar.	Urban roads with less traffic.

(Continued)

Table 11 (continued)

Ref.	Year	Algorithms adopted	Advantages	Drawbacks	Scenarios
[114]	2020	**(a)** Range-angle cartesian plot of Radar data transformed into an image and utilized for training of targets and classification of targets with YOLO V3. **(b)** SVM gets target boundary boxes from the YOLO V3 model to improve classification, and each classification result is combined.	Considering classification accuracy, the proposed method outperforms YOLO and SVM.	The accuracy of classification in humans is slightly lower than that of vehicles due to consistent changes in the arms and torsos of humans.	Urban roads with pedestrians and vehicles.
[116]	2020	The CNN model with YOLO.	**(a)** The Mean average precision (mAP), called a general deep learning performance index, with a 0.5 IoU threshold value, is obtained as 93.44%. **(b)** Provides better recognition for long vehicles than SVM.	Classification performance of pedestrians is lower than that of trailers and cars.	Roads with different types of vehicles and human targets.
[120]	2020	**(a)** PCA and t-SNE algorithms. **(b)** SVM and KNN.	Range-Doppler plots and Doppler vs. time plots show that the slow walking and fast walking of pedestrians are easier to distinguish.	Slow walking with hands in pockets is the same as walking with free hands, which is not easily recognized.	Roads for pedestrians.
[125]	2019	An Artificial Neural Network.	At range 10 m, recognition accuracy is observed to be 99%.	The Accuracy of classification decreases with an increase in distance to the target.	Urban roads.
[112]	2019	**(a)** Range-Doppler image obtained by 2D DFT, followed by extraction of features of targets by CA-CFAR and DB-SCAN. **(b)** SVM applied for the first stage classification for classifying vehicle samples. **(c)** Remaining image samples with no identified category are used as input into the CNN to retrain.	To improve recall for cyclists in the SVM method and precision of the same in CNN, this hybrid method is used.	Complex computational model.	Roads with pedestrians, cyclists and vehicles.
[111]	2019	A classification method using a DNN based on phase estimation is proposed.	**(a)** Accuracy of classification increases with an increasing number of nodes in the hidden layer of the neural network and is maximum at 25. **(b)** Accuracy decreases with an increase in hidden layers and so is set to 1. **(c)** With these parameters and input of phase difference, higher accuracy is observed.	Large amount of Radar data is required for better classification accuracy.	Urban roads.
[106]	2018	Convolutional LSTM and convolutional GRU.	**(a)** Activation function relu or tanh is used. **(b)** The ReLU-based model performs better than the tanh-based one	Complex computation.	Urban roads.
[107]	2018	Three types of neural network architectures presented, VGG16, but a scaled-down version, the ResNET-50 and CNN with LSTM.	CNN-LSTM provides better classification (93–83)% for car and pedestrian.	Problem of overfitting for cases when less data is available. It is unable to detect differences in spectrograms of multiple target types.	Roads with pedestrian, cyclist, and vehicle.

(Continued)

Table 11 (continued)

Ref.	Year	Algorithms adopted	Advantages	Drawbacks	Scenarios
[113]	2017	SVM is applied based on the magnitude value of RRCS, moving out of the line along RRCS and slopes around RRCS.	**(a)** SVM applied on each feature separately shows that higher classification accuracy is obtained using the magnitude value of RRCS. **(b)** Better accuracy is obtained when all three features are used together for classification rather than using one or two features.		Urban roads.

6 Research Challenges and Future Scope

6.1 Challenges in Automotive Radar Signal Processing

The challenges faced in the signal processing of automotive Radar are explained in brief.

1. Interference—The introduction of more radar-fitted vehicles on the road leads to interference, such as self-interference originating from Radar signals reflected by the vehicle and radome, cross-interference from separate radars on the same vehicle, and cross-interference from Radars on another vehicle. Based on the waveforms, these are primarily FMCW-FMCW and FMCW-PMCW interference, and the interference level depends on the separation between Radars, beam pattern, and signal processing method. Interferences increase the likelihood of false alarms and obscure actual targets.
   Solution: Methods like matched filtering for reducing FMCW waveform interference, and CDMA for reducing PMCW waveform interference are used. Recently, neural network-based mitigation methods have been studied.
2. High resolution—Automotive Radar is required to obtain information on the surrounding targets and classify them. For this purpose, high resolution is required in range, Doppler, elevation, and azimuth angles. High resolution is obtained using 2D-FFT in the range-Doppler domain, increasing the processor cost.
   Solution: To maintain a balance between angular resolution and unambiguous field of view, in uniform rectangular arrays (URA), the resolution and field of view are monitored by horizontal and vertical antenna spacings. More research is underway to properly calibrate the array after vehicle integration and throughout Radar's lifespan.
3. Estimation of parameters in Multipath and clutter scenarios—The operation scenario includes various targets like pedestrians, vehicles, animals, bridges, road structures, etc. Automotive Radar has to operate accurately to detect, track, and classify every target even in the presence of multipath propagation in urban road scenarios. The multi-path effect increases false alarms. The tracking of low-altitude targets, such as vehicles, is affected mainly by ground clutter.
   Solution: Radar detection methods, based on the Convolutional Neural Network, can be used for complex clutter conditions.
4. Multi-target detection and ghost object removal—The detection of multiple targets is a difficult task as it involves proper clustering of Radar data associated with a specific target and tracking the position of every target in motion. Multi-target tracking algorithms can be applied to track the positions of multiple targets continuously. Sometimes, multiple radar reflections of the Radar signal produce ghost targets, i.e., targets which are not present.
   Solution: To eliminate such an ambiguity, neural network-based classifiers can be used.

5. Detection in low SNR environments-Radars can usually operate under low SNR environments, like weather conditions with fog or snow. But in very adverse conditions, especially for automotive purposes, detection problems may occur.
   Solution: During extreme bad weather conditions, continuous wave Radars with longer observation time are required for high range detection and range resolution.
6. Real-time constraints in embedded processing. The Operation of automotive Radar is a time-critical process. It is designed to detect and track targets, update target positions, and monitor the surrounding environment, all within a strict time duration, failing which can lead to accidents.
   Solution: Adaptive signal processing and efficient algorithms with reduced computational complexities help to provide real-time, accurate Radar data.
7. Dataset scarcity and lack of standardization—Authorities such as EURO NCAP and the New Car Assessment Program for Southeast Asia (ASEAN NCAP) are present for automotive Radar standardization. However, a global standardization for regulations is still unavailable commercially. Additionally, the scarcity of real-time Radar data is another challenge to carry out further research in this field.
   Solution: Country-specific Radar datasets are available for public use, which resolves this issue to some extent.

6.2 Innovations and Future Trends

The aim of research in automotive Radar has changed from hardware to millimeter-wave systems and RF signal processing methods. So, recent research has focused on digital modulation techniques, Cognitive Radar, Radar imaging, integrated sensing and communication, machine learning, and Quantum Radar. The research and evolution in this sector are outlined here in a brief [15]:

1. AI-driven Radar and Cognitive Radar-Target classification is required for risk assessment, sensing the resources, and finally, automated control. For target recognition and classification, a machine learning algorithm is usually adopted. In this aspect, a large, real or synthetic Radar dataset is required to be available for further work. Artificial Intelligence and Machine learning algorithms can be further utilized for localization, interference reduction, waveform design, and other specialized technologies. Like, Neural network such as CNN can be applied for the processing of non-clustered target detections [129]. In [130], a Deep Learning and Image Processing-based Height Estimator is applied to create a real time system that uses image data to obtain heights of buildings in the paths of unmanned aerial vehicles. Here, Google Street view images are used, which can be replaced with Radar images. An automated multi-path annotation method converts a conventional large Radar dataset into multi-path labeled data, on which deep learning-based signal processing is applied to challenges present in such scenarios [131]. A Cognitive Radar [132] can sense the environment, reason, and learn with the help of supervised techniques, and finally adapt its parameters to meet the changes in the scenario.
2. Radar imaging and 4D Radar—Imaging Radar is an innovative application, beneficial for measuring target RCS. Here, the echoes from the target are converted into digital form, sent to the data recorder for processing, and finally shown as an image. Range-azimuth imaging can be obtained by application of Super-Resolution Angular Spectra Estimation Network [133]. Another such technique is the 4D Radar [134,135] used to measure elevation and azimuth angles, range, and Doppler of the target, while providing high resolution and wider field-of-view. In the case of 4-dimensional imaging Radar, a waveform for MIMO-PMCW is better suited than the MIMO-FMCW model [136]. Coherent Radar networks can be applied to create a Radar image with better SNR and azimuth resolution and to obtain vectorial velocities of targets [137].

3. Integrated sensing and communication (ISAC)—In case of ISAC, the Radar and communication systems can coexist by either sharing the frequency spectrum, or by sharing the same hardware, or by using waveforms from the communication system for Radar functioning [138]. For understanding ISAC, in-depth knowledge of communication is also required. Like in [139], the structure of cell-free massive MIMO has been described for wireless communication networks and green communication methods.
4. Radar simulation and synthetic data for training—To compensate for the scarcity of real-time Radar data, synthetic data is artificially produced. This is very beneficial for the training process of the ML algorithms used for target tracking and classification.
5. Quantum Radar and metamaterial-based Radars—Recent innovations involve Quantum radar [140], which generates quantum entangled signals related to a reference signal present at the receiver. This Radar works better than conventional ones in low signal echoes and high noise, and is quite resilient to deception and electronic jamming.

6.3 Utility of Autonomous Driving

The main application of automotive Radar is to prevent accidents by using warning signals and automated safety functions, and thus achieve the Vision Zero objectives of zero deaths in traffic accidents. The main utilities of autonomous driving can be listed as

1. Safer Roads—As stated in the introduction, reducing road accidents is one of the most important motivations for autonomous vehicles. Automotive Radar sensors can perceive the environment better than human drivers; thus, driving errors like drunk driving and sleepy driving will be significantly reduced.
2. Improved traffic management and fuel efficiency—Automated vehicles will lead to better traffic management and reduced accident rates. Additionally, as vehicles are designed to enhance efficiency in acceleration and braking, fuel efficiency is expected to improve, resulting in reduced carbon emissions. Thus, helping the environment as a whole.
3. Free time for drivers—In levels 3, 4, and 5 of automation, most of the driving tasks will be done by automation, so drivers will have more time to spend on themselves. Accidents caused by drowsy drivers are a widespread incident, with automation, and drivers can rest on long rides.
4. Improved way of living—Even disabled persons and older citizens would be able to experience driving instead of relying on others.
5. Providing newer job opportunities—Job opportunities will be made in automobile, electronics, and software engineering, among others. With the mass production of automated cars, their price will eventually decrease and become more affordable for the general public.

7 Benchmark Datasets and Standards for Automotive Radar

7.1 Radar Datasets

Recent innovations in automotive Radar for target detection, tracking, and classification are being achieved by using ML algorithms. For the training data of the ML algorithms, a large Radar dataset is required, which contains an authentic and detailed description of the surrounding environment. Several Radar datasets are available publicly, and the important datasets are described concisely in this work. These datasets are presented in a comparative table in the following Table 12.

The nuScenes dataset [141] is the most well-known one that provides a large-scale Radar point cloud dataset obtained from 3-dimensional Radars [142]. This multimodal dataset offers 360-degree coverage of the entire surroundings, encompassing data from nighttime and rainy weather conditions, as well as features of objects and a detailed description of scenes. Stochastic geometry is used for modeling large automotive

Radar networks in crowded urban scenarios, where interfering radar and clutter are assumed to be instances of a spatial stochastic point process [143].

Table 12: A comparative presentation of the different Radar datasets

Radar dataset	Availability of database	Type of data	Volume	Task	Experiment scenario	Limitations
NuScenes [141]	2019	Radar 3D point cloud dataset from 5 Radars.	1.3 M frames.	Target detection and tracking.	Public roads during night and rainy conditions.	Variety of weather conditions are not included.
K-Radar [144]	2022	4D Radar Tensors.	35 K frames.	Target detection and tracking.	Various weather conditions including lightning.	The Radar field-of-view is 107 degrees.
RadarScenes [145]	2020	Radar 3D point cloud dataset from 4 Radars.	118 M points.	Target detection, tracking, classification, and instance segmentation.	Urban roads.	Bounding box annotations are not provided.
Oxford Radar Robotcar [146]	2020	Range-azimuth heatmap from rotating Radar.	240 K frames.	Target localization.	Adverse weather, lightning.	Moving vehicles are only considered as targets.
Astyx [147]	2020	Radar 5D point cloud dataset.	546 frames and 1000 points per frame.	Simultaneous localization and mapping of the target.	Urban roads.	Not tested in changing weather conditions.
View-of-Delft [148]	2022	Radar 4D point cloud dataset.	8.6 K frames.	Target detection and tracking.	Sunny weather, dense traffic.	Only clear weather is considered.
Boreas [149]	2022	Range and azimuth angle heatmap.	7.1 K frames.	Object detection in 3-dimension and localization.	Sunny weather.	Sparse Radar data is provided.
Carrada [150]	2021	Range and angle maps, range and Doppler maps, and range-angle-Doppler maps.	7.1 k annotated frames.	Detection and tracking of target and semantic segmentation.	Urban roads.	Object classification is not done.
RADIATE [151]	2021	Radar images of range and azimuth angle.	200 K labeled road objects with 8 categories.	Target detection, tracking, and understanding of road scenes in adverse weather.	Urban and suburban roads under various weather conditions like night, fog, snow, and rain.	Movement of target is not used as recognition tool.

The KAIST-Radar (K-Radar) [144] dataset is a 3-dimensional target detection dataset using the 4-dimensional Radar tensor, which describes a wide variety of scenarios. The 4-dimensional Radar tensor (DRT) consists of range, elevation, azimuth, Doppler, and power measurements, which help to preserve 3-dimensional spatial information for a proper 3-dimensional impression of targets.

Another dataset, the RadarScenes [145], is mainly available for models that have point-wise interpretations. This dataset is helpful for the development of ML algorithms used for mobile targets on the road, labeling them into 11 categories, including car, truck, train, bus, pedestrian, animal, and others.

The Oxford Radar Robotcar dataset [146] contains range and azimuth heatmap data used for target localization and fusion models of Lidar-Radar. This dataset comprises approximately 240,000 scans from a Navtech Radar, covering various weather conditions, lightning situations, and traffic scenarios.

In the Astyx dataset [147], the radar provides a 5-D point cloud data comprising range, elevation, azimuth, relative radial velocity, and a feedback magnitude. The feedback magnitude defines the reflection strength of the target detected by the Radar.

The main feature of the View-of-Delft (VoD) [148] automotive dataset is the (3 + 1D) Radar data, which includes range, elevation, and azimuth angles with Doppler, along with data from 3-dimensional Lidar and a stereo camera. The dataset has about 123,100+ 3-dimensional bounding box annotations of stagnant and moving objects. It also provides details of the semantic map and localization data of vehicles collected from urban road scenarios.

The Borreas [149] dataset for autonomous driving was accumulated by driving on a specific route map for one year. In this set, over 350 km of driving data are provided, including data collected under harsh weather conditions such as rain and snow. The sensors used here include a 360-degree Navtech Radar, a Lidar, and a camera. This dataset is utilized for object detection in 3D, metric localization, and odometry.

The Camera and Automotive Radar (Carrada) dataset [150] consists of synchronized Radar and camera data with range-angle-Doppler mapping. This is used as a basis for semantic segmentation with range-DOA or range-Doppler Radar presentations for target detection.

Radar Dataset In Adverse Weather (RADIATE) dataset [151] is used for target detection, tracking, and understanding of different road scenarios under various weather conditions like sunny, overcast, nighttime, rain, fog and snow. The unique feature of RADIATE is that eight road objects are labeled here, which include van, bus, truck, car, motorbike, cycle, group of pedestrians, and single pedestrian.

7.2 Standards and Evaluation Metrics

The standards and evaluation metrics are required for the performance evaluation of automotive Radar and comply with regulations. Two of the important standards defined are IEEE Standards Association P3116 [152], and European Telecommunications Standards Institute (ETSI) EN 302 264 [153]. The IEEE standard is used for the evaluation of performance metrics and testing techniques for applications of ADAS and the Automated Driving System (ADS). This standard defines the static parameter metrics, e.g., range, DOA, and velocity resolution, and the Field-of-View, and the dynamic parameter metrics like automotive Radar's ability to resolve different targets in separate trajectories. The ETSI standard is applicable for short-range Radar with the operating frequency of 77 to 81 GHz. This contains technical specifications, tests for integrated transceivers, and separate transmit and receive systems.

The static evaluation metrics of automotive Radar include range, DOA, and Doppler resolution, Field-of-View, maximum and minimum detectable range, maximum and minimum detectable velocity, and RCS.

The dynamic evaluation metrics of automotive Radar include the probability of detection of targets, the ability to detect targets present in separate trajectories, detection in various adverse weather conditions, and the probability of false alarm rate.

8 Lessons Learned

This paper provides an overview of conventional automotive radar signal processing algorithms, highlighting their advantages and limitations for applicability to vehicular radar scenarios, and offers insights into new approaches for performance improvements. In particular, range-Doppler processing, target location and direction detection, tracking, and classification methods are discussed, specifically for high-resolution automotive Radars.

- Overview of Automotive Radar: A brief evolution of Automotive Radar and its application in the ADAS of autonomous vehicles and economic development is provided. A signal processing methodology is

described, including the mathematical model for range and velocity measurement, to give information on the basic working principle of automotive Radar. A brief review of the different waveforms used in automotive Radar, along with their respective mathematical equations, is presented. A comparative analysis of these waveforms is presented in a tabular format to help determine the specific waveform for different functions. This article also examines common waveform interference problems from different types of radars, which are assumed to be the source of interference, and radars assumed to be the victims.

- Target detection and DOA estimation: The target detection signal processing architecture is briefly described. Various DOA evaluation algorithms, along with their numerical models, are studied, including Bartlett beamforming, MVDR beamforming, MUSIC, and ESPRIT. This article presents an extensive study of various relevant algorithms used by researchers for angle estimation. Analytical comparisons of all these algorithms are presented in tabular form, highlighting their merits and demerits. DOA estimation of a target is a primary requirement, and this section provides in-depth knowledge on this.
- Target tracking: After target detection, filtering and tracking techniques for obtaining target motion dynamics are required to stay informed about the target's position. Target tracking involves a motion model for the target, filtering for target state estimation and data association, and track management. The filtering techniques mainly include the KF, the EKF, the UKF, and the Bayesian filter. Tracking targets is essential to avoid a collision, as in the ACC scenario. This paper provides an overview of various relevant algorithms that researchers use for tracking processes. Analytical comparisons of all these algorithms are presented in tabular form, highlighting their merits and demerits.
- Target recognition and classification: It is necessary to classify Radar signals into different categories based on their similarity to other signals. The algorithms used for this purpose include KNN and SVM, among others. This article provides detailed information on various relevant algorithms used by researchers for target classification, helping to better understand the process. Analytical comparisons of all these algorithms are presented in tabular form, highlighting their merits and demerits.
- Research challenges and future scope: Some of the major challenges for automotive Radar cases include interference mitigation, high resolution, parameter estimation in multipath scenarios, and target classification with Machine Learning. A brief knowledge of the various future scopes, like AI Radar, and integrated Radar and communication, is required to understand how the world is progressing in the automotive applications of Radar
- Benchmark datasets for automotive Radar: New research on automotive Radar is done mainly with the help of ML algorithms. For training these algorithms, a large amount of training data is required. An overview of the publicly available Radar datasets, highlighting their types of data and the tasks they can accomplish, is beneficial. Additionally, the standards and metrics for evaluating the parameters of automotive Radars are presented for further research.

9 Conclusions

As the vehicle industry moves towards full automation, various challenges will arise, and innovative solutions will be researched. Improved signal processing techniques will be introduced to utilize automotive Radar efficiently. As per the Automotive Radar Market Size, Share, Analysis Report, this industry is predicted to reach US Dollars 22.83 billion by 2032. There is a vast global demand for ADAS technologies, and the dominant sensor for this is the automotive Radar. Hence, this extensive picture of Radar signal processing is of utmost importance. Automotive radar signal processing techniques, along with a comparative analysis of various waveforms, are summarized here to enhance understanding of the working principles. I have a detailed review of the target detection and various DOA estimation algorithms for you, which is a necessary piece of research on this topic. Along with conventional MUSIC and ESPRIT algorithms, innovative ones

such as E-MUSIC, group-sparsity-based, DML-based, and digital beamforming techniques are reviewed, highlighting their benefits and a few complexities. After target positioning, real-time tracking of the target is necessary, for which various algorithms have been discussed here, along with comparison tables highlighting their respective advantages and disadvantages. The tracking filters, such as KF, EKF, and Bayesian filters, as well as improved versions, like SRCKF and track-before-detect methods, are studied. Also, the entire tracking method, with data associated with measuring tracks and track management, is discussed. Classification of targets is required in real road scenarios to avoid clutter and false targets. It has been observed that target recognition and classification using machine learning (ML) algorithms are becoming increasingly important research topics. Algorithms for this technology have been thoroughly discussed, along with their importance and limitations. For the training purpose of these ML algorithms, a large amount of training data is required to understand the Radar environment. Some databases are openly available for conducting new research. A survey of the radar datasets is presented here, which shows the type of data and the tasks they can accomplish. Standards and parameter metrics of automotive radar are also provided here. The challenges faced in the automotive Radar signal processing field have also been described here to aid in further work to overcome them. A comprehensive picture of the signal processing technique typically used for automotive Radar is provided here to help better understand and inform future research in this area.

Acknowledgement: Pallabi Biswas and Samarendra Nath Sur acknowledge administrative and technical support from Sikkim Manipal Institute of Technology, Sikkim Manipal University, Sikkim, India.

Funding Statement: This work was supported in part by the National Science and Technology Council, Taiwan: NSTC 113-2410-H-030-077-MY2.

Author Contributions: Conceptualization: Samarendra Nath Sur and Rabindranath Bera; Investigation: Pallabi Biswas and Samarendra Nath Sur; Methodology: Rabindranath Bera, Samarendra Nath Sur and Chun-Ta Li; Supervision: Samarendra Nath Sur and Rabindranath Bera; Visualization: Pallabi Biswas and Agbotiname Lucky Imoize; Writing—original draft: Pallabi Biswas, Samarendra Nath Sur and Agbotiname Lucky Imoize; Writing—review and editing: Samarendra Nath Sur, Agbotiname Lucky Imoize and Chun-Ta Li. All authors reviewed the results and approved the final version of the manuscript.

Availability of Data and Materials: Data sharing not applicable to this article as no datasets were generated during the current study.

Ethics Approval: Not required.

Conflicts of Interest: The authors declare no conflicts of interest to report regarding the present study.

Abbreviations

ADAS	Advanced Driver Assistance System
ACC	Adaptive Cruise Control
AEB	Automotive Emergency Braking
LRR	Long Range Radar
MRR	Medium Range Radar
SRR	Short Range Radar
FMCW	Frequency Modulated Continuous Wave
SNR	Signal to Noise Ratio
DOA	Direction of Arrival
RCS	Radar Cross Section
MUSIC	Multiple Signal Classification

ESPRIT	Estimation of Signal Parameters via Rotational Invariance Technique
PMCW	Phase Modulated Continuous Wave
PRF	Pulse Repetition Frequency
MIMO	Multiple Input Multiple Output
TDM/FDM	Time Division Multiplexing/Frequency Division Multiplexing
DDM	Dopple Division Multiplexing
PSD	Power Spectral Density
CFAR	Constant False Alarm Rate
GOCA-CFAR	Greatest of Cell Averaging Constant False Alarm Rate
SOCA-CFAR	Smallest of Cell Averaging Constant False Alarm Rate
OS-CFAR	Order Static Constant False Alarm Rate
MVDR	Minimum Variance Distortionless Response
CS	Compressive Sensing
SVM	Support Vector Machine
CTR	Constant Turn Rate
CTRA	Constant Turn Rate and Acceleration
KF	Kalman filter
EKF	Extended Kalman filter
UKF	Unscented Kalman filter PDF Probability Density Function
CKF/SRCKF	Cubature Kalman Filter/Square root Cubature Kalman Filter
JPDAF	Joint Probabilistic Data Association Filter
DRP	Doppler Range Processing
PD	Probability of Detection
SDR	Signal to Disturbance Ratio
RMSE	Root Mean Square Error
KNN	K-Nearest Neighbor
LSTM	Long Short Term Memory
CNN	Convolutional Neural Network
PCA	Principal Component Analysis

References

1. Sur SN, Bera S, Bera R, Bhaskar D, Shome S. Spread spectrum radar for vehicular application. In: 2018 IEEE MTT-S International Microwave and RF Conference (IMaRC). Kolkata, India: IEEE; 2018. p. 1–4.
2. World Health Organization. Global Status Report on Road Safety. Geneva: World Health Organization; 2023. [cited 2025 Feb 1]. Available from: https://www.who.int/publications/i/item/global-status-report-on-road-safety-2023.
3. Kukkala VK, Tunnell J, Pasricha S, Bradley T. Advanced driver-assistance systems: a path towards autonomous vehicles. IEEE Consum Electron Mag. 2018;7(5):18–25. doi:10.1109/mce.2018.2828440.
4. Giuffrida L, Masera G, Martina M. A survey of automotive radar and lidar signal processing and architectures. Chips. 2023;2(4):243–61. doi:10.3390/chips2040015.
5. Barbosa FM, Osório FS. Camera-radar perception for autonomous vehicles and ADAS: concepts, datasets and metrics. arXiv:2303.04302. 2023.
6. Alland S, Stark W, Ali M, Hegde M. Interference in automotive radar systems. IEEE Signal Process Mag. 2019;36(5):45–59.
7. Yan B, Roberts IP. Advancements in millimeter-wave radar technologies for automotive systems: a signal processing perspective. Electronics. 2025;14(7):1436. doi:10.3390/electronics14071436.
8. Waldschmidt C, Hasch J, Menzel W. Automotive radar—from first efforts to future systems. IEEE J Microw. 2021;1(1):135–48. doi:10.1109/jmw.2020.3033616.
9. Magosi ZF, Eichberger A. A novel approach for simulation of automotive radar sensors designed for systematic support of vehicle development. Sensors. 2023;23(6):3227. doi:10.3390/s23063227.

10. Abd El-Hameed AS, Ouf EG, Elboushi A, Seliem AG, Izumi Y. An improved performance radar sensor for K-band automotive radars. Sensors. 2023;23(16):7070. doi:10.3390/s23167070.
11. Patole S, Torlak M, Wang D, Ali M. Automotive radars: a review of signal processing techniques. IEEE Signal Process Mag. 2017;34(2):22–35. doi:10.1109/msp.2016.2628914.
12. Loeffler A, Zergiebel R, Wache J, Mejdoub M. Advances in automotive radar for 2023. In: 2023 24th International Radar Symposium (IRS). Berlin, Germany; 2023. p. 1–8.
13. Tavanti E, Rizik A, Fedeli A, Caviglia DD, Randazzo A. A short-range FMCW radar-based approach for multi-target human-vehicle detection. IEEE Trans Geosci Remote Sens. 2022;60:1–16. doi:10.1109/tgrs.2021.3138687.
14. Händel C, Konttaniemi H, Autioniemi M. State-of-the-Art Review on Automotive Radars and Passive Radar Reflectors. Arctic Challenge Research Project; 2018. [cited 2024 Dec 1]. Available from: https://urn.fi/URN:ISBN:978-952-316-223-5.
15. Engels F, Heidenreich P, Wintermantel M, Stäcker L, Kadi MA, Zoubir AM. Automotive radar signal processing: research directions and practical challenges. IEEE J Sel Top Signal Process. 2021;15(4):865–78. doi:10.1109/jstsp.2021.3063666.
16. Bera S, Sur SN, Singh AK, Bera R. RCS measurement and ISAR imaging radar in VHF/UHF radio channels. Int J Remote Sens. 2024;45(7):2159–81. doi:10.1080/01431161.2024.2326533.
17. Bilik I, Longma O, Villeval S, Tabrikian J. The rise of radar for autonomous vehicles: signal processing solutions and future research directions. IEEE Signal Process Mag. 2019;36(5):20–31. doi:10.1109/msp.2019.2926573.
18. SAE International. SAE J3016 Update; 2021. [cited 2025 Mar 13]. Available from: https://www.sae.org/blog/sae-j3016-update.
19. Malaquin C, Bonnabel A. Radar and Wireless for Automotive: Market and Technology Trends 2019; 2019. [cited 2025 Feb 1]. Available from: https://medias.yolegroup.com/uploads/2019/03/YD19009_Radar_and_Wireless_for_Automotive_2019_Sample-2.pdf.
20. Srivastav A, Mandal S. Radars for autonomous driving: a review of deep learning methods and challenges. IEEE Access. 2023;11:1–22. doi:10.1109/access.2023.3312382.
21. Gerstmair M, Melzer A, Onic A, Huemer M. On the safe road towards autonomous driving. IEEE Signal Process Mag. 2019;36(5):60–99.
22. Venon A, Dupuis Y, Vasseur P, Merriaux P. Millimeter wave FMCW RADARs for perception, recognition and localization in automotive applications: a survey. IEEE Trans Intell Veh. 2022;7(3):533–55. doi:10.1109/tiv.2022.3167733.
23. Gamba J. Radar signal processing for autonomous driving. In: Signals and communication technology. Singapore: Springer Nature Singapore Pte Ltd.; 2020.
24. Sun S, Zhang YD. 4D automotive radar sensing for autonomous vehicles: a sparsity-oriented approach. IEEE J Sel Top Signal Process. 2021;15(4):879–91. doi:10.1109/jstsp.2021.3079626.
25. Thornton CE, Howard WW, Buehrer RM. Online learning-based waveform selection for improved vehicle recognition in automotive radar. In: ICASSP 2023–2023 IEEE International Conference on Acoustics, Speech and Signal Processing (ICASSP). Greece: Rhodes Island; 2023. p. 1–5.
26. Ramasubramanian K, Ginsburg B. AWR1243 Sensor: Highly Integrated 76-81 GHz Radar Front-End for Emerging ADAS Applications. Texas Instruments; 2017. [cited 2025 Feb 1]. Available from: https://www.ti.com/lit/wp/spyy005/spyy005.pdf.
27. Hakobyan G, Yang B. High-performance automotive radar: a review of signal processing algorithms and modulation schemes. IEEE Signal Process Mag. 2019;36(5):32–44. doi:10.1109/msp.2019.2911722.
28. Caffa M, Biletta F, Maggiora R. Binary-phase vs. frequency modulated radar measured performances for automotive applications. Sensors. 2023;23(11):5271. doi:10.3390/s23115271.
29. Kahlert M, Fei T, Tebruegge C, Gardill M. Stepped-frequency PMCW waveforms for automotive radar applications. IEEE Trans Radar Syst. 2025;3:233–45. doi:10.1109/trs.2025.3528773.
30. Shome S, Bera R, Maji B, Sur SN, Bera S. Embedded digital MIMO radar using SDR for target detection and RCS measurement. IETE J Res. 2016;62(1):100–5. doi:10.1080/03772063.2015.1084244.

31. Sun S, Petropulu AP, Poor HV. MIMO radar for advanced driver-assistance systems and autonomous driving. IEEE Signal Process Mag. 2020;37(4):98–117. doi:10.1109/msp.2020.2978507.
32. Uysal F, Sanka S. Mitigation of automotive radar interference. In: 2018 IEEE Radar Conference (RadarConf18). Oklahoma City, OK, USA: IEEE; 2018.
33. Sur SN, Bera S, Bera R, Shome S. Spread spectrum radar for target characterization. Telecommun Radio Eng. 2019;78(14):1223–31.
34. Tamang ND, Sur SN, Bera S, Bera R. A review on spread spectrum radar. In: Advances in electronics, communication and computing: ETAEERE-2016. Singapore: Springer; 2017. p. 653–64 doi:10.1007/978-981-10-4765-7_68.
35. Sur SN, Bera S, Singh AK, Shome S, Bera R, Maji B. Polyphase coded radar for target characterization in the open range environment. Measurement. 2021;167:108247. doi:10.1016/j.measurement.2020.108247.
36. Mazher KU, Graff A, González-Prelcic N, Heath RW. Automotive radar interference characterization: FMCW or PMCW? In: ICASSP 2024–2024 IEEE International Conference on Acoustics, Speech and Signal Processing (ICASSP). Seoul, Republic of Korea; 2024. p. 13406–10.
37. Chen S, Klemp M, Taghia J, Kühnau U, Pohl N, Martin R. Improved target detection through DNN-based multichannel interference mitigation in automotive radar. IEEE Trans Radar Syst. 2023;1:75–89. doi:10.1109/trs.2023.3279013.
38. Kazazi J, Kamarei M, Fakharzadeh M. RD-CFAR: fast and accurate constant false alarm rate algorithm for automotive radar application. TechRxiv. 2025 Feb 07. doi:10.36227/techrxiv.173895066.68496282/v1.
39. Zhang J, Fang C, Zheng Q, Tong Z. A novel method for micro-motion target detection and ghost track suppression in automotive radar. IET Conf Proc. 2024;2023(47):883–8. doi:10.1049/icp.2024.1203.
40. Kazazi J, AleMohammad SMM, Kamarei M. U-Net-based automotive radar target detection and recognition. In: 2024 32nd International Conference on Electrical Engineering (ICEE). Tehran, Iran; 2024. p. 1–5.
41. Cho S, Song H, You KJ, Shin HC. A new direction-of-arrival estimation method using automotive radar sensor arrays. Int J Distrib Sens Netw. 2017;13(6):155014771771362. doi:10.1177/1550147717713628.
42. Sim H, Lee S, Kang S, Kim SC. Enhanced DOA estimation using linearly predicted array expansion for automotive radar systems. IEEE Access. 2019;7:47714–27. doi:10.1109/access.2019.2910120.
43. Xu S, Wang J, Yarovoy A. Super resolution DOA for FMCW automotive radar imaging. In: IEEE Conference on Antenna Measurements & Applications (CAMA). Sweden: IEEE; 2018. p. 1–4.
44. Sun R, Suzuki K, Owada Y, Takeda S, Umehira M, Wang X, et al. A millimeter-wave automotive radar with high angular resolution for identification of closely spaced on-road obstacles. Sci Rep. 2023;13(1):1–15. doi:10.1038/s41598-023-30406-4.
45. Li Y, Zhang C, Song Y, Huang Y. Enhanced beamspace MUSIC for cost-effective FMCW automotive radar. IET Radar, Sonar Navig. 2020;14(2):257–67.
46. Maisto MA, Dell'Aversano A, Brancaccio A, Russo I, Solimene R. A computationally light MUSIC based algorithm for automotive RADARs. IEEE Trans Comput Imaging. 2024;10:446–60. doi:10.1109/tci.2024.3369412.
47. Kahlert M, Xu L, Fei T, Gardill M, Sun S. High-resolution DOA estimation using single-snapshot music for automotive radar with Mixed-ADC allocations. In: 2024 IEEE 13rd Sensor Array and Multichannel Signal Processing Workshop (SAM). Corvallis, OR, USA; 2024. p. 1–5. doi:10.1109/sam60225.2024.10636418.
48. Lee S, Yoon YJ, Lee JE, Sim H, Kim SC. Two-stage DOA estimation method for low SNR signals in automotive radars. IET Radar Sonar Navig. 2017;11(11):1613–9.
49. Shao M, Fan Y, Zhang Y, Zhang Z, Zhao J, Zhang B. A novel gridless non-uniform linear array direction of arrival estimation approach based on the improved alternating descent conditional gradient algorithm for automotive radar system. Remote Sens. 2025;17(2):303. doi:10.3390/rs17020303.
50. Zaherfekr A, Ghoreishian MJ, Ebrahimzadeh A. DOA estimation in FMCW automotive radars with interference: ML and VMD approaches. In: 2024 11th International Symposium on Telecommunications (IST). Tehran, Iran; 2024. p. 795–800.
51. Karim BA, Ali HK. Computationally efficient MUSIC-based DOA estimation algorithm for FMCW Radar. J Electr Sci Technol. 2023;21(1):100192. doi:10.1016/j.jnlest.2023.100192.

52. Van Trees HL. Optimum array processing: Part IV of detection, estimation, and modulation theory. New York, NY, USA: John Wiley & Sons; 2002.
53. Capon J. High-resolution frequency-wavenumber spectrum analysis. Proc IEEE. 1969;57(8):1408–18. doi:10.1109/proc.1969.7278.
54. Schmidt R. Multiple emitter location and signal parameter estimation. IEEE Trans Antennas Propag. 1986;34(3):276–80. doi:10.1109/tap.1986.1143830.
55. Roy R, Kailath T. ESPRIT-estimation of signal parameters via rotational invariance techniques. IEEE Trans Acoust Speech Signal Process. 1989;37(7):984–95. doi:10.1109/29.32276.
56. Mehta P, Appaiah K, Velmurugan R. Robust direction-of-arrival estimation using array feedback beamforming in low SNR scenarios. IEEE Access. 2023;11:80647–55. doi:10.1109/access.2023.3300709.
57. Godara LC. Application of antenna arrays to mobile communications. II. Beam-forming and direction-of-arrival considerations. Proc IEEE. 1997;85(8):1195–245. doi:10.1109/5.622504.
58. Zhang W, Wang P, He N, He Z. Super resolution DOA based on relative motion for FMCW automotive Radar. IEEE Trans Veh Technol. 2020;69(8):8698–709. doi:10.1109/tvt.2020.2999640.
59. Yuan S, Fioranelli F, Yarovoy AG. Vehicular-motion-based DOA estimation with a limited amount of snapshots for automotive MIMO Radar. IEEE Trans Aerosp Electr Syst. 2023;59(6):7611–25. doi:10.1109/taes.2023.3291335.
60. Amani N, Jansen F, Filippi A, Ivashina MV, Maaskant R. Sparse automotive MIMO radar for super-resolution single snapshot DOA estimation with mutual coupling. IEEE Access. 2021;9:146822–9. doi:10.1109/access.2021.3122967.
61. Xu Z, Chen Y, Zhang P. A sparse uniform linear array DOA estimation algorithm for FMCW radar. IEEE Signal Process Lett. 2023;30:823–7. doi:10.1109/lsp.2023.3292739.
62. Moussa A, Liu W. A two-stage sparsity-based method for location and doppler estimation in bistatic automotive radar. In: 2023 IEEE Statistical Signal Processing Workshop (SSP). Hanoi, Vietnam: IEEE; 2023. p. 487–91. doi:10.1109/ssp53291.2023.10207941.
63. Moussa A, Liu W, Zhang YD, Greco MS. Multi-target location and doppler estimation in multistatic automotive radar applications. IEEE Trans Radar Syst. 2024;2(2):215–25. doi:10.1109/trs.2024.3362706.
64. Moussa A, Liu W. Estimation of doppler, range, and direction of targets in wideband bistatic automotive radar. In: ICASSP, 2025–2025 IEEE International Conference on Acoustics, Speech and Signal Processing (ICASSP). Hyderabad, India; 2025. p. 1–5.
65. Correas-Serrano A, González-Huici MA. Experimental evaluation of compressive sensing for DoA estimation in automotive radar. In: 19th International Radar Symposium (IRS). Bonn, Germany: IEEE; 2018. p. 1–10.
66. Zheng L, Long J, Lops M, Liu F, Hu X, Zhao C. Detection of ghost targets for automotive radar in the presence of multipath. IEEE Trans Signal Process. 2024;72(3):2204–20. doi:10.1109/tsp.2024.3384750.
67. Sim H, Kang S, Lee S, Kim SC. Improved DOA estimation method by distinction of different transmit signals in automotive MIMO frequency-modulated continuous wave radar systems. IET Radar Sonar Navig. 2020;14(8):1135–42. doi:10.1049/iet-rsn.2019.0634.
68. Wu Y, Li C, Hou YT, Lou W. Real-time DOA estimation for automotive radar. In: 18th European Radar Conference (EuRAD). London, UK: IEEE; 2022. p. 437–40.
69. Wu Y, Li C, Hou YT, Lou W. A real-time super-resolution doa estimation algorithm for automotive radar sensor. IEEE Sensors J. 2024;24(22):37947–61. doi:10.1109/jsen.2024.3462350.
70. Jauch A, Meinl F, Blume H. DoA estimation in automotive MIMO radar with sparse array via fast variational bayesian method. In: 2023 IEEE Conference on Antenna Measurements and Applications (CAMA); Genoa, Italy; 2023. p. 892–7.
71. Jauch A, Meinl F, Blume H. Hardware-friendly variational bayesian method for DoA estimation in automotive MIMO radar. In: 2024 9th International Conference on Frontiers of Signal Processing (ICFSP). Paris, France; 2024. p. 174–8.
72. Fuchs J, Gardill M, Lübke M, Dubey A, Lurz F. A machine learning perspective on automotive radar direction of arrival estimation. IEEE Access. 2022;10:6775–97. doi:10.1109/access.2022.3141587.

73. Song Y, Li Y, Zhang C, Huang Y. Data driven low-complexity DOA estimation for ultra-short range automotive radar. In: 2019 IEEE International Workshop on Signal Processing Systems (SiPS). Nanjing, China: IEEE; 2019. p. 313–7. doi:10.1109/sips47522.2019.9020602.
74. Chen M. Short-range target tracking using high-resolution automotive radars [doctoral dissertation]. Hamilton, ON, Canada: McMaster University; 2024. [cited 2025 Jan 3]. Available from: http://hdl.handle.net/11375/29759.
75. Shamsfakhr F, Macii D, Palopoli L, Corrà M, Ferrari A, Fontanelli D. A multi-target detection and position tracking algorithm based on mmWave-FMCW radar data. Measurement. 2024;234(11):114797. doi:10.1016/j.measurement.2024.114797.
76. Zhou T, Yang M, Jiang K, Wong H, Yang D. MMW radar-based technologies in autonomous driving: a review. Sensors. 2020;20(24):7283.
77. Eltrass A, Khalil M. Automotive radar system for multiple-vehicle detection and tracking in urban environments. IET Intell Trans Syst. 2018;12(8):783–92. doi:10.1049/iet-its.2017.0370.
78. Khalil M, Eltrass AS, Elzaafarany O, Galal B, Walid K, Tarek A, et al. An improved approach for multi-target detection and tracking in automotive radar systems. In: International Conference on Electromagnetics in Advanced Applications (ICEAA). Cairns, QLD, Australia: IEEE; 2016. p. 480–3.
79. Uysal F, Aubry PJ, Yarovoy A. Accurate target localization for automotive radar. In: 2019 IEEE Radar Conference (RadarConf). Boston, MA, USA: IEEE; 2019. p. 1–5.
80. Li Y, Liang C, Lu M, Hu X, Wang Y. Cascaded Kalman filter for target tracking in automotive radar. J Eng. 2018;2019(19):6264–7. doi:10.1049/joe.2019.0159.
81. Song S, Wu J, Zhang S, Liu Y, Yang S. Research on target tracking algorithm using millimeter-wave radar on curved road. Math Probl Eng. 2020;2020(4):1–21. doi:10.1155/2020/3749759.
82. Wang CL, Xiong X, Liu HJ. Target tracking algorithm of automotive radar based on iterated square-root CKF. J Phys: Conf Ser. 2018;976:012010. doi:10.1088/1742-6596/976/1/012010.
83. Liu Q, Song K, Xie H, Meng C. Research on invalid target filtering and target tracking algorithm optimization in millimeter-wave radar technology. In: SAE Technical Paper Series. Xi'an, China: SAE International; 2025. doi:10.4271/2025-01-7035.
84. Tan B, Ma Z, Zhu X, Li S, Zheng L, Huang L, et al. Tracking of multiple static and dynamic targets for 4D automotive millimeter-wave radar point cloud in urban environments. Remote Sens. 2023;15(11):2923. doi:10.3390/rs15112923.
85. Koloushani M, Naghsh MM, Reza Taban M, Karbasi SM. Multitarget tracking in the presence of velocity ambiguity for automotive radar. In: ICASSP 2024–2024 IEEE International Conference on Acoustics, Speech and Signal Processing (ICASSP). Seoul, Republic of Korea; 2024. p. 8851–5.
86. Wu Q, Chen L, Li Y, Wang Z, Yao S, Li H. Reweighted robust particle filtering approach for target tracking in automotive radar application. Remote Sens. 2022;14(21):5477. doi:10.3390/rs14215477.
87. Chen Y, Wang Y, Qu F, Li W. A graph-based track-before-detect algorithm for automotive radar target detection. IEEE Sens J. 2021;21(5):6587–99. doi:10.1109/jsen.2020.3042079.
88. Li W, Miao Q, Yuan Y, Tian Y, yi W, Teh K. Automotive radar multi-frame track-before-detect algorithm considering self-positioning errors. IEEE Trans Intell Transp Syst. 2025;1–16. doi:10.1109/tits.2025.3565733.
89. Miao Q, Li PMM, Li W, Yi W. Motion compensation based track-before-detect methods for automotive radar system. In: 2024 Photonics & Electromagnetics Research Symposium (PIERS). Chengdu, China: IEEE; 2024. p. 1–10.
90. Jacobs L, Veelaert P, Steendam H, Philips W. On the accuracy of automotive radar tracking. In: 2023 IEEE 97th Vehicular Technology Conference (VTC2023-Spring). Florence, Italy: IEEE; 2023. p. 1–6.
91. Manjunath A, Liu Y, Henriques B, Engstle A. Radar based object detection and tracking for autonomous driving. In: IEEE MTT-S International Conference on Microwaves for Intelligent Mobility (ICMIM). Munich, Germany: IEEE; 2018. p. 1–4.
92. Held P, Steinhauser D, Koch A, Brandmeier T, Schwarz UT. A novel approach for model-based pedestrian tracking using automotive radar. IEEE Trans Intell Trans Syst. 2022;23(7):7082–95. doi:10.1109/tits.2021.3066680.
93. Huang F, Zhou J, Zhao X. An improved multi-target tracking algorithm for automotive radar. J Phys: Conf Ser. 2021;1971(1):012076. doi:10.1088/1742-6596/1971/1/012076.

94. Honer J, Kaulbersch H. Bayesian extended target tracking with automotive radar using learned spatial distribution models. In: IEEE International Conference on Multisensor Fusion and Integration for Intelligent Systems (MFI). Karlsruhe, Germany: IEEE; 2020. p. 316–22.
95. Tian F, Guo X, Fu W. Target tracking algorithm based on adaptive strong tracking extended kalman filter. Electronics. 2024;13(3):652. doi:10.3390/electronics13030652.
96. de Ramos DC, Ferreira LR, Santos MMD, Teixeira ELS, Yoshioka LR, Justo JF, et al. Evaluation of cluster algorithms for radar-based object recognition in autonomous and assisted driving. Sensors. 2024;24(22):1–31.
97. Ren J, Zhang L, Liu J. Research and implementation of 77 GHz automotive radar target detection technology. In: 2023 6th International Conference on Information Communication and Signal Processing (ICICSP). Xi'an, China; 2023. p. 517–21.
98. Xu L, Lien J, Li J. Doppler-range processing for enhanced high-speed moving target detection using LFMCW automotive radar. IEEE Trans Aerosp Electr Syst. 2021;58(1):568–80. doi:10.1109/taes.2021.3101768.
99. Li Y, Li G, Liu Y, Zhang XP, He Y. A hybrid SVSF algorithm for automotive radar tracking. IEEE Trans Intell Trans Syst. 2022;23(9):15028–42. doi:10.1109/tits.2021.3136170.
100. Tilly JF, Haag S, Schumann O, Weishaupt F, Duraisamy B, Dickmann J, et al. Detection and tracking on automotive radar data with deep learning. In: 2020 IEEE 23rd International Conference on Information Fusion (FUSION). Rustenburg, South Africa: IEEE; 2020. p. 1–7.
101. Cao X, Lan J, Li XR, Liu Y. Automotive radar-based vehicle tracking using data-region association. IEEE Trans Intell Trans Syst. 2022;23(7):8997–9010. doi:10.1109/tits.2021.3089676.
102. Lindenmaier L, Aradi S, Bécsi T, Fekete B. Comparison of track management strategies in automotive track-to-track fusion algorithms. In: 2025 IEEE 23rd World Symposium on Applied Machine Intelligence and Informatics (SAMI). Stará Lesná, Slovakia: IEEE; 2025.
103. Ghatak G. Target tracking: statistics of successive successful target detection in automotive radar networks. arXiv:2411.18252. 2024.
104. Lee KC. Radar target recognition by machine learning of K-nearest neighbors regression on angular diversity RCS. ACES J. 2019;34(1):75–81.
105. Park C, Kwak S, Lee H, Lee S. Bidirectional LSTM-based overhead target classification for automotive radar systems. IEEE Trans Instrum Meas 2024;73(2):1–11. doi:10.1109/tim.2023.3343741.
106. Kim S, Lee S, Doo S, Shim B. Moving target classification in automotive radar systems using convolutional recurrent neural networks. In: 26th European Signal Processing Conference (EUSIPCO). Rome, Italy: IEEE; 2018. p. 1482–6.
107. Angelov A, Robertson A, Murray-Smith R, Fioranelli F. Practical classification of different moving targets using automotive radar and deep neural networks. IET Radar Sonar Navig. 2018;12(10):1082–9.
108. Kwak S, Kim H, Kim G, Lee S. Multi-view convolutional neural network-based target classification in high-resolution automotive radar sensor. IET Radar Sonar Navig. 2022;17(1):15–26. doi:10.1049/rsn2.12320.
109. Wen Q, Cao S. Radar range-doppler flow: a radar signal processing technique to enhance radar target classification. IEEE Trans Aerosp Electronic Syst. 2024;60(2):1519–29. doi:10.1109/taes.2023.3337757.
110. Richter Y, Balal N, Pinhasi Y. Neural-network-based target classification and range detection by CW MMW radar. Remote Sens. 2023;15(18):4553. doi:10.3390/rs15184553.
111. Lim S, Lee S, Yoon J, Kim SC. Phase-based target classification using neural network in automotive radar systems. In: IEEE Radar Conference (RadarConf). Boston, MA, USA: IEEE; 2019. p. 1–6.
112. Gao T, Lai Z, Mei Z, Wu Q. Hybrid SVM-CNN classification technique for moving targets in automotive FMCW radar system. In: 11th International Conference on Wireless Communications and Signal Processing (WCSP). Xi'an, China: IEEE; 2019. p. 1–6.
113. Lee S, Yoon YJ, Lee JE, Kim SC. Human-vehicle classification using feature-based SVM in 77-GHz automotive FMCW radar. IET Radar Sonar Navig. 2017;11(10):1589–96. doi:10.1049/iet-rsn.2017.0126.
114. Kim W, Cho H, Kim J, Kim B, Lee S. Target classification using combined YOLO-SVM in high-resolution automotive FMCW radar. In: IEEE Radar Conference (RadarConf20). Florence, Italy: IEEE; 2020. p. 1–5.

115. Gupta S, Rai PK, Kumar A, Yalavarthy PK, Cenkeramaddi LR. Target classification by mmWave FMCW radars using machine learning on range-angle images. IEEE Sens J. 2021;21(18):19993–20001. doi:10.1109/jsen.2021.3092583.
116. Kim W, Cho H, Kim J, Kim B, Lee S. YOLO-based simultaneous target detection and classification in automotive FMCW radar systems. Sensors. 2020;20(10):2897. doi:10.3390/s20102897.
117. Sohail M, Khan AU, Sandhu M, Shoukat I, Jafri M, Shin H. Radar sensor based machine learning approach for precise vehicle position estimation. Sci Rep. 2023;13(1):13837. doi:10.1038/s41598-023-40961-5.
118. Lamane M, Tabaa M, Klilou A. Classification of targets detected by mmWave radar using YOLOv5. Procedia Comput Sci. 2022;203(18):426–31. doi:10.1016/j.procs.2022.07.056.
119. Lee H, Kwak S, Lee S. Multiple-output network for simultaneous target classification and moving direction estimation in automotive radar systems. Expert Syst Appl. 2025;259(10):125280. doi:10.1016/j.eswa.2024.125280.
120. Senigagliesi L, Ciattaglia G, De Santis A, Gambi E. People walking classification using automotive radar. Electronics. 2020;9(4):588. doi:10.3390/electronics9040588.
121. Chipengo U, Sligar AP, Canta SM, Goldgruber M, Leibovich H, Carpenter S. High fidelity physics simulation-based convolutional neural network for automotive radar target classification using micro-doppler. IEEE Access. 2021;9:82597–617. doi:10.1109/access.2021.3085985.
122. Lee Y, Kim J, Kim S, Lee H, Lee S. Estimation of moving direction and size of vehicle in high-resolution automotive radar system. IEEE Trans Intell Trans Syst. 2024;25(7):7174–86. doi:10.1109/tits.2023.3339811.
123. Dubey A, Santra A, Fuchs J, Lübke M, Weigel R, Lurz F. Integrated classification and localization of targets using bayesian framework in automotive radars. In: ICASSP 2021-IEEE International Conference on Acoustics, Speech and Signal Processing (ICASSP). Toronto, ON, Canada: IEEE; 2021. p. 4060–4.
124. Kanona MEA, Alias MY, Hassan MK, Mohamed KS, Khairi MHH, Hamdan M, et al. A machine learning based vehicle classification in forward scattering radar. IEEE Access. 2022;10(2):64688–700. doi:10.1109/access.2022.3183127.
125. Cai X, Sarabandi K. A Machine learning based 77 GHz radar target classification for autonomous vehicles. In: 2019 IEEE International Symposium on Antennas and Propagation and USNC-URSI Radio Science Meeting. Atlanta, GA, USA: IEEE; 2019. p. 371–2.
126. Cai X, Giallorenzo M, Sarabandi K. Machine learning-based target classification for MMW radar in autonomous driving. IEEE Trans Intell Veh. 2021;6(4):678–89. doi:10.1109/tiv.2020.3048944.
127. Duong S, Kahrizi D, Mettler S, Klöck C. Moving target classification with a dual automotive FMCW radar system using convolutional neural networks. In: 2021 21st International Radar Symposium (IRS). Berlin, Germany; 2021. p. 1–9.
128. Ulrich M, ser Glä C, Timm F. DeepReflecs: deep learning for automotive object classification with radar reflections. In: 2021 IEEE Radar Conference (RadarConf21). Atlanta, GA, USA; 2021. p. 1–6.
129. Kung YC, Zhou X, Shen H, Ahn J, Wang J. Convolutional neural networks for interpreting unclustered radar data in automotive applications. In: 2023 IEEE International Automated Vehicle Validation Conference (IAVVC). Austin, TX, USA; 2023. p. 1–6.
130. Pattanaik S, Imoize AL, Li CT, Francis SAJ, Lee CC, Roy DS. Data-driven diffraction loss estimation for future intelligent transportation systems in 6G networks. Mathematics. 2023;11(13):3004. doi:10.3390/math11133004.
131. Danino S, Bilik I. Automatic multipath annotation for conventional automotive radar datasets. IEEE Sens J. 2024;24(8):13500–17. doi:10.1109/jsen.2024.3364497.
132. Gurbuz SZ, Griffiths HD, Charlish A, Rangaswamy M, Greco MS, Bell K. An overview of cognitive radar: past, present, and future. IEEE Aerosp Electr Syst Mag. 2019;34(12):6–18. doi:10.1109/maes.2019.2953762.
133. Zheng R, Sun S, Caesar H, Chen H, Li J. Redefining automotive radar imaging: a domain-informed 1D deep learning approach for high-resolution and efficient performance. 2024. doi:10.48550/arXiv.2406.07399.
134. Fan L, Wang J, Chang Y, Li Y, Wang Y, Cao D. 4D mmWave radar for autonomous driving perception: a comprehensive survey. IEEE Trans Intell Veh. 2024;9(4):4606–20. doi:10.1109/tiv.2024.3380244.
135. Chan PH, Shahbeigi Roudposhti S, Ye X, Donzella V. A noise analysis of 4D RADAR: robust sensing for automotive? IEEE Sens J. 2025;25(10):18291–301. doi:10.36227/techrxiv.24517249.v1.

136. Sichani NK, Ahmadi M, Raei E, Alaee-Kerahroodi M, M.R. BS, Mehrshahi E, et al. Waveform selection for FMCW and PMCW 4D-imaging automotive radar sensors. In: 2023 IEEE Radar Conference (RadarConf23). San Antonio, TX, USA; 2023. p. 1–6.
137. Gottinger M, Hoffmann M, Christmann M, Schütz M, Kirsch F, Gulden P, et al. Coherent automotive radar networks: the next generation of radar-based imaging and mapping. IEEE J Microw. 2021;1(1):149–63. doi:10.1109/jmw.2020.3034475.
138. Dong F, Wang W, Li X, Liu F, Chen S, Hanzo L. Joint beamforming design for dual-functional MIMO radar and communication systems guaranteeing physical layer security. IEEE Trans Green Commun Netw. 2023;7(1):537–49. doi:10.1109/tgcn.2022.3233863.
139. Imoize AL, Obakhena HI, Anyasi FI, Sur SN. A review of energy efficiency and power control schemes in ultra-dense cell-free massive MIMO systems for sustainable 6G wireless communication. Sustainability. 2022;14(17):11100. doi:10.3390/su141711100.
140. Maccone L, Ren C. Quantum radar. Phys Rev Lett. 2020;124:1–5.
141. Caesar H, Bankiti V, Lang AH, Vora S, Liong VE, Xu Q, et al. NuScenes: a multimodal dataset for autonomous driving. In: 2020 IEEE/CVF Conference on Computer Vision and Pattern Recognition (CVPR). Seattle, WA, USA: IEEE; 2020. p. 11618–28.
142. Muckenhuber S, Museljic E, Stettinger G. Performance evaluation of a state-of-the-art automotive radar and corresponding modeling approaches based on a large labeled dataset. J Intell Trans Syst. 2022;26(6):655–74. doi:10.1080/15472450.2021.1959328.
143. Ram SS, Ghatak G. Emerging trends in radar: automotive radar networks. IEEE Aerosp Electron Syst Mag. 2025;40(6):54–9. doi:10.1109/maes.2025.3539254.
144. Paek DH, Kong SH, TirtaWijaya K. K-radar: 4D radar object detection for autonomous driving in various weather conditions. In: 36th Conference on Neural Information Processing Systems (NeurIPS 2022) Track on Datasets and Benchmarks. New York, USA: Neurips; 2022. p. 1–8.
145. Schumann O, Hahn M, Scheiner N, Weishaupt F, Tilly JF, Dickmann J, et al. RadarScenes: a real-world radar point cloud data set for automotive applications. In: 2021 IEEE 24th International Conference on Information Fusion (FUSION). Sun City, South Africa: IEEE; 2021. p. 1–8.
146. Barnes D, Gadd M, Murcutt P, Newman P, Posner I. The oxford radar robotcar dataset: a radar extension to the oxford robotcar dataset. In: 2020 IEEE International Conference on Robotics and Automation (ICRA). Paris, France: IEEE; 2020. p. 6433–8.
147. Meyer M, Kuschk G. Automotive radar dataset for deep learning based 3D object detection. In: 2019 16th European Radar Conference (EuRAD). Paris, France: IEEE; 2019. p. 129–32.
148. Palffy A, Pool E, Baratam S, Kooij JFP, Gavrila DM. Multi-class road user detection with 3+1D radar in the view-of-delft dataset. IEEE Robot Autom Lett. 2022;7(2):4961–8. doi:10.1109/lra.2022.3147324.
149. Burnett K, Yoon DJ, Wu Y, Li AZ, Zhang H, Lu S, et al. Boreas: a multi-season autonomous driving dataset. Int J Rob Res. 2023;42(1–2):33–42. doi:10.1177/02783649231160195.
150. Ouaknine A, Newson A, Rebut J, Tupin F, Pérez P. CARRADA dataset: camera and automotive radar with range-angle-doppler annotations. In: 2020 25th International Conference on Pattern Recognition (ICPR). Milan, Italy: IEEE; 2021. p. 5068–75.
151. Sheeny M, De Pellegrin E, Mukherjee S, Ahrabian A, Wang S, Wallace A. RADIATE: a radar dataset for automotive perception in bad weather. In: 2021 IEEE International Conference on Robotics and Automation (ICRA). Xi'an, China: IEEE; 2021. p. 1–7.
152. Rafieinia F, Castro R, Wyglinski A, Mcnew J. Standard for automotive radar performance metrics and testing methods for advanced driver assistance systems (ADAS) and automated driving system(ADS) applications. IEEE; 2019. [cited 2025 Feb 1]. Available from: https://standards.ieee.org/ieee/3116/10712/.
153. Short Range Devices; Transport and Traffic Telematics (TTT); Short Range Radar equipment operating in the 77 to 81 GHz band. Harmonised Standard covering the essential requirements of article 3.2 of Directive 2014/53/EU; 2017. [cited 2025 Jan 3]. Available from: https://www.etsi.org/deliver/etsi_en/302200_302299/302264/02.01.01_30/en_302264v020101v.pdf.